AUG 12 1965
LIBRARY

REACTOR MATERIALS

A Quarterly Technical Progress Review

Prepared for DIVISION OF TECHNICAL INFORMATION, USAEC, by
R. W. DAYTON, E. M. SIMONS, and ASSOCIATES, BATTELLE MEMORIAL INSTITUTE

Summer 1965

● VOLUME 8

● NUMBER 2

TECHNICAL PROGRESS REVIEWS

To meet the needs of industry for concise summaries of current atomic developments, the Atomic Energy Commission is publishing this series, Technical Progress Reviews. Issued quarterly, each of the reviews digests and evaluates the latest findings in a specific area of nuclear technology and science.

The five journals published in this series are:

Isotopes and Radiation Technology, P. S. Baker, A. F. Rupp, and associates, Oak Ridge National Laboratory

Nuclear Safety, Wm. B. Cottrell, W. H. Jordan, and associates, Oak Ridge National Laboratory

Power Reactor Technology, W. H. Zinn and J. R. Dietrich, Combustion Engineering, Inc., Nuclear Division

Reactor Fuel Processing, Stephen Lawroski and associates, Chemical Engineering Division, Argonne National Laboratory

Reactor Materials, R. W. Dayton, E. M. Simons, and associates, Battelle Memorial Institute

Each journal may be purchased from the Superintendent of Documents, U. S. Government Printing Office, Washington, D. C., 20402. *Isotopes and Radiation Technology* at $2.00 per year for subscription or $0.55 for individual issues; the other four journals at $2.50 per year and $0.70 per issue. See back cover for remittance instructions and foreign postage requirements.

The views expressed in this publication do not necessarily represent those of the United States Atomic Energy Commission, its divisions or offices, or of any Commission advisory committee or contractor.

Availability of Reports Cited in This Review

Unclassified AEC reports are available for inspection at AEC depository libraries and are sold by the Clearinghouse for Federal Scientific and Technical Information, National Bureau of Standards, U. S. Department of Commerce, 5285 Port Royal Road, Springfield, Va., 22151. Some of the reports cited are not available owing to their preliminary nature; however, the information contained in them will eventually be made available in formal progress or topical reports.

Unclassified reports issued by other Government agencies or private organizations should be requested from the originator.

Unclassified British and Canadian reports may be inspected at AEC depository libraries. British reports are sold by the British Information Service, 45 Rockefeller Plaza, New York, N. Y.; Canadian reports (AECL series) are sold by the Scientific Document Distribution Office, Atomic Energy of Canada, Ltd., Chalk River, Ontario, Canada.

Classified U. S. and foreign reports identified in this journal as Classified may be purchased by properly cleared Access Permit Holders from the Division of Technical Information Extension, U. S. Atomic Energy Commission, P. O. Box 1001, Oak Ridge, Tenn., 37831. Such reports may be inspected at classified AEC depository libraries.

REACTOR MATERIALS

A REVIEW OF RECENT DEVELOPMENTS

Prepared for DIVISION OF TECHNICAL INFORMATION, USAEC,
by R. W. DAYTON, E. M. SIMONS, and ASSOCIATES,
BATTELLE MEMORIAL INSTITUTE

SUMMER 1965

VOLUME 8

NUMBER 2

Foreword

Reactor Materials is one of a series of quarterly technical progress reviews broadly covering the field of nuclear science and technology. Under the auspices of the AEC Division of Technical Information, *Reactor Materials* is prepared by Battelle personnel from worldwide literature. It covers properties, behavior, and fabrication processes of materials applicable to nuclear reactor components and associated equipment.

The reader will recognize that the scope of this Review is too broad to permit detailed coverage of every topic. Rather, the authors and editors attempt to combine the highlights of significant new developments into an informative summary of current research for both management and the technical specialist. As a rule, enough of the results are presented to define the research and summarize the findings. For readers desiring more information on any particular topic, a complete set of references is provided at the end of each section.

Each quarter a number of bibliographies, monographs, and books appear on subjects within the scope of *Reactor Materials*. Although the main purpose of this Review is to call attention to findings that are new and significant, such publications are noted in the text because they often represent excellent compilations of available information on important materials topics.

R. W. DAYTON
E. M. SIMONS
R. W. ENDEBROCK
Battelle Memorial Institute

DEPOSITED BY THE
UNITED STATES OF AMERICA

Contents

I Fuel and Fertile Materials 57
Uranium Metal and Alloys 57
Plutonium 61
Thorium and Its Alloys 63
Metal-Ceramic Fuels 64
Coated-Particle Fuel Materials 65
Uranium Oxides 67
Uranium and Thorium Carbides, Nitrides, and Sulfides 68
Mechanism of Corrosion of Fuels . . . 71
Basic Studies of Irradiation Effects in Fuel Materials 71
References 71

II Moderator Materials 74
Graphite 74
Beryllium Metal and Alloys 75
Beryllium Oxide 77
Beryllium Intermetallic Compounds . . 80
Solid Hydrides 80
References 81

III Nuclear Poisons 83
Metallic Poison Materials 83
Dispersion and Nonmetallic Poison Materials 84
References 85

IV Cladding and Structural Materials . 86
Corrosion 86
Selected Mechanical Properties of Cladding and Structural Materials . . 91
Metallurgical Aspects of Cladding Materials 93
Diffusion Studies 97
Ceramic Technology 98
Radiation Effects in Nonfuel Materials . . 100
References 101

V Special Fabrication Techniques . . . 105
Melting and Hot and Cold Working . . . 105
Cladding 106
Explosive Joining 109
Welding and Brazing 112
Nondestructive Testing 115
References 117

Issued quarterly by the U. S. Atomic Energy Commission. Use of funds for printing this publication approved by the Director of the Bureau of the Budget on October 14, 1963.

Section

I

Reactor Materials

Fuel and Fertile Materials

Uranium Metal and Alloys

Unalloyed Uranium

The effects of grain size and plastic deformation at 300°C on the tensile properties of commercial-purity uranium were investigated by the British,[1] with particular reference to the brittle-ductile phenomenon. It was established that increasing amounts of cold work lower the transition temperature appreciably, whereas decreasing the grain size has only a slight lowering effect on the transition temperature. The cleavage fracture stress (σ_c) and grain size (d) do not obey the predicted relation $\sigma_c \propto d^{-\frac{1}{2}}$. The criterion for brittle fracture in uranium is considered to be associated with the increasing incidence of the twinning mode of deformation with decreasing temperature.

Investigators at Iowa State University[2] studied the influence of rate of loading on the tensile properties of gamma-extruded alpha uranium. The tests were conducted in the temperature range from 25 to 600°C at three constant loading rates (0.0017/min, 0.0130/min, and 0.0400/min). The results led to the following conclusions:

1. Tensile properties of uranium are influenced by the rate of loading; however, they are much less sensitive to loading rate than to temperature.

2. Tensile strength, yield strength, and Young's modulus are the properties of uranium most affected by the rate of loading, especially at the higher temperatures. A general statement cannot be made on the influence of loading rate on the elongation and reduction in area for uranium, but the lowest strain rate seemed to give the lowest values for both of these properties in the majority of cases.

3. The slope of the uranium stress-strain curve in the region of plastic flow is affected by the rate of loading; and, in general, the smallest slope occurs at the lowest rate of loading.

4. The lowest rate of loading appears to cause the smallest amount of strain hardening in uranium at a specific temperature.

5. The predominance of the twinning and slip mechanisms of deformation in uranium may be affected by rate of loading, as well as by temperature.

The anisotropic growth during neutron irradiation of mechanically worked uranium is related to the texture of the uranium. In fact, it has been established that preferred-orientation measurements in unirradiated uranium can be used to compute a growth index, G, from which irradiation growth can be predicted. In Britain, Slattery and Connolly[3] have derived generalized growth indices, G, from inverse pole figures and used them to predict the irradiation growth patterns of both rolled and extruded uranium—unalloyed, and with small additions of molybdenum, chromium, and aluminum.

Hanford Atomic Products Operation workers[4] used NaK-filled controlled-temperature capsules to irradiate small, unclad, high-purity, tubular uranium specimens over the temperature range 300 to 650°C to burnups of 0.03 to 0.4 at.%. It was established that fission gases play a minor role in the irradiation behavior of these uranium specimens. Below 600°C the interaction and recovery of fission-induced defects produce gross specimen distortion, and, between 400 and 600°C, they account for very large volume increases. Above 600°C the volume increase is much smaller, and agglomeration of fission gas into pores becomes a contributing factor; below 350°C no volume change occurs.

Alpha-Phase Uranium Alloys

Workers at Mallinckrodt Chemical Works[5,6] have determined the phase relations existing in binary uranium alloys containing small amounts of silicon and iron. Figures I-1 and I-2 present results obtained with the aid of differential, thermal, metallographic, and microprobe analyses.

The British have reported in Ref. 7 on the resistance to deformation of uranium–1, 2, and 5 wt.% molybdenum alloys at several strain rates. Determinations were made using a cam plastometer. In general, resistance to deformation decreases with increasing temperature. The information obtained was utilized to formulate hot-rolling schedules for the uranium–1 and 2 wt.% molybdenum alloys.

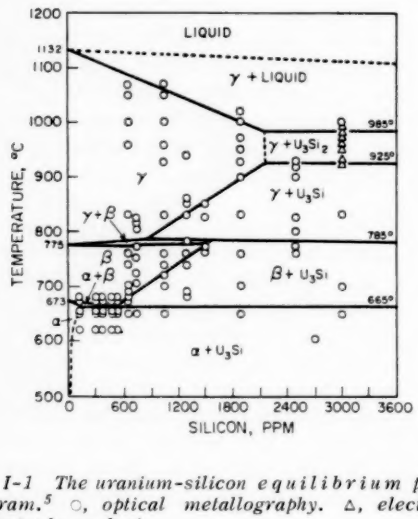

Fig. I-1 The uranium-silicon equilibrium phase diagram.[5] ○, *optical metallography.* △, *electron-microprobe analysis.*

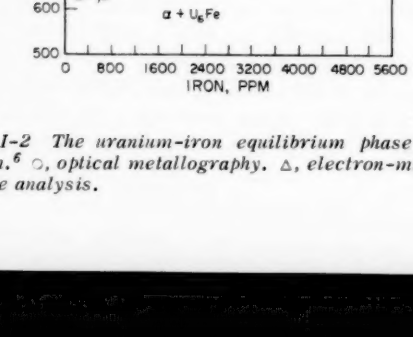

Fig. I-2 The uranium-iron equilibrium phase diagram.[6] ○, *optical metallography.* △, *electron-microprobe analysis.*

Investigators at Nuclear Metals Division of Textron Inc.,[8] attempted to improve the high-temperature properties of high-uranium alloys containing iron, silicon, and aluminum. The following compositions were evaluated by hot-hardness and metallographic tests to assess the effects of molybdenum and chromium additions:

1. U–350 ppm Fe–350 ppm Si–800 ppm Al–1000 ppm Mo
2. U–250 ppm Fe–250 ppm Si–250 ppm Al–250 ppm Cr
3. U–250 ppm Fe–350 ppm Si–800 ppm Al–200 ppm Cr

None of the three alloys showed significant amounts of stable-solution hardening of alpha uranium attributable to the molybdenum or chromium. When the U-Fe-Si-Al alloys were aged 100 hr at 600°C, additions of molybdenum or chromium added only slightly to the hardness. In the solution-treated condition, the chromium addition in alloy 2 caused some increase in hardness, but neither the chromium in alloy 3 nor the molybdenum in alloy 1 caused any significant change in hardness.

Metallographic analysis of alloy 1 showed that the molybdenum combines with uranium and silicon to form $U_4Mo_5Si_3$. Formation of this compound reduces the concentration of molybdenum in solution and its associated hardening effect. It was observed that $U_4Mo_5Si_3$ is relatively insoluble in gamma uranium at 800°C.

The hot hardness and microstructure of the following additional alloys, in various conditions of heat-treatment, were examined by workers at Nuclear Metals:[9]

4. U–350 ppm Si
5. U–350 ppm Si–800 ppm Al
6. U–350 ppm Si–800 ppm Al–350 ppm Fe
7. U–250 ppm Si–250 ppm Al–250 ppm Fe

The investigation revealed that all compositions were responsive to heat-treatment; i.e., the alloy content could be dissolved in beta or gamma uranium and subsequently be precipitated in the alpha phase. For the aluminum-bearing alloys, the amount of precipitate formed in alpha uranium was greater than that predicted from the respective binary equilibrium diagrams. These results suggest the formation of some unknown complex compound or compounds.

The rate of precipitation of the alloy phases in solution-treated uranium is approximately the same for the alloys studied; aging at 600°C for about 5 to 24 hr resulted in the greatest number of fine particles. After such treatment the modal size of the small particles decreases with increasing aluminum content; the modal size for particles in alloy 5 was about 0.035 μ.

The distribution of precipitated particles in the aluminum-bearing alloys is such that some dispersion hardening can be obtained, whereas dispersion hardening in alloy 4 is improbable. After similar precipitation treatments, alloy 5 was 5, 50, and 75% harder at room temperature, 400°C, and 600°C, respectively, than alloy 4. This difference in hardness is attributed primarily to dispersion hardening. The hot hardness of uranium solution treated in the beta phase increases with increasing iron and silicon content, whereas the hot hardness of uranium solution treated in the gamma phase increases with increasing iron, silicon, and aluminum content.

The swelling of irradiated uranium-zirconium alloys on annealing at temperatures to 900°C was measured in terms of density change, and the effect of annealing temperature on the release of fission-product gas was determined at Argonne National Laboratory.[10] The data show that phase changes influenced the swelling and gas release. The present state of knowledge of the physical metallurgy and in-pile behavior of uranium and uranium alloys containing up to 0.25 wt.% of alloying elements is summarized in Ref. 11.

Gamma-Phase Uranium Alloys

The isothermal time-temperature-transformation (TTT) characteristics of gamma-phase alloys of uranium with molybdenum, niobium, and zirconium were studied at Lawrence Radiation Laboratory.[12] Results of this study are shown in Figs. I-3 to I-8.

It was found that niobium and molybdenum stabilize the gamma phase of uranium. The greater the addition of either element required to form a binary alloy with uranium, the longer the delay in the initiation of the gamma-phase transformation. During heat-treatment at temperatures ranging from 450°C to the eutectoid temperature, the "nose" of the TTT curve lies between 500 and 550°C. Varying the amount of the alloying element does not change this temperature appreciably. Below 450°C no evidence of gamma-phase transformation is found until the elapse of considerable time; when transformation does occur, the final product is ordered gamma (γ') and alpha in the molybdenum-uranium alloys and niobium-rich gamma (γ_2) plus alpha in the uranium-niobium alloys.

The elevated-temperature transformation of the gamma phase in a uranium-molybdenum binary alloy is accelerated by the addition of

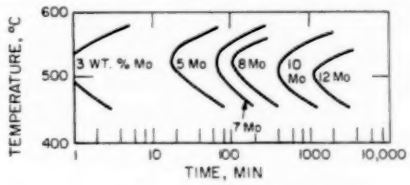

Fig. I-3 Isothermal transformations of uranium-molybdenum alloys.[12]

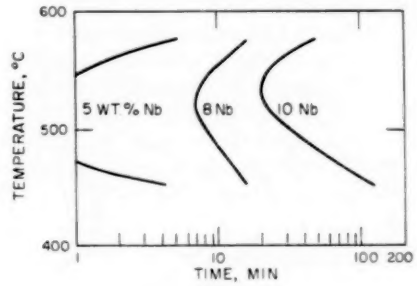

Fig. I-4 Isothermal transformations of uranium-niobium alloys.[12]

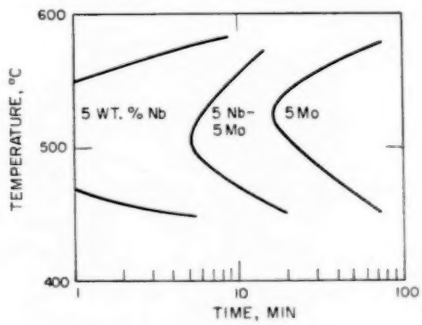

Fig. I-5 Isothermal transformations of uranium—5 wt.% niobium, uranium—5 wt.% niobium—5 wt.% molybdenum, and uranium—5 wt.% molybdenum alloys.[12]

niobium. Molybdenum, on the other hand, when added to a uranium-niobium binary alloy, retards the decomposition of the gamma phase.

Alloying the uranium-molybdenum binary with zirconium hastens the transformation of the gamma phase. Since $ZrMo_2$ is formed, the amount of effective stabilizing molybdenum is reduced; this is reflected in the shorter transformation time. On the other hand, increasing the amount of zirconium in a U-Nb-Zr alloy retards the high-temperature decomposition of the gamma phase. As the temperature of heat-treatment falls from 450°C to room temperature, zirconium has an accelerating effect on the transformation, and a new nose appears at about 350°C. From 350°C to room temperature, the reaction slows down. An increase in the amount of niobium reduces the rate of transformation at the lower nose, but the zirconium content, up to 6 wt.%, has slight effect on the nose position.

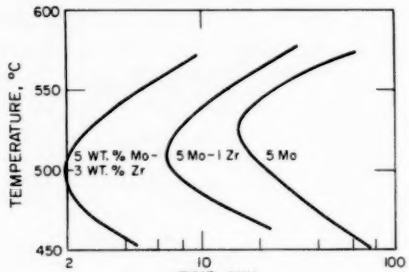

Fig. I-6 The effect on the isothermal transformation of zirconium additions to uranium—5 wt.% molybdenum alloy.[12]

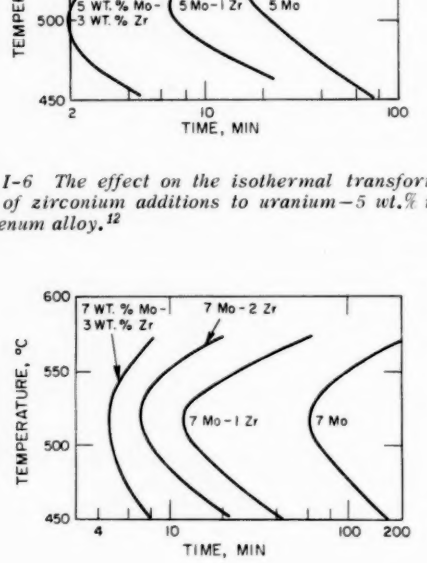

Fig. I-7 The effect on the isothermal transformation of zirconium additions to uranium—7 wt.% molybdenum alloy.[12]

In all the alloys the transformation at the elevated temperatures is of the cellular or nodular type, resulting in a lamellar product. The transformations are not rapid and produce very slight lattice stresses, as seen by the small hardening effect. The low-temperature transformation, common to the zirconium-bearing alloys, is very rapid and produces great hardening. This transformation appears to be martensitic in nature, the M_s temperature occurring at approximately 470°C.

It is suggested that the alloys with zirconium will be less corrosion resistant than the uranium-molybdenum or uranium-niobium gamma-phase binary alloys. On the other hand, there are advantages in obtaining high strengths through heat-treatment. The uranium—7.5 wt.% niobium—2.5 wt.% zirconium alloy is attractive for this reason.

Dilute Uranium Alloys

British investigators[13] have determined the phase relations existing in high-purity palladium-uranium alloys containing up to 25 at.% uranium. They found that the terminal face-

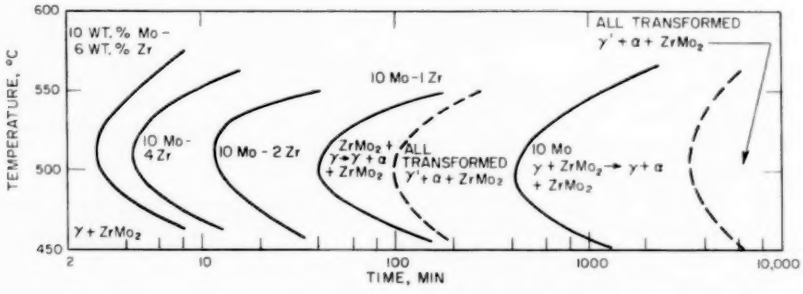

Fig. I-8 The effect on the isothermal transformation of zirconium additions to uranium—10 wt.% molybdenum alloy.[12]

centered cubic (fcc) phase undergoes two eutectoidal transformations: the first, at 13.5 at.% uranium at 694°C, gives the compounds $Pd_{17}U_2$ and $Pd_{11}U_2$; and the second, at 15.5 at.% and 1015°C, gives $Pd_{11}U_2$ and Pd_5U. The Pd_5U forms by peritectic reaction at 18.8 at.% uranium and 1440°C and exists over a small solubility range. The nominal compound Pd_4U forms by a peritectic reaction at 1525°C. (M. S. Farkas)

Plutonium

Plutonium Metal and Alloys

Investigators at Nuclear Materials & Equipment Corp.[14] are attempting to grow single crystals of alpha plutonium. In experiments to date, using a modified Andrade technique, little or no success was noted when the wire-specimen temperature was varied over the range of 120 to 205°C (beta phase), followed by transformation to alpha at 76°C. Likewise, progressive beta-to-alpha cycling had little or no effect on grain size. Plans call for the application of pressures up to 500,000 psi to stabilize the alpha phase up to temperatures of about 400°C, and thus promote grain growth through accelerated solid-state diffusion.

The fracture behavior of alpha plutonium has been studied at Los Alamos Scientific Laboratory using electron microfractography.[15] For high-purity alpha plutonium, the fracture mode is temperature dependent, with an equicohesive temperature between 191 and 297°K. Below this temperature range alpha plutonium fractures in a ductile, transgranular manner; and at higher temperatures fractures are intergranular.

The plutonium-cadmium phase diagram, as determined at Mound Laboratory[16] by differential thermal analysis and metallographic examination, is shown in Fig. I-9.

The effects of small additions of alloying elements on phase transformations in plutonium and delta-stabilized plutonium–3.5 at.% gallium alloys have been investigated using differential-thermal-analysis techniques. The following observations were made:

1. Additions of 0.1 at.% iron, cobalt, or nickel to plutonium caused additional phase transformations in the temperature range 405 to 412°C. Solidus and liquidus temperatures for the alloys were near 624 and 640°C, respectively.
2. Additions of 0.1 at.% iron or cobalt to delta-stabilized plutonium introduced additional phase transformations at 405°C and lowered the solidus and liquidus temperatures.
3. The combined addition of iron and nickel, each at 0.05 at.%, depressed the plutonium-iron eutectic temperature about 15°C. In the delta-stabilized plutonium, the same eutectic was lowered 10°C.

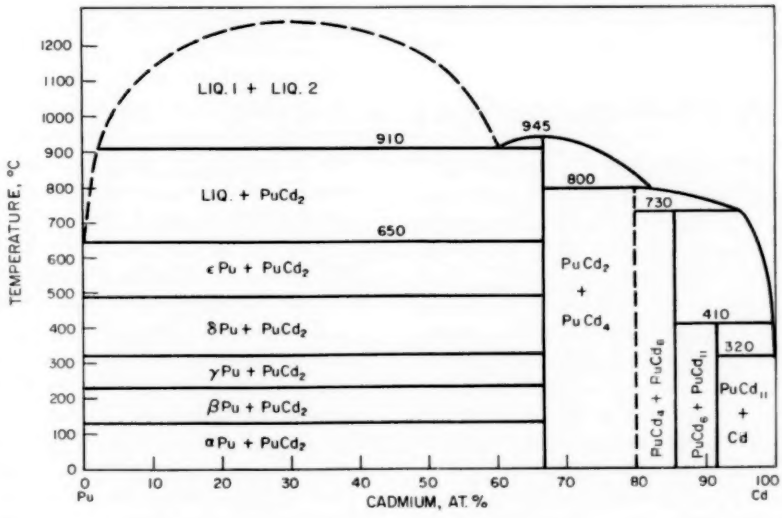

Fig. I-9 Plutonium-cadmium binary phase diagram.[16]

Densities of liquid plutonium–1 wt.% gallium alloy were measured at temperatures from 682 to 847°C using a vacuum pycnometric method. The equation representing density as a function of temperature is

$$\rho = 16.725 - (9 \times 10^{-4})\ T \pm 0.085$$

where ρ is the density in grams per cubic centimeter and T is the temperature in degrees centigrade.

Viscosities of several liquid plutonium-cerium alloys measured at Mound Laboratory are shown as a function of temperature in Fig. I-10.

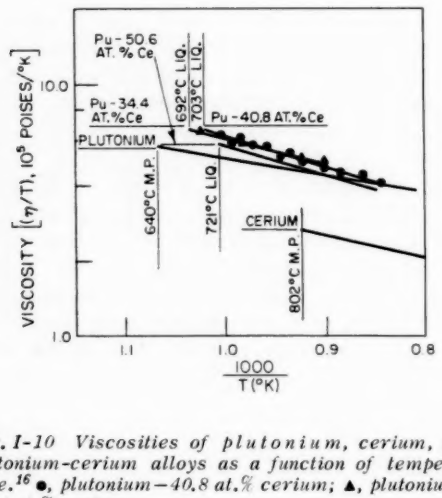

Fig. I-10 Viscosities of plutonium, cerium, and plutonium-cerium alloys as a function of temperature.[16] ●, plutonium–40.8 at.% cerium; ▲, plutonium–34.4 at.% cerium.

United Kingdom investigators report[17] that uranium–25 at.% plutonium–4, 6, and 8 at.% iron alloys all ignite in air at temperatures between 100 and 315°C. Data are tabulated in Table I-1.

Argonne is continuing the investigation and development of uranium-plutonium-fizzium alloys.[18] Transformation kinetic studies indicate that transformation in a uranium–10 wt.% plutonium–10 wt.% fizzium alloy is essentially complete after 30 min at 450 or 500°C. The reaction is apparently eutectoidal, with the products being alpha uranium and gamma prime (U_2Mo), both of which contain plutonium. Compressive creep tests of uranium–15 wt.% plutonium–10 wt.% fizzium alloy were conducted at 650, 750, and 850°C with a load of 11.6 (10^{-3}) kg/mm^2. After 50 hr the rods had contracted 0.04% at 650°C, 0.08% at 750°C, and 0.32% at 850°C. Compatibility tests of uranium–15 wt.% plutonium–10 wt.% fizzium alloy with a vanadium–20 wt.% titanium cladding alloy in the temperature range 600 to 750°C show that the fuel penetration rate into the cladding is somewhat higher than with a uranium–10 wt.% plutonium–10 wt.% fizzium alloy. The data can be described by

$$X^2 = Kt$$

where X equals the penetration into the cladding in centimeters, t equals the time in seconds, and K equals the penetration coefficient in square centimeters per second.

(V. W. Storhok)

Table I-1 OXIDATION AND IGNITION BEHAVIOR OF URANIUM-PLUTONIUM-IRON ALLOYS[17]

Iron content, at.%	Casting temp., °C		Surface condition	Atmosphere	Sustained oxidation temp., °C	Ignition temp., °C
	Melt	Mold				
4	980	625	Oxidized	Moist air		~100
4	980	625	Oxidized	Moist air		140
4	980	200	Oxidized	Moist air	190	270
4	1200	325–805	As cast	Moist air	190	270
4	1200	325–805	Polished	Moist air	190	270
4	1200	325–805	Mechanical	Dry air	280	290
4	1200	325–805	Mechanical	Dry air	270	280
6	1200	~70	As cast	Dry air	290	315
6	1200	~70	As cast	Dry air	280	300
6	1200	~70	As cast	Moist air	235	290
8	1150	660	Slightly oxidized	Moist air	210	240
8	1150	660	Slightly oxidized	Moist air	160	220
8	1150	660	Slightly oxidized	Moist air	165	200

Plutonium Compounds

Mound Laboratory has compiled a comprehensive review[19] of the solubilities of numerous plutonium compounds in various media. A second compilation[20] by Battelle Memorial Institute lists the known physical properties of about 50 compounds, discusses their fuel potential, and presents some experimental results on PuAs, PuP, and Pu_xSi_y compounds. A quite useful presentation[21] of thermodynamic data for plutonium oxides as a function of composition and temperature has been published by British workers.

A study[22] of the $(U,Pu)O_2$ system shows that increased plutonium contents lead to a considerable decrease in electrical resistivity and that PuO_2 is a classical semiconductor, as demonstrated by the resistivity change with temperature. Chalk River workers[23] indicate that the addition of PuO_2 to UO_2 decreases the sinterability markedly in neutral or oxidizing atmospheres, but only slowly in reducing atmospheres; however, this is in contradiction with earlier results of Russell and coworkers in the United Kingdom.

Hanford reports an interaction in the PuO_2-hydrogen-platinum system[24] at 1050°C, but no apparent reaction[25] between PuO_2 and type 304 stainless steel after 400 hr at 900°C. Both results agree with earlier information generated at Battelle. It is concluded that β-Pu_2O_3 exists over a narrow homogeneity range at 1450°C. The β-Pu_2O_3 compound and UO_2 are reported in Ref. 26 to be mutually soluble over a very wide range of composition. There was a transition from a fluorite to a body-centered cubic (bcc) structure between 50 and 60% Pu_2O_3 and an abrupt increase in cell size at approximately 30% Pu_2O_3. Attempts to prepare plutonium or (plutonium, uranium) monoxides resulted in polyphase mixtures, which exhibit substantial weight loss on sintering.[27]

Solubility limits and eutectic compositions and temperatures have been reported for the systems PuO_2-Al_2O_3, PuO_2-BeO, PuO_2-MgO, and PuO_2-ThO_2-BeO, with the most significant results[28] summarized in Tables I-2 and I-3.

Plutonium nitride studies conducted over a two-year period are summarized in two recent Battelle reports,[29,30] including synthesis methods, fabrication studies, and chemical reactivity of PuN and several of its alloys. A 2500-μ-thick reaction zone between $(U_{0.8}Pu_{0.2})N$ and type 304 stainless steel after irradiation to 5×10^{20} fissions/cm^3 at 600°C is probably indicative of considerable free plutonium in the specimen. This seems most probable since a nominally identical composition irradiated to 2.5×10^{20} fissions/cm^3 showed no change in the solid-solution lattice parameter.[31] The reasonable degree of stability associated with PuN is further indicated[32] by the reported absence of reaction with PuO_2 at 1500°C. (W. M. Pardue)

Table I-2 TERMINAL SOLID SOLUBILITY OF SOME BINARY SYSTEMS[28] INVOLVING PuO_2 OR ThO_2

Solubility of	Weight %*	Mole %*
PuO_2 in Al_2O_3	0.75 to 0.04	0.28 ± 0.02
Al_2O_3 in PuO_2	0.05 ± 0.05	0.14 ± 0.14
PuO_2 in BeO	0.48 ± 0.03	0.016 ± 0.001
BeO in PuO_2	N.D.†	N.D.
PuO_2 in MgO	0.21 ± 0.04	0.032 ± 0.006
MgO in PuO_2	0.5 ± 0.2	3.2 ± 1.5
ThO_2 in BeO	5.5 ± 0.4	0.54 ± 0.04
BeO in ThO_2	N.D.	N.D.

*The errors given are those determined by the counting statistics of the microbe analyzer.
†Not determined.

Table I-3 EUTECTIC TEMPERATURES AND COMPOSITIONS OF PuO_2-MgO, PuO_2-BeO, AND PuO_2-Al_2O_3 BINARIES[28]

System	Predicted values		Experimental values	
	Composition, mole % PuO_2	Temp., °C	Composition, mole % PuO_2	Temp., °C
PuO_2-MgO	53	1923	40	2260
PuO_2-BeO	48	1870	34	2135
PuO_2-Al_2O_3	42	1803	42	1910

Thorium and Its Alloys

The addition of 10 vol.% ThO_2 to thorium-base alloys containing 2 and 5 wt.% zirconium resulted in a decrease of the hot tensile strength of these alloys, according to workers at Oak Ridge National Laboratory.[33] As part of the same program, the hot hardness and 800°C tensile properties of thorium–2 and 5 wt.% indium alloys were measured, with the results shown in Fig. I-11 and Table I-4. The 5 wt.% indium addition appears best on the basis of hardness, strength, and ductility.

The 700 and 900°C sections of the ternary Th-Pu-U phase diagram have been worked out by investigators at Argonne,[34] as shown in Figs. I-12 and I-13. Figure I-14 shows a portion of

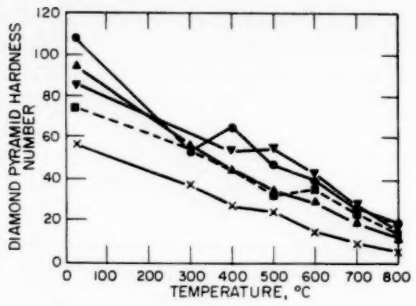

Fig. I-11 Hardness (1-kg load) of thorium and thorium-indium alloys at elevated temperatures.[33] ×, thorium (calcium reduced). ▲, thorium–2 wt.% indium. ■, thorium–3 wt.% indium. ▼, thorium–4 wt.% indium. ●, thorium–5 wt.% indium.

Table I-4 TENSILE RESULTS AT 800°C ON THORIUM-INDIUM ALLOYS[33]

Indium content, wt.%		Ultimate tensile strength, psi	Yield strength (0.2% offset), psi	Elongation, %
Nominal	Actual			
2	1.78	6475	5550	10.0
3	2.60	7315	6330	6.0
4	3.68	6940	6120	5.5
5	4.38	7810	7130	20.0

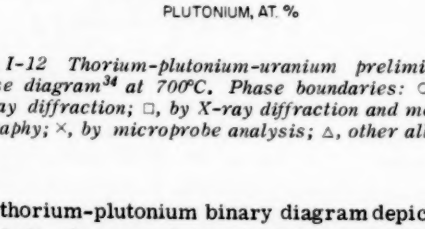

Fig. I-12 Thorium-plutonium-uranium preliminary phase diagram[34] at 700°C. Phase boundaries: ○, by X-ray diffraction; □, by X-ray diffraction and metallography; ×, by microprobe analysis; △, other alloys.

the thorium-plutonium binary diagram depicting the beta phase as determined between 700 and 900°C.

A metastable phase, designated alpha double prime by investigators in the United Kingdom,[35] with an orthorhombic structure has been observed in the composition range 22 to 30 at.% thorium in the zirconium-thorium system. It is believed to be a product of deformation strains on the beta phase with atom positions intermediate between those of the beta- and the close-packed hexagonal alpha prime phases.

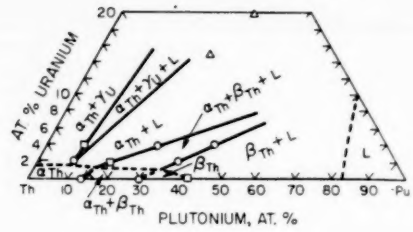

Fig. I-13 Thorium-plutonium-uranium preliminary phase diagram[34] at 900°C. Phase boundaries: ○, by X-ray diffraction; □, by X-ray diffraction and metallography; ×, by microprobe analysis; △, other alloys.

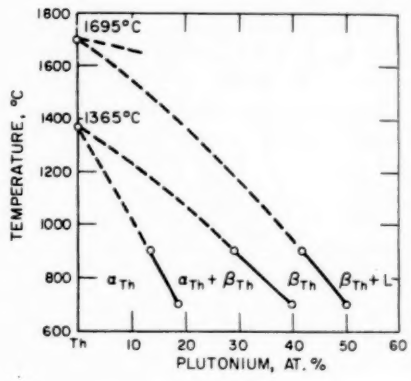

Fig. I-14 Portion of binary thorium-plutonium phase diagram[34] showing the beta phase between 700 and 900°C.

(R. L. Martin)

Metal-Ceramic Fuels

Fuel plates containing either U_3O_8 or niobium-coated UO_2–15 wt.% ZrO_2 particles dispersed in X8001 aluminum matrices were roll bonded at 500°C with Alclad 6061 aluminum. Microstructures were examined at Oak Ridge,[36] and the results indicated that the irregular-shaped U_3O_8 particles were stringered and fragmented; however, the structure was satisfactory for testing. The spherical UO_2–15 wt.% ZrO_2 particles appeared intact after similar reductions, but the structures revealed more particle clumping. These particles were coated with niobium to minimize observed chemical reactions that have occurred previously between the

ceramic oxide and aluminum matrix. Compatibility tests are planned to evaluate the niobium-coated UO_2-ZrO_2 particles and aluminum and to determine the maximum temperature of the system.

Oak Ridge has irradiated fuel plates containing 27.5 vol.% UO_2–type 347 stainless-steel dispersions clad with type 347 stainless steel at maximum surface temperatures of 477 to 507°C and 538 to 450°C to burnups of 0.36 to 0.39×10^{21} and 1.7 to 2.0×10^{21} fissions/cm^3, respectively. The specimens irradiated at the lower temperatures showed density decreases of approximately 0.5%, whereas the other specimens suffered gross swelling and cracking of the type 347 stainless-steel matrix and indicated density decreases of 6 to 13%. Correlation of data[37] with experimental information of other investigators suggests that the maximum tolerable burnup prior to failure is 1.6×10^{21} fissions/cm^3 at a surface temperature of 482°C. Irradiation testing has been continued on tubular and plate 35 vol.% UO_2–stainless-steel fuel dispersions of Martin Marietta Co. in the Oak Ridge Research Reactor (ORR) pressurized-water loop.[33] The centerline temperature has been maintained between 482 and 538°C, and the fuel burnup is currently estimated at 6×10^{20} fissions/cm^3.

British workers[38,39] have devised a simple fabrication technique to give consistent and high controllable densities of dispersion fuels with little or no damage to the ceramic particles. Dispersions of UO_2 and stainless steel are blended, cold pressed, and sintered. After the specimens are sintered, they are further densified by a series of coining operations with intermediate annealings. Annealing removes the residual work hardening after coining and renders the material amenable to further plastic deformation. Three or four coining operations under pressures ranging from 50 to 100 tsi suffice to raise the density from 80 to 97% of the theoretical. Since the forces are primarily compressive and the amount of deformation is limited to that necessary to close the matrix voids, the UO_2 withstands the fabrication process without fragmentation or deformation and with minimum effect on its distribution within the matrix.

To prepare 30 vol.% UO_2–stainless-steel irradiation pins (3 ft long) applicable for fast reactors, Hanford workers[24] are further reducing dense Dynapak specimens by hot extrusion. Area reductions of approximately 10 times resulted in a cladding-thickness variation of 0.0015 in. along the extrusion length. The amount of UO_2-particle stringering was significantly reduced by using the Dynapak billets for extrusion.[31] Similar improvement in structure was reported[29] for sol-gel UO_2–type 347 stainless-steel dispersions fabricated at Battelle by hot rolling at 1200°C. Subsequent cold rolling from 1 to 15% had little effect on the sol-gel UO_2 particles, whereas previous fuel plates without sol-gel UO_2 could withstand a cold-rolling reduction of only 3% before extensive UO_2 breakage.[40] The higher cold-rolling reductions did create small voids at the ends of the sol-gel UO_2 particles, and the voids tended to increase in size with increased cold reduction. These voids may possibly be beneficial in collecting fission gases during irradiation.

(D. L. Stoltz)

Coated-Particle Fuel Materials

Particle Coating

A brief review of development work by Minnesota Mining & Manufacturing Co. on pyrolytic carbon (PyC)-coated fuel particles is given in Ref. 41. During the development program several methods of particle agitation were studied, including vibration, rotating drums, fluidized beds, and a continuous-particle elevator-drop system. The rotating-drum and the fluidized-bed systems were studied in more detail. Each of these coating systems has its own unique advantages.

Oak Ridge reports[33] that microvoids 100 A in diameter have been revealed in low-density PyC deposits by the use of transmission techniques. Annealing of massive deposits of PyC at 2650°C for 3 hr did not change the apparent microstructure but did cause the microvoids to disappear.

Italian workers[42] developed a method for deposition of 80 wt.% nickel–20 wt.% chromium-alloy coatings on UO_2 pellets with diameters between 1 and 4 mm. Approximately 10 μ of nickel is deposited in about 1 hr from an electroless nickel-plating bath to form a conducting surface on the pellets. Additional nickel is then electrodeposited in a normal Watts bath in a rotary barrel. Chromium is then

Table I-5 COATED-PARTICLE FUEL IRRADIATIONS (REFS. 29, 40, 45, AND 46)

Laboratory	Fuel particle: Material	Fuel particle: Diameter, μ	Fuel particle: Density, % of theoretical	Coating: Type of PyC	Coating: Thickness, μ	Irradiation temp., °C	Burnup, at.% of heavy metal	Fission-gas release, R/B,* 10^{-6}	Failed coatings,†%
ORNL	UO_2	229	90	Duplex	118	1370	2.5	1–2	0
ORNL	$(Th,U)O_2$	206		Duplex	100	1200	0.6	1–3	0
BMI	UO_2	200	77	Columnar	73	815	8	1–2	<0.2
BMI	UO_2	200	77	Columnar	73	1200–1300	3	1–2	<0.2
BMI	UO_2	200	78	Laminar	50	815	2	60–200	~10
BMI	UO_2	460	65	Laminar	113	815	2	<0.01	0
ORNL	UC_2	186	Dense	Duplex	107	1370	14.9	3–12	0
ORNL	UC_2	205	Dense	Duplex	138	1010	2.5	1–3	0
ORNL	$(Th,U)C_2$	213	Dense	Duplex	117	1370	14.2		0
ORNL	$(Th,U)C_2$	213	Dense	Duplex	113	1260	9.5		0
ORNL	UC_2	220	Dense	Columnar	101	1370	9.3		15
ORNL	$(Th,U)C_2$	175	Dense	Laminar	105	1260	13.2		0

*R/B value is the rate of release of a fission product divided by the rate of birth.
†Determined metallographically, except at Battelle. The Battelle values are estimates based on the fission-gas release.

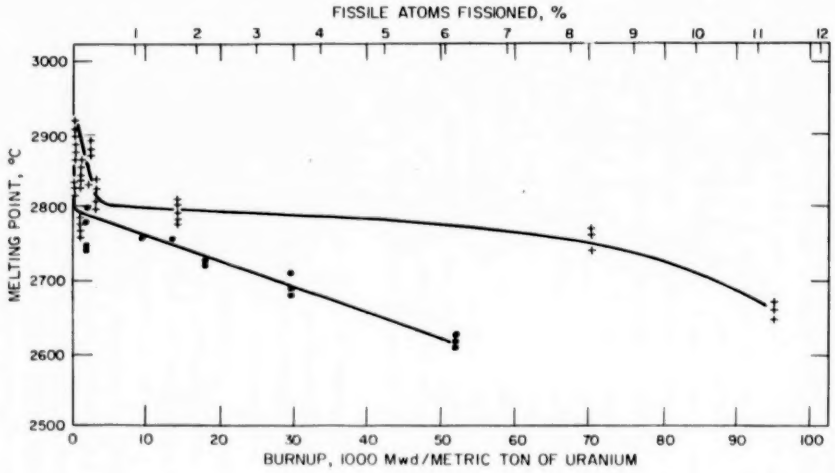

Fig. I-15 Melting point of irradiated uranium dioxide.[47] ●, *Westinghouse data.* +, *1962 Hanford data (USAEC Report HW-69234).*

electroplated on the nickel in a specially developed model of an oscillating cradle platter. The coated product is heat-treated to interdiffuse the nickel and chromium.

A review[43] of the U. S. development of PyC coatings, as well as the development of Al_2O_3, BeO, MgO, and stabilized ZrO_2 coatings, was presented in a 1964 Geneva Conference paper. The authors point out that PyC- or ceramic-coated fuel dispersed in a graphite or ceramic matrix is most useful in gas-cooled reactors operated at temperatures of about 1400 to 1500°C. Problems remaining to be solved are (1) the deposition of impermeable coatings, so that release of certain volatile fission products can be controlled, and (2) the prevention of failure of the coating in fabrication or service. The PyC coating is most promising for use in nonpurged unclad fuel elements for gas-cooled reactors at temperatures as high as 1370°C and heavy-metal burnups to 20 at.%.

(N. D. Veigel)

Irradiation and Evaluation of Coated-Particle Fuels

OXIDE-BASE FUEL

The irradiation behavior of PyC coatings on oxide fuel particles is being studied by Oak Ridge[45] and Battelle.[29,40,46] A summary of recent data is given in Table I-5.

In short irradiations at Oak Ridge,[45] the duplex type coating has shown the same good performance on relatively dense UO_2 and $(Th,U)O_2$ particles as was found earlier with dense UC_2 particles. The coating thicknesses were 100 μ or more, with 200-μ substrate particles. The work at Battelle has been concentrated on porous UO_2 substrates with monolithic coatings. This was true even with UO_2 of only 50% of the theoretical density. With 200-μ, 78% dense UO_2, Battelle found 50-μ coatings to be inadequate, but 73-μ coatings performed very well.[29,40,46] Extremely good performance is also being observed by Battelle for a 113-μ monolithic coating on 460-μ, 65% dense UO_2 particles.

CARBIDE-BASE FUEL

A large number of UC_2 and $(Th,U)C_2$ particles coated with PyC have been evaluated in-pile by Oak Ridge.[45] These are also listed in Table I-5. The fuel in these particles was dense.

Irradiations of duplex coatings (all thicker than 100 μ) have continued at Oak Ridge,[45] and no failures were observed (see Table I-5). Metallography showed wedge-shaped cracks in the inner layers of the coatings, but they did not penetrate the outer coatings. One surprising result in the Oak Ridge data is the excellent performance of the laminar coating on dense $(Th,U)C_2$. Considering earlier results for monolithic coatings, one would have expected considerable failure. (C. W. Townley)

Uranium Oxides

Properties and Behavior

Westinghouse[47] has reported melting points for UO_2 irradiated at different levels from 2000 to 52,000 Mwd per metric ton of uranium. These results are presented in Fig. I-15, along with earlier Hanford data. The Westinghouse data indicate a 32°C decrease in the melting point of UO_2 per 10,000 Mwd per metric ton of uranium.

The thermal conductivity of sintered UO_2 was determined at temperatures up to 2400°C at Combustion Engineering.[48] Minimum thermal conductivity was observed at 1400°C, with values ranging from 0.025 to 0.033 watt/(cm)(°C). Above 1400°C there was a definite increase in thermal conductivity, with values of 0.034 to 0.046 watt/(cm)(°C) at 2000°C and 0.048 to 0.059 watt/(cm)(°C) at 2400°C. Onset of small grain growth was noted at temperatures between 1400 and 1700°C. The onset of massive, blocky grain growth occurred from about 1940 to 2200°C and depended on the magnitude of the thermal gradient to which the sample was exposed.

Diffusion kinetics for nitrogen in UO_2 pellets were studied experimentally by Ferrari[49] at temperatures ranging from 1000 to 1600°C. These studies were performed by measuring nitrogen release from uniformly dispersed UN in UO_2. The diffusion coefficient for nitrogen in UO_2 followed the expression:

$$D = 2.25 \times 10^{-9} \exp(-33{,}400/RT) \quad \text{cm}^2/\text{sec}$$

(R. H. Barnes)

Fabrication

Japanese investigators[50] are studying the effect of the vibration frequency and acceleration on the compaction density using sinusoidal

wave vibrations generated by an electrodynamic shaker. Stainless-steel tubes 40 in. long by 0.5 in. in diameter have been loaded to densities in excess of 88% of theoretical with sized fused UO_2 by using a stepwise acceleration-increase technique.

Workers at Hanford[51] report that the oxygen-to-uranium ratio of fuel mixture for pneumatic impaction may be adjusted to the optimum level for this process by simply blending a calculated amount of U_3O_8 with the fuel. When the mixture of particles was heated under vacuum at 1200°C for 80 min, the excess oxygen was found to equilibrate among the various UO_2 particle-size fractions.

Fuel pellets have been cold compacted at Atomics International[52] from fully enriched 10 wt.% UO_2 and 90 wt.% ZrH_2. Various amounts of Eu_2O_3 and HfH_2 were added to the fuel composition. Because of difficulty experienced in pelletizing the UO_2-ZrH_2 as-blended mix, the material was first granulated by compacting at 12 tsi and then breaking the loosely compacted briquettes into the desired size fractions. The sized granules were then compacted into pellets by cold pressing at 35 tsi. Densities averaged 75% of the theoretical.

Thoria–2 wt.% urania compositions have been fabricated by Canadian investigators.[53] The powders are first dry mixed with 0.5 wt.% Sterotex and then granulated. Excellent-appearing pellets resulted after sintering if powder compacts that had been performed in a steel die at 1000 psi were hydrostatically pressed at 25,000 psi. Densities approaching 94% of the theoretical were obtained.

Arthur and Scott[54] have studied the effect of various oxide additions on the density of hydrogen-sintered UO_2. Of the oxides studied, TiO_2 had the greatest effect, followed by Nb_2O_5 and V_2O_5. To study the mechanism of which TiO_2 acts as a sintering aid, Arthur and Scott examined the UO_2-TiO_2 diagram, in hydrogen, and found it to be a simple eutectic system. The eutectic temperature is 1645°C. Therefore at the temperature at which the effect of TiO_2 on sintering is the most pronounced, 1300°C, no liquid is present.

The feasibility of thermochemical deposition as a one-step process of fabricating ceramic fuels is being investigated at Oak Ridge.[55] Uranium dioxide can be produced as a powder, as a needlelike crystalline deposit, or as a solid according to the reaction:

$$UF_6 + 2H_2O + H_2 \rightarrow UO_2 + 6HF$$

Crystalline needlelike deposits of UO_2 have been formed, with the needles consisting of dendritic platelets that, in turn, constitute a low-bulk-density material. The density can be increased by raising the UF_6 concentration while decreasing the overall system pressure. High-density uniform deposits having an oxygen-to-uranium ratio equal to 2.048 and an alcohol immersion density of 11.04 g/cm^3 have been formed. (T. R. Wright)

Uranium and Thorium Carbides, Nitrides, and Sulfides

Properties

A review of data in the literature on the constitution and physical and thermodynamic properties of selected refractory carbides and nitrides, including those of thorium, uranium, and plutonium, has been prepared by Los Alamos.[56]

According to a U. S. Bureau of Mines report,[57] a preliminary examination of alloys in the quasi-ternary system UC-UN-"UO" suggests that the sodium chloride structure exists as a single phase in a triangular region roughly bounded by lines or planes connecting the compositions UC, UN, and $U(C_{0.75}O_{0.25})$.

Oak Ridge[33] reports that UC forms a eutectic with UBe_{13} at 1610°C and at a composition near 65 at.% beryllium–20 at.% uranium–15 at.% carbon. At 1610°C the solubility of beryllium in UC is about 4 at.%. The solubility of beryllium in UC decreases to approximately 2 at.% at 1500°C.

It was also found[33] that UC_2 and ThC_2 form a continuous series of solid solutions below the solidus and at temperatures ranging down to 1415°C at ThC_2, down to 1110°C at 37 mole % ThC_2, and down to 1820°C at UC_2. At room temperature the body-centered tetragonal UC_2 solid solution exists to 30 mole % ThC_2; a body-centered tetragonal solid solution also exists from 40 to 70 mole % ThC_2; and the monoclinic ThC_2 solid solution exists from 80 to 100 mole % ThC_2. A two-phase region was found by X-ray techniques between 30 and 40

mole % ThC_2 but not between 70 and 80 mole % ThC_2.

Atomics International[58] reports that, when hypostoichiometric UC (about 4.3 wt.% carbon) is held in intimate contact with stainless steel, the relatively small amount of free uranium at the grain boundaries of the UC structure begins to react with the steel at all temperatures from 650 to 870°C. The reaction occurs by solid-state processes at temperatures below the uranium-iron eutectic at 730°C. The reaction becomes more extensive at 760°C; and at 870°C there were indications of reaction between the UC and the steel, as well as between the free uranium and the steel.

The thermal conductivity of UC_2 is apparently similar to that of UO_2. Kubota, Seki, and Takahashi[59] found that the thermal conductivity of 95% dense UC_2 was 0.014 to 0.016 cal/(sec)(cm)(°C) between 200 and 400°C. A comparable sample of 95% dense UC had a thermal conductivity of 0.04 to 0.05 cal/(sec)(cm)(°C) from 100 to 400°C.

Los Alamos[60] reports that ThN has a congruent melting point of 2790°C at a pressure of about 9.8 atm of nitrogen (Fig. I-16). Uranium mononitride has a congruent melting point of 2850°C at about 3 atm; NpN has a congruent melting point of 2830°C at about 12 atm; and PuN has a melting point above 2700°C and 20 atm.

The fabrication, properties, and irradiation behavior of uranium monocarbide[58,61] have been reviewed in a 1964 Geneva Conference paper. The collations of swelling and gas-release data for UC (Figs. I-17 and I-18) suggest that the processes of swelling and gas release become

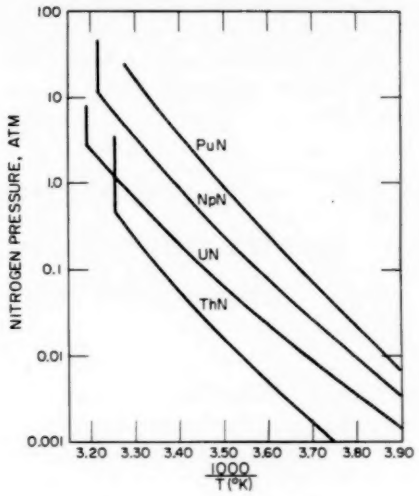

Fig. I-16 Decomposition pressure of the actinide mononitrides.[60]

active at temperatures above 1000°C (1832°F). This temperature appears to coincide with the equicohesive temperature of UC as determined by mechanical-property tests.

Atomics International[62] has obtained data supporting the findings obtained at United Nuclear Corp. to the effect that the irradiation behavior of hypostoichiometric UC is strongly influenced by the amount of free uranium present. Specimens of slightly hypostoichiometric UC were irradiated to about 1 at.% total burnup at a maximum centerline temperature of about 1650°F (900°C). Samples containing 4.53 wt.% carbon showed diameter

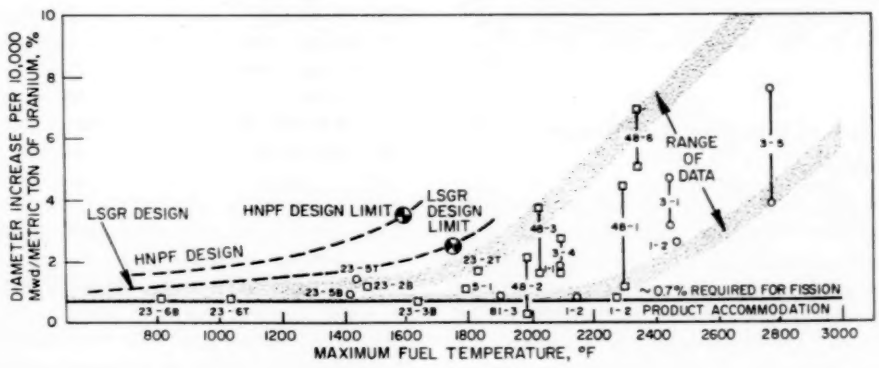

Fig. I-17 Diameter increase in UC due to irradiation.[58] ○, *hypostoichiometric UC (< 4.8 wt.% carbon);* □, *hyperstoichiometric UC (> 4.8 wt.% carbon).*

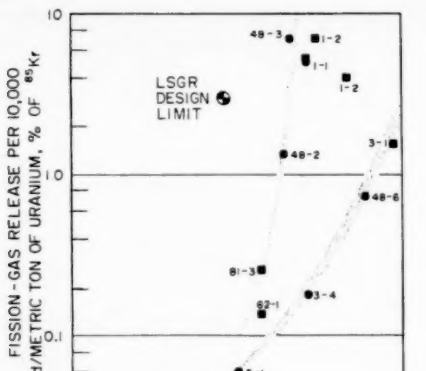

Fig. I-18 Fission-gas release from UC due to irradiation.[58] ■, hypostoichiometric UC (< 4.8 wt.% carbon); ●, hyperstoichiometric UC (> 4.8 wt.% carbon).

changes of about 3% and density changes of about 7%, whereas samples containing about 4.6 wt.% carbon showed diameter changes of about 1% and density changes of about 4%. Metallographic examination of a 4.4 wt.% carbon alloy from this group disclosed severe separation of the carbide grains. This separation was clearly associated with the network of free uranium metal in the grain boundaries. No evidence for radial redistribution of the uranium was observed.

Results of an irradiation of US do not appear promising. At Hanford it was found[32] that an 85% dense sample of US became friable, fragmented, and released 3.8% of its fission gas during irradiation to 3.3×10^{20} fissions/cm^3 (1.4 at.% burnup) at a maximum temperature of 600°C. (W. Chubb)

Fabrication of Uranium Carbides and Nitrides

An analysis of data from hollow-cathode-discharge (HCD) melting experiments with uranium carbide was made by Atomics International[62] to determine relations between furnace operating variables and the carbon content of the product. In conventional arc melting of uranium carbide, the carbon content is strongly influenced by the pickup of carbon in the melt from the graphite electrode. The HCD process does not utilize a graphite electrode; the only carbon source is the melt stock itself. The HCD process is similar to electron-beam melting. However, uranium volatilization losses, and consequent compositional control problems, are expected to be less severe in the HCD process because of the higher allowable furnace operating pressures (20 to 200 μ, as compared with the 0.01-μ range required for electron-beam operation). From results of the analysis, the investigators concluded that, although initial melt-stock carbon content and furnace variables (such as pressure, voltage, amperage, and melt time) all have significant effects on the final UC carbon content, it should be possible to control the cast UC composition within ±0.1 wt.% carbon with the HCD process.

Some time ago, on the basis of preliminary results, it was reported that UAl_2 was an effective sintering aid for uranium carbide powders and thus allowed the achievement of high sintered densities at relatively low sintering temperatures. Further work showed that impurities in the UC or excess carbon "seriously impaired" its effectiveness, and UBe_{13} was then shown to be an effective sintering aid for UC. It has since been found that the effectiveness of UBe_{13} is seriously impaired by the excessive oxygen or above-stoichiometric carbon in the carbide, and preliminary work now indicates that U_3Si_2 may be an effective sintering aid.[55] In vacuum at 1550°C arc-cast UC powders of high purity sintered to 97% of the theoretical density with 1.5 to 2.0 wt.% of U_3Si_2 added as a sintering aid. The same sintered density was also achieved with U_3Si_2 and "impure" carbide starting material at 1600°C. In the tests the sintering crucible also contained UBe_3, but not mixed with carbide, to "scavenge sintering inhibiting oxide films" with beryllium vapor.

British workers say that solid-state sintering of uranium carbide to greater than 95% of the theoretical density became possible at 1500 to 1600°C once it was realized that the main factor inhibiting solid-state sintering was the presence of an oxidized layer on the surface of powders of sinterable particle size. They also say that the oxidation was minimized by careful control of the handling atmosphere (UKAEA Reports AERE-R-4151, AERE-R-4328, and AERE-R-4486, referenced in AERE-R-4662). They applied the same approach to UN powders and indicate that UN powder will sinter

to 95% of the theoretical density when suitably milled, compacted, and sintered at 1700°C in pure argon.[63] One pellet had 97% of the theoretical density when sintered for 10 hr at 1700°C. Free uranium metal was not observed in the pellet by microscopic examination. They obtained some results to support their premise that the sinterability was reduced by oxidation of the powder with exposure to the glove-box atmosphere.

It was observed in the above work that after the powders were milled to reduce the particle size, they were free flowing and contained many minute lustrous particles just visible to the unaided eye. Working with arc-fused UN material prepared at Battelle, Japanese workers[64] have determined that all the lustrous flat planes are (1 0 0) planes and that rectangular edges take the (1 0 0) direction. Laue back-reflection photographs and diffractometer charts from cleavage faces confirmed that UN single crystals cleave along the (1 0 0) planes only. Freshly cleaved surfaces were examined by electron-diffraction methods, but in no instance could the pure UN structure be obtained. Whether in air or in inert media, all surfaces exhibited Kirchner-Roether lines accompanied by vague halos, indicating formation of an amorphous thin layer on the freshly cleaved surface. They have since further identified the components of the very thin layer as a higher nitride intermediate between U_2N_3 and UN_2 and a face-centered cubic or pseudocubic UO_{2+x} which grows simultaneously and epitaxially on the UN (1 0 0) face and which gives the UN a fair resistance to further oxidation in air at low temperatures. Changes in the characteristics of the surface films on heating were also studied.

A topical report[65] on the preparation and properties of cast UN has been issued by Battelle. The UN single crystals referred to above were produced as an offshoot of the arc-melting experiments described in Ref. 65.

(E. O. Speidel)

Mechanism of Corrosion of Fuels

Oxygen has been found to retard the reaction of uranium in humid atmospheres according to studies conducted by the British.[66] Experiments with ^{18}O have shown that oxygen did not combine directly with the uranium but reacted with hydrogen to form water. Evolution of hydrogen was negligible, and corrosion rates were low in a gaseous system until all oxygen was consumed.

(W. E. Berry)

Basic Studies of Irradiation Effects in Fuel Materials

Metals

The process of bubble diffusion and coalescence during the annealing of material containing insoluble radioinduced gases was analyzed by Speight.[67] He developed an expression, which depends on the influence of dislocations, for the average bubble size in terms of annealing time and temperature and then compared this expression with experimental results. The analysis included the case where solid precipitates in the material impede bubble movement.

The elongation of uranium single crystals in the [0 1 0] direction during thermal-neutron irradiation was investigated[68] at 110 and 425°K. The growth coefficients were 150 at 110°K and 9700 at 425°K.

Ceramics

The release of xenon from lightly irradiated UC powders was studied[69] in the temperature range 150 to 975°C. Release in this range is much higher than that calculated by extrapolating high-temperature-diffusion data. The kinetics of the release agree with a model in which the xenon in the first three or four unit cells is released over a range of activation energies.

(F. A. Rough)

References

1. D. M. R. Taplin and J. W. Martin, The Effect of Grain Size and Cold Work on the Tensile Properties of Alpha-Uranium, *J. Less-Common Metals*, 7: 89-97 (August 1964).
2. P. A. Loretan and G. Murphy, Influence of Rate of Loading on the Tensile Properties of Normal Alpha Uranium, USAEC Report IS-757, Ames Laboratory, Iowa State University, August 1963.
3. G. F. Slattery and D. E. Connolly, Irradiation Growth Rates of Mechanically Worked Uranium, *J. Nucl. Energy, Pts. A & B*, 18: 347-359 (June 1964).

4. R. D. Leggett, B. Mastel, and T. K. Bierlein, Irradiation Behavior of High-Purity Uranium, USAEC Report HW-79559, Hanford Atomic Products Operation, November 1963.
5. J. A. Straatmann and N. F. Neumann, Equilibrium Structures in the High Uranium-Silicon Alloy System, USAEC Report MCW-1486, Mallinckrodt Chemical Works, Oct. 23, 1964.
6. J. A. Straatmann and N. F. Neumann, Equilibrium Structures in the High Uranium-Iron Alloy System, USAEC Report MCW-1487, Mallinckrodt Chemical Works, Nov. 6, 1964.
7. G. A. Whitlow, Resistance to Deformation of Some Uranium-Molybdenum Alloys — Its Dependence on Temperature and Rate of Deformation, British Report AWRE-0-66/64, August 1964.
8. R. W. Anderson, Effect of Heat Treatment on U-Fe-Si-Al Alloys Containing Additions of Chromium and Molybdenum, USAEC Report NMI-7097-2, Nuclear Metals Division of Textron Inc., July 22, 1964. (Classified)
9. R. W. Anderson, Effect of Heat Treatment on the Properties of High-Uranium Alloys Containing Additions of Iron, Silicon, and Aluminum, USAEC Report NMI-7097-1, Nuclear Metals Division of Textron Inc., July 28, 1964. (Classified)
10. B. A. Loomis, Swelling of Irradiated Uranium-Zirconium Alloys on Annealing, *Nucl. Sci. Eng.*, 20: 112-113 (September 1964).
11. S. F. Pugh and B. R. Butcher, Metallic Fuels, in Reactor Technology, Selected Reviews — 1964, USAEC Report TID-8540, pp. 331-410.
12. C. A. W. Peterson, W. J. Steele, and S. L. DiGiallonardo, Isothermal Transformation Study of Some Uranium-Base Alloys, USAEC Report UCRL-7824, University of California, Lawrence Radiation Laboratory, August 1964.
13. G. P. Pells, The Palladium-Uranium Phase Diagram Up to 25 At.% Uranium, *J. Inst. Metals*, 92: 416-418 (August 1964).
14. Nuclear Materials & Equipment Corp., Growth of Single Crystals of Plutonium, Quarterly Progress Report, July 1 – September 30, 1964, USAEC Report NUMEC-3428-3.
15. S. E. Bronisz and D. L. Douglass, An Electron-Micrographic Study of Alpha Plutonium Fracture Surfaces, USAEC Report LA-3140-MS, Los Alamos Scientific Laboratory, August 1964.
16. L. J. Wittenberg and G. R. Grove, Reactor Fuels and Materials Development Plutonium Research, April – June 1964, USAEC Report MLM-1208, Mound Laboratory, June 30, 1964.
17. G. Picton and J. F. Sackman, The Corrosion and Ignition Behavior of Some Uranium-Plutonium-Iron Alloys, British Report AWRE-0-58/64, Aug. 19, 1964.
18. Argonne National Laboratory, Reactor Development Program, Progress Report, September 1964, USAEC Report ANL-6944, Oct. 15, 1964.
19. J. S. Griffo, W. B. Brown, and F. D. Lonadier, Solubility of Plutonium Compounds, USAEC Report MLM-1191, Mound Laboratory, Oct. 30, 1964.
20. W. M. Pardue, V. W. Storhok, R. A. Smith, and D. L. Keller, An Evaluation of Plutonium Compounds as Nuclear Fuels, USAEC Report BMI-1698, Battelle Memorial Institute, Oct. 29, 1964.
21. T. L. Markin, R. J. Bones, and E. R. Gardner, Thermodynamic Data for Plutonium Oxides, British Report AERE-R-4724, September 1964.
22. H. E. Schmidt, Study of Physical Properties of UO_2 and UO_2-PuO_2, USAEC-Euratom Report EURAEC-1110, Commissariat à l'Énergie Atomique, Centre d'Études Nucléaires, April 1964.
23. Atomic Energy of Canada Ltd., 1964. (Unpublished)
24. F. W. Albaugh, Reactor and Fuels Laboratory Monthly Report, September 1964, USAEC Report HW-84291A, Hanford Atomic Products Operation, Oct. 15, 1964. (Classified)
25. F. W. Albaugh, Reactor and Fuels Laboratory Monthly Report, October 1964, USAEC Report HW-84474A, Hanford Atomic Products Operation, Nov. 16, 1964.
26. N. H. Brett, Solid Solution in the UO_2-Pu_2O_3 System, British Report AERE-R-4689, July 1964.
27. D. Stahl, A. Strauser, J. Andersen, and K. Taylor, Study of Uranium-Plutonium Monoxides, Progress Report, February 1 – July 31, 1964, USAEC Report UNC-5096 (EURAEC-1222), United Nuclear Corp. and Carborundum Co., Oct. 5, 1964.
28. A. Hough and J. A. C. Marples, The Pseudo-Binary Phase Diagrams of PuO_2 with Alumina, Beryllia, and Magnesia and the Pseudo-Ternary PuO_2-ThO_2-BeO, British Report AERE-R-4749, October 1964.
29. R. W. Dayton and R. F. Dickerson, Progress Relating to Civilian Applications During October 1964, USAEC Report BMI-1697, Battelle Memorial Institute, Nov. 1, 1964. (Classified)
30. W. M. Pardue, V. W. Storhok, R. A. Smith, P. H. Bonnell, J. E. Gates, and D. L. Keller, Synthesis, Fabrication, and Chemical Reactivity of Plutonium Mononitride, USAEC Report BMI-1693, Battelle Memorial Institute, Sept. 15, 1964.
31. F. W. Albaugh, Reactor and Fuels Laboratory Monthly Report, November 1964, USAEC Report HW-84529A, Hanford Atomic Products Operation, Dec. 15, 1964. (Classified)
32. Hanford Atomic Products Operation, Ceramics Research and Development Operation Quarterly Report, April – June 1964, USAEC Report HW-81601A. (Classified)
33. Oak Ridge National Laboratory, Metals and Ceramics Division Annual Progress Report for Period Ending June 30, 1964, USAEC Report ORNL-3670, October 1964.
34. W. L. R. Rice (Ed.), Nuclear Fuels and Materials Development, USAEC Report TID-11295(3rd ed.), July 1964.
35. C. G. Hanson, V. G. Rivlin, and B. A. Hott, The Beta Phase Transformation of Some Zirconium-Thorium Alloys, *J. Nucl. Mater.*, 12: 83-93 (May-June 1964).
36. Oak Ridge National Laboratory, September 1964. (Unpublished)
37. W. C. Thurber, F. R. McQuilkin, E. L. Long, Jr., and M. F. Osborne, Irradiation Testing of Fuel for Core B of the Enrico Fermi Fast Breeder Reactor, USAEC Report ORNL-3709, Oak Ridge National Laboratory, November 1964.
38. L. H. Cope, A Coining Technique for the Fabrication of Medium-Volume Cermet Nuclear Fuels, *Metallurgia*, 70: 59-63 (August 1964).
39. L. H. Cope and R. J. Warmer, Improvements Relating to the Manufacture of Cermet Nuclear Fuels and Fuel Elements Containing Such Fuels, British Patent 969,975, Sept. 16, 1964.
40. R. W. Dayton and R. F. Dickerson, Progress Re-

lating to Civilian Applications During September 1964, USAEC Report BMI-1694, Battelle Memorial Institute, Oct. 1, 1964. (Classified)
41. H. G. Sowman, R. L. Surver, and J. B. Johnson, The Development of Spherical Pyrolytic-Carbon-Coated UC_2 and $UThC_2$ Fuel Particles, *Nucl. Sci. Eng.*, 2: 227-234 (October 1964).
42. F. Barbesino, E. Brutto, R. Di Pietro, A. Gioia, G. Perona, and R. Sesini, UO_2 Fuel Elements Shaped as Small Spheres, presented at the Third United Nations International Conference on the Peaceful Uses of Atomic Energy, Geneva, 1964, Paper A/Conf.28/P/554.
43. R. W. Dayton, W. V. Goeddel, and W. O. Harms, Ceramic-Coated-Particle Nuclear Fuels, presented at the Third United Nations International Conference on the Peaceful Uses of Atomic Energy, Geneva, 1964, Paper A/Conf.28/P/235.
44. Reference deleted.
45. Oak Ridge National Laboratory, Nov. 3, 1964. (Unpublished)
46. R. W. Dayton and R. F. Dickerson, Progress Relating to Civilian Applications During November 1964, USAEC Report BMI-1704, Battelle Memorial Institute, Dec. 1, 1964. (Classified)
47. Westinghouse Electric Corp., Atomic Power Division, Yankee Core Evaluation Program, Quarterly Progress Report for the Period Ending September, 30, 1964, USAEC Report WCAP-6064, October 1964.
48. W. P. Chernock, C. E. Burdg, E. I. Veil, G. Zuromsky, and J. J. Koziol, The Development and Testing of UO_2 Fuel Systems for Water Reactor Applications, Progress Report, April 1–July 31, 1964, USAEC Report CEND-2863-217, Combustion Engineering, Inc., August 1964.
49. H. M. Ferrari, Diffusion of Nitrogen in Uranium Dioxide, *J. Nucl. Mater.*, 12: 142 (July 1964).
50. K. Naruki, Vibratory Compaction of Uranium Dioxide, I. Effect of Vibration Character, *J. Nucl. Sci. Technol. (Tokyo)*, 1: 57-58 (May 1964).
51. F. W. Albaugh, Reactor and Fuels Laboratory Monthly Report, August 1964, USAEC Report HW-83820A, Hanford Atomic Products Operation, Sept. 15, 1964. (Classified)
52. W. M. Jones, Cold Compaction of UO_2 + ZrH_2 Fuel Pellets for Critical Experiments, USAEC Report NAA-SR-Memo-9411, Atomics International, Jan. 13, 1964.
53. E. Mizzan, Atomic Energy of Canada Ltd., 1964. (Unpublished)
54. G. Arthur and D. Scott, The Effect of TiO_2 Additions on the Sintering of UO_2, *Trans. Brit. Ceram. Soc.*, 63: 417-429 (August 1964).
55. Oak Ridge National Laboratory, November 1964. (Unpublished)
56. E. K. Storms, A Critical Review of Refractories, USAEC Report LA-2942, Los Alamos Scientific Laboratory, March 1964.
57. U. S. Bureau of Mines, Albany Metallurgy Research Center, Quarterly Metallurgical Progress Report No. 24, July 1–September 30, 1964, USAEC Report USBM-RC-1135.
58. Atomics International, Annual Technical Progress Report, AEC Unclassified Programs, Fiscal Year 1964, USAEC Report NAA-SR-9999, Aug. 31, 1964.
59. T. Kubota, Y. Seki, and S. Takahashi, Thermal Conductivity of UO_2, UC, and UC_2, *J. Nucl. Sci. Technol. (Tokyo)*, 1: 93-100 (June 1964).
60. R. J. Beals, J. H. Handwerk, and J. F. Schumar (Comps.), A Seminar on Groups V and VI Anions, Held at Argonne National Laboratory, February 26 and 27, 1964, USAEC Report ANL-6856, March 1964.
61. H. Pearlman and R. F. Dickerson, Carbide Fuel Fabrication and Performance, presented at the Third United Nations International Conference on the Peaceful Uses of Atomic Energy, Geneva, 1964, Paper A/Conf.28/P/234.
62. Atomics International, AEC Unclassified Programs, Quarterly Technical Progress Report, July–September 1964, USAEC Report NAA-SR-10501, Dec. 1, 1964.
63. J. R. McLaren and P. W. M. Atkinson, The Sintering of Uranium Mononitride, British Report AERE-R-4662, July 1964.
64. Oxide and Carbide Fuels, Japan–U. S. Research Newsletter No. 3, August 1964.
65. R. W. Endebrock, E. L. Foster, Jr., and D. L. Keller, Preparation and Properties of Cast UN, USAEC Report BMI-1690 (EURAEC-1206), Battelle Memorial Institute, Aug. 28, 1964.
66. M. McD. Baker, J. W. Bleloch, N. Less, and S. Orman, Uranium Compatibility Studies, Part 3: The Influence of Oxygen on the Uranium-Water Reaction, British Report AWRE-0-40/64, June 1964.
67. M. V. Speight, Bubble Diffusion and Coalescence During the Heat Treatment of Materials Containing Irradiation-Induced Gases, *J. Nucl. Mater.*, 12: 216-220 (July 1964).
68. B. A. Loomis, T. H. Blewitt, A. C. Klank, and S. B. Gerber, Elongation of Uranium Single Crystals During Neutron Irradiation, *Appl. Phys. Letters*, 5: 135-137 (Oct. 1, 1964).
69. A. Auskern, Release of Xenon from Uranium Carbide at Low Temperatures, *J. Am. Ceram. Soc.*, 47: 390-394 (August 1964).

Section

II

Reactor Materials

Moderator Materials

Graphite

Data on the kinetics of the reaction of CO_2 with hydrogen at temperatures below 800°C are reported by Hanford Laboratories in Ref. 1. The rates of CO and water-vapor formation were determined at 775°C as functions of CO_2 concentration. The results show that, in the partial-pressure range from 200 to 600 torrs, the reaction rate is proportional to the CO_2 concentration. The rate of the reaction as a function of the hydrogen pressure was also investigated and was found to be proportional to the 0.3 power of the hydrogen concentration in the partial-pressure range from 16 to 500 torrs. The activation energy is 39.2 kcal/mole. The rate expression is as follows:

$$\frac{-d[CO_2]}{dt} = k[H_2]^{0.3}[CO_2]$$

Previous experimenters have suggested that oxygen affects the rate of the reaction of CO_2 with hydrogen, although no quantitative data were given. In the experiments at Hanford, the oxygen concentration was maintained at 5 ppm or less by passing the reactants over copper turnings at 300°C. When the copper turnings were cooled to room temperature, the oxygen content increased to 11 ppm and the rate of the reaction increased to 20 times its original value. Thus the differences in the reaction rate reported by various authors might be due to slight differences in oxygen content.

Reference 2 is a Hanford report that presents the results of an investigation of the longest term reactor irradiation [16,000 Mwd/adjacent ton, or approximately 1.52×10^{21} neutrons/cm^2 ($E > 0.18$ Mev)] yet carried out by Hanford for graphite grades CSF, KC, CSGBF, WSF, SGBF, and TSGBF. The physical properties investigated were (1) dimensions, (2) electrical resistivity, (3) thermal resistivity, (4) apparent crystallite size, and (5) crystallite lattice spacings. Irradiation was conducted in the temperature range 450 to 600°C. In general, the observations and conclusions from this study confirm the results of earlier investigations reported for lower doses. Specimens cut parallel to the extrusion direction exhibited only contraction occurring at a linear rate throughout most of the exposure period. The contractions observed for parallel samples after 16,000 Mwd/adjacent ton were about −0.27, −0.32, −0.38, −0.33, and −0.37% for KCF, CSF, CSGBF, WSF, and SGBF, respectively. Perpendicular specimens showed a small expansion initially, followed by a linear contraction in the later stages of exposure, but a lower contraction rate than for parallel specimens. Contractions after 16,000 Mwd/adjacent ton were about −0.052, −0.21, −0.23, −0.21, −0.22, and −0.25% for KC, XCSGBF, CSF, TSGBF, WSF, and SGBF. Electrical resistivity tended to saturate at low exposures (about 3000 to 4000 Mwd/adjacent ton). Saturation values in general ranged between 1.75 and 2.0 times the unirradiated values. Thermal resistivity also exhibited saturation but required higher exposures to reach final saturation. The indicated values of saturation dosages for thermal resistivity were likely affected by temperature increases during irradiation from a low of 450°C to a high of 600°C, and thus an annealing effect was introduced. The increase in thermal resistivity was generally found to be between 200 and 300%.

The impervious carbon materials referred to as "vitreous" or "glassy" carbons are relatively new materials, and neither their methods of manufacture nor their property characteristics are well known. Recent data on the oxidation of vitreous carbon in CO_2 and water vapor have been reported by Harwell in Ref. 3. The samples of carbon tested were prepared by

curing a phenol formaldehyde liquid resin at 90°C, followed by a closely controlled heating schedule in argon to 1600°C. X-ray diffraction indicated that the carbon contained randomly oriented small graphite crystallites with dimensions $L_c \approx 30$ A and $L_a \approx 50$ A. Its permeability was low; the coefficient for krypton at room temperature was 2.5×10^{-11} cm^2/sec.

Oxidation tests over the temperature range 900 to 1400°C were conducted on pure vitreous carbon samples, or samples loaded with fission-product elements, and samples containing uranium or thorium. In general, a linear rate of oxidation was quickly established, with the rate constant increasing with increasing temperature and chemical contamination of the sample.

Much of the attack was localized at pits; the effect was most pronounced in, and led to the formation of very large pits with, the contaminated samples. An unusual observation was the formation of films in the thickness range of 400 to 2600 A which could be stripped from the carbon samples. This film thickness increased steadily with oxidation time until extensive attack resulted in powdering of the films. It was proposed that the films consist of a loose agglomeration of graphite crystallites and that film formation is directly related to the submicroscopic structure of the vitreous carbon.

Of particular interest is a comparison of reaction rates of the vitreous carbon and Pile Grade A graphite on the basis of their true surface areas. A sample of Pile Grade A graphite (1.5 × 0.5 × 0.5 cm), oxidized in carbon dioxide at 1000°C and 100 cm^3/min, had a reaction rate based upon the geometric area of 0.835 mg/(cm^2)(hr) compared with a rate of 0.11 to 0.17 mg/(cm^2)(hr) for vitreous carbon. On the basis of surface areas measured after oxidation, the rates were 5.6×10^{-4} mg/(cm^2)(hr) for Pile Grade A and 4×10^{-4} mg/(cm^2)(hr) for vitreous carbon after 16 hr and 590 hr, respectively. Although these data are not conclusive, they suggest that the carbon atoms had a similar reactivity in the two materials.

(M. C. Brockway)

Beryllium Metal and Alloys

This review covers some of the papers presented at the AIME (American Institute of Mining, Metallurgical and Petroleum Engineers) Second International Conference on Beryllium Technology held in Philadelphia, Pa., Oct. 15 to 17, 1964. Because of the large number of papers presented, a complete review of each one is not practicable. A list of all of the papers with abstracts has been published (Ref. 4). Persons interested in obtaining copies of the papers should contact the appropriate authors. Publication of the proceedings in book form is planned by AIME.

Physical Metallurgy

The British Atomic Weapons Research Establishment (AWRE)[5a] investigated slip modes along the c-axis in high-purity zone-refined single crystals of beryllium near 200°C. Pyramidal slip occurred out of the basal plane at temperatures above 180°C. The maximum critical resolved shear stress (crss) for $(11\bar{2}5)$ slip was calculated to be between 11,700 and 19,000 psi. Indications were that the crss is sensitive to purity, and it was suggested that the occurrence of pyramidal slip influences the ductile-to-brittle transition in polycrystalline beryllium.

The same group at AWRE investigated the effects of heat-treatment on the ambient-temperature flow stress in comparable-purity beryllium.[5b] A low-temperature (<550°C) aging effect, previously reported in material of lower purity, was not observed in the single crystals in this study. It was suggested that aging below 575°C involved two types of solutes: the interstitials, which are relatively mobile below 575°C, and the substitutional elements, which are removed from solution only by overaging above 575°C. This lack of low-temperature aging response is consistent with the fact that interstitial content is very low in the high-purity materials. The studies also suggest that strain-hardening effects may have masked any effect of overaging in the low-temperature range.

Franklin Institute[5c] studied work-hardening mechanisms by observing dislocation networks in high-purity beryllium single crystals. Observations were made on thin films cut from bulk tensile specimens oriented for basal and prismatic slip and on slip lines on the surfaces of the specimens. Two-stage work hardening was observed in basal slip, whereas three definite stages were noted in specimens oriented

for prismatic slip. The observed dislocation networks in each type of specimen and their effects on work hardening are discussed in detail.

Reference 5*d* is a paper presented at Autonetics which reviews the effects of crystallographic orientation, purity, and grain size on mechanical properties of polycrystalline beryllium sheet. The author postulates that, by varying rolling schedules, significant improvement in short-transverse ductility can be made by producing sheet with many grains that have their *c*-axes oriented greater than 20° out of the plane of the sheet. Improved purity, in conjunction with fine grain size, would also be necessary for improved ductility. He suggests that fine grain size can be achieved only by a powder-metallurgy approach.

Purification of Beryllium

Alloyd General Corporation reported[5*e*] on the purification of beryllium by electron-beam distillation without the use of a crucible. Impurities such as copper, nickel, carbon, and oxygen were reduced by factors of 2 to 5. Distillate purity was influenced by both rate of distillation and purity of source material.

Another method of purification of beryllium by distillation was described[5*f*] by the University of California Lawrence Radiation Laboratory. A crucible-free induction-melting operation was used to eliminate contamination from the crucible. Volatile and insoluble impurities are first removed by a vacuum-induction casting process, and then the beryllium is distilled from the casting. The distilled beryllium is deposited on a tantalum condenser plate in the form of a very high-purity (~100-ppm total impurity) polycrystalline layer. The plate is designed to produce semifinished shapes of beryllium.

Powder Metallurgy

Nuclear Metals[5*g*] investigated "splat cooling" as a means for producing a fine-grained powder for hot pressing. A fine-grained platelet (1- to 10-μ average grain diameter) was produced by quenching drops of molten beryllium on a rotating copper disk. The "splats" were compacted at temperatures of 700°C or lower, with virtually no grain growth. The layered structure produced by the orientation of the splats during loading for hot pressing caused some variation in mechanical properties in various directions. However, significantly high elongations and reductions in area coupled with high tensile strengths were recorded in some samples.

The effects of chemical composition and particle-size distribution on the hot-pressing characteristics of commercial beryllium powders were investigated by the British.[5*h*] Powder from electrolytic flake was ball-milled with various concentrations of activating elements to form an even dispersion of these elements prior to hot pressing. The length-to-diameter ratio of a body capable of being hot pressed to greater than 98% of theoretical density was increased from less than 1 to greater than 2 by adding 500 ppm of silicon or the atomic equivalent of iron, nickel, or chromium. The mechanism for the distribution of silicon in the reaction was not clear, but a gaseous transport mechanism was favored.

Battelle reported[5*i*] on the use of the gas-pressure-bonding process for hot isostatically pressing various grades of beryllium powder. Beryllium powders were compacted to theoretical density in the temperature range 700 to 950°C at isostatic pressures of 10,000 to 15,000 psi. Powders were preconsolidated by vibratory packing, hydrostatic pressing, plasma-arc spraying, or explosive compaction. Brush NP-50A powder compacted at 788°C yielded tensile strengths in excess of 49,000 psi, as compared with 35,000 psi minimum guaranteed strengths for vacuum-hot-pressed block.

Fabrication of Beryllium

Forging of beryllium components was discussed[5*j*] by the Ladish Co. Fabrication of various hardware items was described. Some of these components include seamless rings (such as used in the Minuteman Spacer), gimbal rings, shafts, rotors, pressure vessels, and various jet-engine components. In addition to the component fabrication, metallurgical factors affecting forgeability were described. It was noted that different lots of source material with comparable chemistry have vastly different forging characteristics. Some of the contributing factors to varying forgeability are described, and the role of metallic contaminants is hypothesized. On the basis of metallurgical studies, Ladish has established specifications for a forging grade of beryllium.

Rocketdyne's interest in beryllium forgings for structural applications led to a detailed study[5k] of commercial forgings. Mechanical properties were determined on pancake forgings of high-oxide fine-grain material (I-400/HPI-40 type), and average levels were 99,300 psi for the ultimate tensile strength, 76,200 psi for the yield strength, and 6.6% for the elongation. Compatibility with nitrogen tetroxide and monomethylhydrazine propellants was determined to be satisfactory. Zinc-brazed test specimens showed an average strength of 78,200 psi.

Forming and deformation characteristics of beryllium under high pressures at room temperature were reported[5l] by Pressure Technology Corp. Tensile tests under hydrostatic pressure indicated increased elongation and reduction in area with increasing pressures. Fluid-to-fluid extrusion was successfully used to produce sound extrusions of commercial beryllium at room temperature. Under pressure, commercial beryllium sheet was bent without fracturing, the bend angle increasing with increased environmental pressure. It is hypothesized that hydrostatic pressure introduces additional deformation modes in the beryllium. (H. D. Hanes)

Beryllium Oxide

Enthalpy measurements have been made by General Electric researchers[6] on unirradiated and irradiated specimens of AOX-grade and UOX + MgO-grade BeO compositions at temperatures of approximately 300, 600, and 900°C. The results indicate no change, within about 2%, after irradiation to approximately 10^{21} neutrons/cm^2 at 1000°C.

Room-temperature modulus-of-rupture values for unirradiated EBOR samples given in Ref. 7 (UOX BeO + 1 wt.% bentonite) ranged from 1.8 to 2.5 × 10^3 kg/cm^2 (25,600 to 35,600 psi). The grain size of these specimens ranged from an average of 17.4 to 28.6 μ; density ranged from 2.78 to 2.96 g/cm^3. Some AOX and UOX-MgO samples of different grain sizes and densities were tested at room and elevated temperatures after radiation exposures ranging from about 0.4 to 1.0 × 10^{21} neutrons/cm^2 (≥ 1 Mev). The data of Table II-1 show that, in general, the elevated-temperature and room-temperature strengths of irradiated samples differed from strengths of unirradiated samples by similar percentages. Also, large grains and low irradiation temperatures appear to be conducive to the greatest deterioration in post-irradiation strength.

In Ref. 8 Austerman has reported measurements of the crystallographic expansion associated with the hexagonal-to-tetragonal transformation of BeO at approximately 2050 to 2100°C. The crystallographic expansion was measured by X-ray diffraction and by visual measurement with a traveling microscope. By the latter method it was determined that expansion parallel to the c-axis was 5.9 ± 1%, and normal to the c-axis it was 0.0 ± 1.0%. By X-ray diffraction from single crystals, expansion was measured to be 6.1 ± 0.3% parallel to the c-axis and −0.9 ± 0.3% normal to the c-axis.

Oak Ridge researchers[9] have reported additional data on irradiation effects on BeO. Figure II-1 presents volume increases for

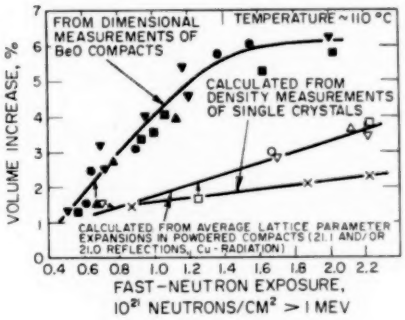

Fig. II-1 Volume increase of ½-in. BeO compacts and single crystals vs. fast-neutron exposure.[7] ○, low density (~2.7 g/cm^3), small grain size (~17 μ); □, low density (~2.7 g/cm^3), large grain size (~34 μ); △, high density (~2.9 g/cm^3), small grain size (~25 μ); ▽, high density (~2.9 g/cm^3), large grain size (~74 μ); ×, single crystals.

samples irradiated at approximately 110°C. The values of $\Delta a/a_0$ ranged from 0.00115 to 0.00159, and the c-parameter expansion $\Delta c/c$ increased from 0.0130 to 0.0356 over the range 0.7 to 2.23 × 10^{21} neutrons/cm^2. It was suggested that self-constraint in the relatively large single crystals might account for the lower values of volume increases calculated from density changes as compared with values calculated from lattice expansion of powdered specimens. Lattice-parameter changes for the single crystals will be reported later. Grain-

Table II-1 MODULUS-OF-RUPTURE DATA ON BeO IRRADIATED AT ELEVATED TEMPERATURES[7]

Specimen description			Irradiation conditions			Radiation expansion, vol.%	Modulus of rupture					
							At room temperature			At 600°C		
							Irradiated		% of unirradiated value	Irradiated		% of unirradiated value
Composition	Grain size, μ	Density, g/cm³	Temp., °C	Flux, 10^{14} neutrons/(cm²)(sec) (≥ 1 Mev)	Exposure, 10^{20} neutrons/cm² (≥ 1 Mev)		10^3 psi	10^3 kg/cm²		10^3 psi	10^3 kg/cm²	
AOX	5	2.75	650	2.0	9.1	2.2	7.6	0.53	25	4.5	0.32	12
			600	1.9	8.7	2.3	7.8	0.55	26	4.9	0.34	14
			750	2.4	11.1	1.6				14.4	1.01	41
			775	2.2	10.2	1.5	13.3	0.94	44	9.4	0.66	27
			600	1.9	9.0	2.1	10.0	0.70	40	6.6	0.46	23
			600	1.8	8.5	2.0	11.4	0.80	46	9.4	0.66	33
	5	2.60	550	2.0	9.5	2.7				4.7	0.33	13
			650	1.9	8.9	1.9	10.0	0.70	32	8.6	0.60	23
			750	2.3	10.6	1.3	14.2	1.00	47	12.2	0.86	33
			775	2.2	10.4	1.1	12.7	0.89	42	11.6	0.82	31
	20	2.75	600	1.7	8.0	2.6	1.6	0.11	5	1.3	0.09	4
			550	1.8	8.5	3.1	1.0	0.07	3	2.1	0.15	6
			750	2.0	9.4	1.8	4.0	0.28	14	3.9	0.27	11
			775	2.0	9.3	2.0	3.5	0.25	12	3.6	0.25	10
			750	2.1	9.8	1.7	5.8	0.41	20	3.6	0.25	10
			775	2.0	9.5	1.8	4.7	0.33	16	3.6	0.25	11
	20	2.60	750	2.2	10.2	1.7	4.5	0.32	21	3.2	0.22	13
			800	2.2	10.0	1.7	3.8	0.27	17	3.2	0.22	13
			550	1.3	6.0	2.5	1.9	0.13	8	2.4	0.17	9
	80	2.90	750	2.1	9.8	2.4				1.1	0.08	6
			800	2.0	9.4	2.2	1.4	0.10	9	1.1	0.08	6
			550	1.5	7.1					0.2	0.01	1
			750	2.2	10.0	2.2	1.5	0.10	9	1.3	0.09	6
			800	2.1	9.7	2.2	1.7	0.12	10	1.7	0.12	9
	80	2.75	650	1.8	8.2	3.8				0.9	0.06	5
			750	2.0	9.2	2.8	1.8	0.13	13	1.3	0.09	8
			600	1.7	8.0	4.2				0.6	0.04	4

Table II-1 (Continued)

Table II-1 (Continued)

Specimen description			Irradiation conditions				Modulus of rupture					
							At room temperature			At 800°C		
							Irradiated		% of unirradiated value	Irradiated		% of unirradiated value
Composition	Grain size, μ	Density, g/cm³	Temp., °C	Flux, 10^{14} neutrons/(cm²)(sec) (≥ 1 Mev)	Exposure, 10^{20} neutrons/cm² (≥ 1 Mev)	Radiation expansion, vol.%	10^3 psi	10^3 kg/cm²		10^3 psi	10^3 kg/cm²	
AOX	5	2.75	850	2.0	9.0	1.0				11.3	0.80	38
			1000	3.2	11.5	1.0	31.0	2.18	103	24.2	1.70	69
			970	3.1	11.3	1.0	34.4	2.42	132	34.8	2.45	99
			940	2.8	10.0	1.2	36.8	2.59	141	37.2	2.62	106
	20	2.90	900	2.1	5.1	0.8	24.1	1.69	79	32.9	2.31	93
			900	2.1	5.1	0.8	34.5	2.43	108	39.6	2.78	107
	20	2.75	950	2.5	11.3	0.9	22.5	1.58	81	18.8	1.32	58
			970	2.1	5.0	0.6	26.2	1.84	101	31.2	2.19	103
	20	2.60	900	2.4	11.0	1.2	24.8	1.74	104	20.3	1.43	73
			900	2.4	10.8	1.1	31.4	2.21	131	28.5	2.00	102
			900	2.3	10.2	1.0	32.4	2.28	136	35.9	2.52	129
			850	2.0	9.2	1.1	21.4	1.50	89	27.7	1.95	100
			800	2.0	8.8	1.3	13.4	0.94	56	13.5	0.95	49
	80	2.90	900	2.4	11.0	1.4	2.2	0.15	14	3.4	0.24	19
			930	2.4	10.8	1.2	4.0	0.28	26	5.7	0.40	33
			900	2.3	10.1	1.3				3.2	0.22	19
			850	2.0	9.2	1.5	1.4	0.10	9	1.4	0.10	8
	80	2.75	950	2.8	10.0	1.0	5.7	0.40	39	7.5	0.53	46
			930	2.3	8.2	1.0	5.7	0.40	41	10.4	0.73	64
UOX-MgO	20	2.90	950	2.3	5.5	0.6	22.7	1.60	70	24.0	1.69	70
AOX	5	2.75	1000	2.5	9.0	0.9	36.2	2.54	139	31.9	2.24	90
	20	2.90	1040	1.5	3.6	0.5	27.2	1.91	85	28.5	2.00	77
			1040	1.8	4.2	0.6	31.7	2.23	90	24.6	1.73	66
			1025	2.0	4.7	0.7	30.4	2.14	95	30.2	2.12	81
	20	2.75	1050	2.3	5.5	0.7	30.5	2.14	117	27.6	1.94	91
			1050	2.3	5.5	0.7	28.4	2.00	109	27.8	1.95	92

Specimen description			Irradiation conditions				Modulus of rupture					
							At room temperature			At 1000°C		
							Irradiated		% of unirradiated value	Irradiated		% of unirradiated value
Composition	Grain size, μ	Density, g/cm³	Temp., °C	Flux, 10^{14} neutrons/(cm²)(sec) (>1 Mev)	Exposure, 10^{20} neutrons/cm² (>1 Mev)	Radiation expansion, vol.%	10^3 psi	10^3 kg/cm²		10^3 psi	10^3 kg/cm²	
AOX	50	2.90	1100	1.8	4.3	0.4	22.6	1.59	120	21.4	1.50	98
			1000	2.4	5.6	0.7	18.0	1.26	96	24.3	1.71	111
			1100	2.3	5.5	0.5	22.0	1.55	117	22.1	1.55	101
			1100	2.1	4.9	0.4	21.3	1.50	113	22.4	1.58	103
			1100	2.3	5.5	0.5	22.1	1.55	118	24.2	1.70	111
			1000	2.4	5.6	0.7	20.1	1.41	107	16.5	1.16	75
	80	2.75	1000	2.5	9.0	1.0	5.8	0.41	40	7.5	0.53	46
			1000	3.0	10.8	1.0	6.4	0.45	44	7.9	0.56	48
UOX-MgO	20	2.90	1050	1.8	4.3	0.4	25.7	1.81	85	29.6	2.08	84
			1030	2.1	5.1	0.5	27.9	1.96	92	29.8	2.10	84
			1030	2.1	5.1	0.5	25.3	1.78	83	32.5	2.28	92
			1030	1.7	4.0	0.4	23.2	1.63	76	34.7	2.44	98

boundary separation of course explains the larger expansions observed in the polycrystalline compacts.

Data were also presented which compare the radiation-induced effects on BeO (UOX grade) with those on BeO containing bentonite additive (EBOR BeO). In both cases, $\frac{1}{2}$-in.-diameter by $\frac{1}{2}$-in.-long cylinders were irradiated at 800 and 1100°C over the fast-neutron exposure range of 1.5 to 4.85 × 10^{21} neutrons/cm^2 (> 1 Mev). There was no significant gross damage to either type of BeO. Dimensional measurements revealed apparent differences in volume expansion as shown in Table II-2. Metallographic and other examinations will be conducted for a more complete comparison, but Table II-2 data indicate greater expansion for EBOR BeO at both temperatures. (M. C. Brockway)

Table II-2 VOLUME EXPANSION OF IRRADIATED EBOR BeO WITH BENTONITE ADDITIVE AND BeO CONTAINING NO ADDITIVE[7]

Type	Temp., °C	Fast-neutron exposure, 10^{21} neutrons/cm^2	Volume expansion, %
EBOR	800	2.5	3.5
EBOR	800	4.7	3.7
No additive	800	1.5	1.2
No additive	800	4.4	2.0
EBOR	1100	2.5	3.3
EBOR	1100	4.7	4.2
No additive	1100	3.5	1.9
No additive	1100	4.85	3.2

Beryllium Intermetallic Compounds

The "pest" degradation of beryllides and other intermetallic compounds was studied by Westbrook and Wood of the General Electric Research Laboratory.[10] Results of experimental observation of grain-boundary hardness and grain-boundary broadening were used to propose a model for degradation based on preferential diffusion of a gaseous element (oxygen and/or nitrogen) along grain boundaries, coupled with a temperature-dependent hardening process caused by concentration of the gaseous element in the grain boundary. The authors point out that grain-boundary hardening, which precedes degradation, has a temperature dependence that may be used to predict roughly the range of temperature of pest susceptibility for a given compound.

The Russians[11] prepared beryllium-niobium specimens of 0.7 to 58 wt.% niobium by induction melting in argon. Solubility, microstructures, phases, microhardness, and degree of segregation in the cast state were analyzed. These same characteristics were studied after cyclic annealing and quenching of the cast structure.

The rate of vaporization of beryllium during thermal dissociation of $LaBe_{13}$ and YBe_{13} was studied[12] in the temperature range 1040 to 1290°C; these compounds dissociate at temperatures above 1050°C. From these studies the following equations for the equilibrium vapor pressure of beryllium during dissociation were derived:

$$\log P = (-16{,}600/T) + 8.73 \text{ for } LaBe_{13}$$

$$\log P = (-16{,}420/T) + 8.30 \text{ for } YBe_{13}$$

where P is in millimeters of mercury. The heat of vaporization was 75.8 kcal/mole for $LaBe_{13}$ and 75.0 kcal/mole for YBe_{13}.

(R. W. Getz)

Solid Hydrides

Zirconium Hydride

The solubility of hydrogen in zirconium at room temperature was studied by Straumanis and Wiebe.[13] The solid-solubility limit was 310 ppm, as determined by the parametric X-ray method. A value of 280 ppm was derived from the increase of tensile and yield strength of zirconium wires with increasing hydrogen content. Within the solid-solubility range, the strength of the wires increased only slightly, but in the two-phase region it increased greatly. The a_0 value for zirconium increased from 3.2360 A for pure metal to 3.2378 A for zirconium containing 310 ppm hydrogen in solid solution. At the same time, c_0 changed from 5.1508 A to 5.1572 A. The experimentally measured density of pure zirconium was 6.481 g/cm^3, as compared to the X-ray density of 6.4840 g/cm^3 at 25°C. The experimental density decreased more rapidly than the X-ray density as the hydrogen content of the zirconium was increased; this result indicates an increase of vacancy aggregations as the hydrogen is absorbed.

Hydrogen-absorption isotherms determined at Hanford[14] show the boundaries of the beta-phase zirconium hydride to extend from $ZrH_{0.28}$ to $ZrH_{0.99}$ at 750°C. These data are in agreement with the commonly accepted phase diagram for the zirconium-hydrogen system at the higher hydrogen content, but the lower boundary is usually given as $ZrH_{0.15}$ at this temperature. The boundaries of the beta-plus-delta-phase region are given as $ZrH_{0.99}$ and $ZrH_{1.43}$ in the Hanford study, which is in good agreement with findings of previous investigators.

Hydrided Zirconium Alloys

The combustion behavior of zirconium–10 wt.% uranium fuel elements hydrided to $ZrH_{1.9}$ was examined at Lockheed.[15] An arc-image furnace equipped with 14-in. elliptical mirrors made it possible to reach a temperature near the melting point of the alloy. A strongly endothermic dehydrogenation occurred, resulting in a lowered temperature. There was no violent disintegration, and the amount of oxidation varied from almost none to almost complete in various samples. Formation of water was also observed.

The effect of hydriding on the properties of zirconium–1 wt.% niobium used for fuel-element cladding in water-moderated water-cooled power reactors has been reported by the Russians.[16] The clad fuel elements were hydrided to 0.06 wt.% hydrogen and operated for 4000 hr in water at 100-atm pressure and 300°C surface temperature. The integrated neutron flux was 1.5×10^{20} neutrons/cm^2. The zirconium hydride stringers in the alloy were found to be displaced toward the cooler portion of the cladding. With increasing hydrogen content from 20 to 600 ppm, the tensile strength showed an increase of 45 to 85% when compared with the strength of nonirradiated specimens. At the same time the ultimate strength decreased from 53 to 47 kg/mm^2. Thus the presence of a hydrided surface layer affects the ductility and the load-carrying capacity of the cladding. Hydriding under stress showed that at stresses up to 3.0 kg/mm^2 the hydride stringers were concentric, but they changed to a radial orientation above 4.4 kg/mm^2.

Similar results were found by Sawatzky[17] for specimens of zirconium–2.5 wt.% niobium and Zircaloy-2 exposed at 280°C to an integrated neutron flux of 10^{21} neutrons/cm^2. The tensile strength of both alloys increased, whereas impact strength decreased.

Yttrium Hydride

Some thermodynamic properties of yttrium deuteride, YD_2, have been measured by the British.[18] The heat of formation is reported to be −51.7 kcal/mole, and the associated entropy change is 46.4 cal/(mole)(°C). The dissociation pressure is given by

$$\log P\,(\text{mm}) = 10.15 - \frac{\sqrt{11{,}300}}{T(^\circ\text{K})}$$

Ternary Hydrides

Ternary metal-carbon-hydrogen compounds of various transition metals have been prepared at Iowa State University.[19] They all have the composition $MC \cdot MH_x$ and have a wide range of hydrogen contents. All are more stable thermally than the simple metal hydride. The dissociation pressures, heats of formation, and lattice constants of the hexagonal close-packed metal atoms are tabulated below:

	$\log P\,(\text{mm}) = A - B/T$		ΔH, kcal/mole of hydrogen	a_0, A	c_0, A
	A	B			
$TiC \cdot TiH_{0.46}$	10.91	9,560	−43.7	3.083	5.042
$ZrC \cdot ZrH_{1.46}$	9.82	10,670	−48.8	3.347	5.469
$HfC \cdot HfH_{0.86}$	9.24	9,870	45.2	3.291	5.385

The values for the lattice constants of the zirconium compound were verified at Atomics International.[20] In addition, the existence of a similar nitrogen compound, $ZrN \cdot ZrH_x$, has been established. It also has a hexagonal structure, with $a_0 = 3.288$ A and $c_0 = 5.468$ A. Efforts to prepare the corresponding boron compound have been unsuccessful, and apparently it does not exist. (H. H. Krause)

References

1. F. W. Albaugh, Reactor and Fuels Laboratory Monthly Report, November 1964, USAEC Report HW-84529A, Hanford Atomic Products Operation, Dec. 15, 1964. (Classified)
2. S. S. Jones and E. M. Woodruff, Radiation Effects in Some Hanford Reactor Graphites, USAEC Report HW-82152, Hanford Atomic Products Operation, June 1964.
3. J. K. Higgins and J. E. Antill, Oxidation of Vitreous Carbon in Carbon Dioxide and Water Vapour, British Report AERE-R-4547, Aug. 21, 1964.

4. *J. Metals*, 16(9): 693-699 (September 1964).
5. Papers presented at the AIME Second International Conference on Beryllium Technology held at the Franklin Institute in Philadelphia, Pa., Oct. 15 to 17, 1964.
   a. D. Beasley and A. Moore, Slip in Beryllium Single Crystals Compressed Along the *c*-Axis Near 200°C.
   b. D. Beasley and A. Moore, Effects of Heat Treatment on the Flow Stress of Beryllium Single Crystals.
   c. V. V. Damiano and M. Herman, Dislocations in Deformed Beryllium Single Crystals.
   d. A. G. Gross, Jr., The Crystallography of Beryllium Sheet.
   e. M. J. Hordon and W. T. Hess, Electron-Beam Vaporization of Beryllium.
   f. R. F. Bunshah and R. S. Juntz, Purification of Beryllium by Crucible-Free Vacuum Melting and Distillation Process, USAEC Report UCRL-7591.
   g. A. R. Kaufman and W. C. Muller, Fine Grain Size in Beryllium by Splat Cooling.
   h. J. W. Butcher and J. N. Lowe, Activated Sintering in Beryllium Powders by Selective Addition of Trace Elements.
   i. E. S. Hodge, P. J. Gripshover, and H. D. Hanes, Properties of Gas-Pressure-Consolidated Beryllium Powder.
   j. J. A. Yoblin, Forging Beryllium for Structural Applications.
   k. L. L. Soffa and G. J. Bash, High-Strength Forged Beryllium for Structural Applications.
   l. E. A. Stark and A. Bobrowsky, Deformation and Forming of Beryllium at Room Temperature Under Pressure.
6. General Electric Company, Advanced Technology Services, High-Temperature Materials Program Progress Report No. 42, Part A, USAEC Report GEMP-42A, Dec. 18, 1964.
7. General Electric Company, Advanced Technology Services, High-Temperature Materials Program Progress Report No. 40, Part A, USAEC Report GEMP-40A, Oct. 15, 1964.
8. S. B. Austerman, Crystallographic Expansion of BeO at the Alpha-Beta BeO Transformation Temperature, USAEC Report NAA-SR-9260, Atomics International, Oct. 15, 1964.
9. W. C. Thurber (Comp.), High-Temperature Materials Program Quarterly Progress Report for Period Ending October 31, 1964, USAEC Report ORNL-TM-980, Oak Ridge National Laboratory, December 1964. (Classified)
10. J. H. Westbrook and D. L. Wood, "Pest" Degradation of Beryllides, Silicides, Aluminides, and Related Compounds, *J. Nucl. Mater.*, 12: 208-215 (July 1964).
11. N. D. Nagorskaya, L. V. Molchanova, et al., Crystallization in the Beryllium-Niobium System, *Metalloved. i Term. Obrabotka Metal.*, 6: 12-15 (1964).
12. V. M. Amonenko, A. A. Kruglykh, V. S. Pavlov, and G. F. Tikhinakii, Vaporization Rate of Components During Thermal Dissociation of Yttrium and Lanthanum Beryllide, *Izv. Akad. Nauk SSSR, Met. i Gorn. Delo*, No. 3: 158-160 (May-June 1964).
13. M. E. Straumanis and D. H. Wiebe, Solubility of Hydrogen in Zirconium at Room Temperature and Properties of the Solid Solutions, Report AD-604409, University of Missouri, Rolla School of Mines and Metallurgy, August 1964.
14. Hanford Atomic Products Operation, Metallurgy Research Operation. Quarterly Progress Report, April-June 1964, USAEC Report HW-82651, July 15, 1964.
15. F. E. Littman and A. E. Levy-Pascal, Combustion and Disintegration of Zirconium Hydride-Uranium Fuel Rods, in Proceedings of Aerospace Nuclear Safety, USAEC Report SC-DC-3553, Sandia Corp., 1963.
16. A. D. Amaev et al., Influence of Some Factors on Hydriding and Variation of Properties of Zirconium Alloy with 1% Niobium Used for Fuel Element Cladding in Water-Moderated Water-Cooled Power Reactors, presented at the Third United Nations International Conference on the Peaceful Uses of Atomic Energy, Geneva, 1964, Paper A/Conf.28/P/342.
17. A. Sawatzky, The Effect of Neutron Irradiation on the Mechanical Properties of Hydrided Zirconium Alloys, Canadian Report AECL-1986, June 1964.
18. P. M. S. Jones, J. Southall, and K. Goodhead, The Thermal Stability of Metal Hydrides. Part I. Rare Earth and Yttrium Hydrides and Deuterides, British Report AWRE-0-22/64, June 1964.
19. J. Rexer and D. T. Peterson, Ternary Metal-Carbon-Hydrogen Compounds of Some Transition Metals, USAEC Report IS-875, Ames Laboratory, April 1964.
20. Atomics International, Annual Technical Progress Report, AEC Unclassified Programs, Fiscal Year 1964, USAEC Report NAA-SR-9999, Aug. 31, 1964.

Section

III

Reactor Materials

Nuclear Poisons

Metallic Poison Materials

Considerable research has recently been undertaken concerning phase diagrams of hafnium with various other metals. Workers at the U. S. Bureau of Mines have published the hafnium-tantalum[1,2] and hafnium-iridium[2] phase diagrams shown in Figs. III-1 and III-2. Both the Russians[3] and Americans[4] have determined tentative phase diagrams for hafnium-niobium. As can be seen in Fig. III-3, there are substantial differences between the two.

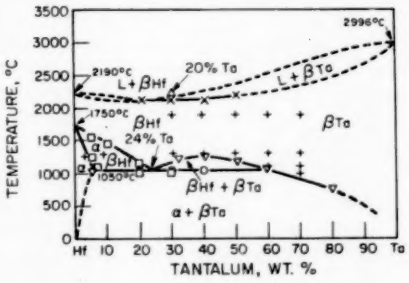

Fig. III-1 Hafnium-tantalum phase diagram.[1] ×, solidus; Δ, liquidus; +, single phase; □, two phase; ○, thermal analysis; ▽, X-ray diffraction.

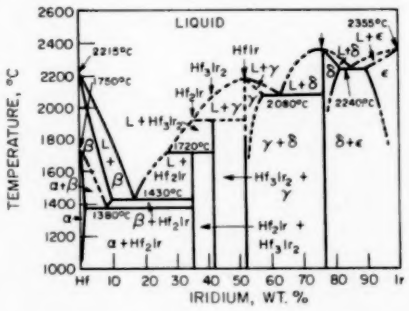

Fig. III-2 Hafnium-iridium phase diagram.[2]

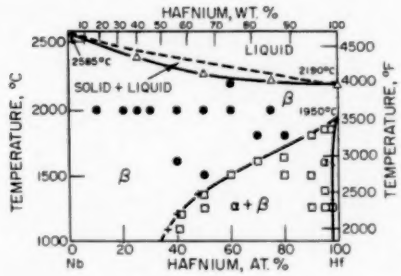

(a) By Taylor and Doyle.[4] ●, single-phase beta. □, two-phase alpha plus beta. +, boundary by X-rays. Δ, melting point.

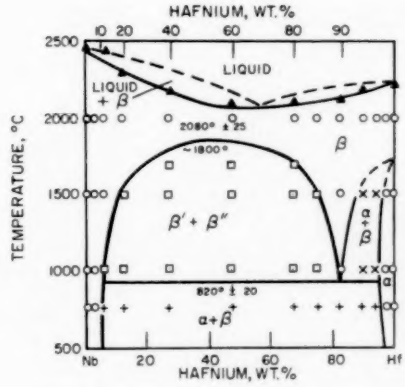

(b) By Tilkina, Tsyganova, and Savitskii.[3] ○, single-phase. Δ, melting or freezing point. □, two-phase beta prime plus beta double prime. ×, +, two-phase alpha plus beta.

Fig. III-3 Tentative niobium-hafnium phase diagrams.

The diffusion coefficient of oxygen in hafnium over the temperature range 500 to 1100°C has been determined to be $D = 0.660 \exp(-50{,}820/RT)$ by the anodization technique[5] and $D = 30$

exp $(-58{,}000/RT)$ by internal-friction measurements (Ref. 6). The diffusion coefficient of nitrogen in hafnium was found (Ref. 6) to be $D = 0.20 \exp(-50{,}000/RT)$ over the same temperature range.

Postirradiation measurements of the silver-indium-cadmium absorber sections of fuel assemblies from core I of the Yankee reactor indicated a density decrease of about 1%, based on the measured volume increase of 1% (Ref. 7). These assemblies had operated at temperatures up to 340°C for almost two years, much of the time with the reactor at full power of 485 Mw(t).

The chromium-gadolinium system was studied at the Bureau of Mines.[8] Liquid immiscibility was found at temperatures above the monotectic isotherm, 1830°C, which extended from less than 0.25 to about 85 wt.% gadolinium. The only eutectic point was at 96 wt.% gadolinium and 1170°C. No compounds were found. The solid solubility of gadolinium in chromium was 0.25 wt.% at 1730°C; that of chromium in gadolinium was 0.10 wt.% at 1160°C. (M. Kangilaski)

Dispersion and Non-metallic Poison Materials

An article[9] translated from the Russian described how stoichiometric ZrB_2 of high purity can be produced commercially from reacting B_4C and ZrO_2. The effect of composition of the starting materials and of the conditions of preparation on the chemical and phase compositions of the ZrB_2 produced was also discussed.

High-density specimens of ZrB_2 and HfB_2, covering a range of boron-to-metal ratios, have been prepared at ManLabs, Inc.[10] The specimens were formed by high-pressure hot pressing and were later characterized by X-ray, metallographic, pycnometric, and chemical analyses. Oxidation measurements on metal-rich ZrB_2, metal-rich HfB_2, boron-rich HfB_2, and tantalum-doped boron-rich HfB_2 were performed at temperatures up to 1830°K and at oxygen pressures of 0.4 and 40 mm Hg. The metal-rich HfB_2 (B/Me = 1.88) was found to have a parabolic oxidation-rate constant, which is one-eighth that of boron-rich HfB_2 (B/Me = 2.12), whereas metal-rich ZrB_2 has a rate constant one-third that of stoichiometric ZrB_2. Additions of hafnium to boron-rich HfB_2 without complete homogenization did not improve the oxidation resistance expected on the basis of B/Me ratios.

It was found possible to sinter ZrB_2 to near theoretical density at 2100°C in the presence of impurities. Other physical-property measurements made included thermal conductivity and emissivity of TiB_2, ZrB_2, HfB_2, and NbB_2 between 1000 and 1700°C and electrical resistivity of ZrB_2 and HfB_2 up to 1500°C. The free energies of formation of the monoborides of hafnium and zirconium were estimated so as to provide information to construct Hf-B and Zr-B phase diagrams.

Oak Ridge National Laboratory[11] developed procedures for consolidating Eu_2O_3 and studied the compatibility of arc-fused Eu_2O_3 and $Eu_{5.3}MoO_{11}$ with stainless steel, iron, nickel, and chromium. Optimum parameters were established for melting Eu_2O_3 in 300- to 500-g quantities. Although small quantities could be arc melted in one operation, a two-step operation is more suitable for larger quantities. In the initial step low-density cold-pressed pellets are partially fused to remove the major portion of the volatiles and to increase the bulk density. In the second step the material is melted completely. In each step an equimolar mixture of helium and argon flows through the electrode tip at a system pressure of 300 mm Hg.

No reactions were observed between either Eu_2O_3 or $Eu_{5.3}MoO_{11}$ with iron or nickel powder as a result of treatment at 1150°C in vacuum or argon. However, these oxides did react with chromium, but this may have been because of impurities within the powder. Neither of the oxides was compatible with types 302B and 304L stainless-steel powders.

The Japanese[12] used plasma fusion to fabricate UO_2 pellets containing spherical particles of ZrB_2 as a burnable poison. Low-density ZrB_2 rod was fabricated and then spheroidized by plasma-flame techniques to form spherical particles of 50- to 100-μ diameter. This material was then mixed with UO_2 powder (oxygen-to-uranium ratio 2.04) having an average particle size of 1.6 μ. The powders were blended, cold pressed, and then slowly heated to 1600°C and held at temperature for 2 hr.

The average sintered density of the UO_2 pellets containing ZrB_2 was 10.96 g/cm^3, and permeability measurements indicated them to have 0.4% closed porosity and 2.2% open porosity. Chemical analysis of the pellets showed 129 ± 20 ppm boron, greater than 5 ppm carbon,

and 35 ± 10 ppm nitrogen. Metallographic examination showed the ZrB_2 particles to be homogeneously dispersed in the UO_2 matrix, and there was no evidence of reaction with the matrix.

Later experiments were made using UO_2 and ZrB_2 powders blended, pressed, and sintered in vacuum at 1800 and 2000°C for 2 hr. Evaluation of the resulting structure indicated that there was no reaction between the UO_2 and ZrB_2, although a thermodynamic study indicated that they should react. (E. G. Smith, Jr.)

References

1. L. L. Oden, D. K. Deardorff, M. I. Copeland, and H. Kato, The Hafnium-Tantalum Equilibrium Diagram, USAEC Report BM-RI-6521, Bureau of Mines, Albany Metallurgy Research Center, February 1964.
2. W. L. R. Rice (Ed.), Nuclear Fuels and Materials Development, USAEC Report TID-11295 (3rd ed.), July 1964.
3. M. A. Tylkina, I. A. Tsyganova, and S. M. Savitskii, The Hafnium-Niobium System (In Russian), *Zh. Neorgan. Khim.*, 9: 1650-1652 (July 1964).
4. A. Taylor and N. J. Doyle, The Constitution Diagram of the Hafnium-Niobium System, *J. Less-Common Metals*, 7: 37-53 (July 1964).
5. J. P. Pemsler, Diffusion of Oxygen in Hafnium, *J. Electrochem. Soc.*, 111: 1185-1186 (October 1964).
6. E. Bisogni, G. Mah, and C. Wert, Diffusion of Gases in Special Interstitial Sites in Hafnium, *J. Less-Common Metals*, 7: 197-204 (September 1964).
7. Westinghouse Electric Corp., Atomic Power Division, Yankee Core Evaluation, Quarterly Progress Report for Period Ending September 30, 1964, USAEC Report WCAP-6064, October 1964.
8. M. I. Copeland, C. E. Armantrout, and H. Kato, The Chromium-Gadolinium System, Mark I, USAEC Report BM-RI-6503, Bureau of Mines, Albany Metallurgy Research Center, January 1964.
9. V. F. Funke and S. I. Yudkovskii, Preparation of Zirconium Boride, *Soviet Powder Met. Metal Ceram.* (English Translation), No. 4: 293-296 (August 1963).
10. L. Kaufman, Investigation of Boride Compounds for Very High Temperature Applications, Report NP-14192, ManLabs, Inc., May 1964.
11. Oak Ridge National Laboratory, Metals and Ceramics Division Annual Progress Report for Period Ending June 30, 1964, USAEC Report ORNL-3670, October 1964.
12. Oxide and Carbide Fuels, Japan–U. S. Research Newsletter No. 3, August 1964.

Section IV

Reactor Materials

Cladding and Structural Materials

Corrosion

Zirconium Corrosion

FRETTING CORROSION

Studies on the fretting corrosion of Zircaloy in high-temperature water are continuing at Hanford Atomic Products Operation.[1] Recent out-of-reactor tests with a UO_2 fuel element in flowing water at 530°F and a vibration of 0.004-in. amplitude resulted in fretting marks 2 to 3 mils deep after 830 hr of exposure. In addition, the fretting corrosion observed in the Plutonium Recycle Test Reactor (PRTR) pressure tubes and the results of out-of-reactor tests that were conducted to determine the fretting parameters have been summarized.[2]

Fretting corrosion was also believed to be responsible for complete penetration of 0.056-in.-wall Zircaloy-2 cladding in contact with a stainless-steel spacer wire in fuel-assembly tests conducted in the Vallecitos Boiling Water Reactor (VBWR).[3] Penetration apparently occurred after about nine months' operation of the fuel element, which had sustained a total of 8828 hr at operating temperature and a burnup of 8358 Mwd/ton. Other results from the same study indicated that time to transition from cubic to linear corrosion rates of Zircaloy-2 cladding in the VBWR was an order of magnitude less than for out-of-reactor tests at the same temperature (575°F).

HYDROGEN PICKUP

The variation in the corrosion rate and hydriding of Zircaloy-2 as a function of heat flux has been computed by Dyce[4] for exposure to water at 550 to 680°F. The acceleration in corrosion rate and accompanying hydriding was such that the time to reach a hydride level of 500 ppm at a heat flux of 1,000,000 Btu/(hr)(sq ft) was calculated to be about one-half the predicted time under isothermal conditions.

Tritium has been used to study hydrogen solubility as a function of the dissolved oxygen content in oxidized Zircaloy-2 in studies conducted at Chalk River.[5] The results of autoradiography and hardness tests suggested that a range of oxygen contents, which corresponded to Knoop hardnesses of approximately 250 to about 400, increased the hydrogen solubility in Zircaloy-2. The solubility decreased again above this oxygen content.

MISCELLANEOUS

Wet-chemical, activation, and microprobe analyses have been made at Vallecitos Atomic Laboratory[6] of zirconium-alloy corrosion films formed in high-temperature water and steam. It was found that the amount of tin, niobium, and chromium in posttransition oxide films was directly proportional to the amount in the alloy, and the effects of these elements on the posttransition corrosion rates could be associated with the amount of the solute in the corrosion film. (W. E. Berry)

Aluminum Corrosion

A comprehensive review of the aqueous corrosion behavior of aluminum alloys, zirconium alloys, nickel alloys, and stainless steels has recently been issued by the U. S. Atomic Energy Commission.[7] Considerable attention was devoted to the problems of stress-corrosion cracking and corrosion in superheated steam. (W. E. Berry)

Stainless-Steel Corrosion

GENERAL

A useful information manual on stainless steel has been issued by the Savannah River

Laboratory.[8] Data are presented on corrosion, oxidation, and radiation effects for austenitic, ferritic, martensitic, and precipitation-hardening stainless steels. Also included are a discussion of corrosion mechanisms, examples of corrosion attack, means of avoiding corrosion, and a list of tests for producing the various forms of localized attack.

SELECTIVE ATTACK

Intergranular corrosion of irradiated type 304 stainless steel during storage has been reported by Oak Ridge National Laboratory.[9] The attack occurred in sensitized material stored in high-humidity or underwater environments, but the mechanism of corrosion has not yet been established.

Stress-corrosion cracking of the stainless steel in composite stainless-steel–asbestos gaskets in PRTR nozzle tubes has been attributed to chlorides leached from the asbestos as the result of tests conducted at Hanford.[10] Maximum chloride concentration in the asbestos was 1430 ppm.

CORROSION PRODUCTS

Microscopic and microprobe examinations have been made of the oxide film formed on stainless steel in steam at 500°C, in research conducted in Belgium.[11] Two distinct layers were found: an outer layer that contained only iron and an inner layer that was enriched in chromium and nickel. The fact that the two layers were of the same thickness irrespective of the testing time suggested that the opposing diffusion rates of anions and cations in the oxide film were about equal. A similar phenomenon has been observed in boiler-tube steel at England's Central Electricity Authority.[12]

Analysis of corrosion products on the Yankee reactor core I and core II fuel rods has revealed a depletion of iron and an enrichment of chromium and nickel in corrosion films and a slight depletion of nickel and severe depletion of chromium in deposits, as compared with the composition of the cladding metal (type 348 stainless steel).[13] Average oxide-film surface concentrations were 121 mg/dm^2 for core I rods and 104 mg/dm^2 for core II rods. Core I operated for 17 months at an average water temperature of 510°F and *p*H 7.5; the conditions for core II were 12 months at approximately 515°F and *p*H 8.5. (W. E. Berry)

Corrosion of Iron- and Nickel-Base Alloys

STEAM CORROSION

For fuel-element superheat service in nuclear power plants, General Electric Company workers have evaluated alloys 2541 (Fe–25 wt.% Cr–4 wt.% Al–1 wt.% Y) and 80 wt.% Ni–20 wt.% Cr, as well as other alloys, in steam ranging from 500 to 1300°C and at several pressures.[14] Tests at Hanford at 550°C and 333 atm showed the two alloys to be comparable. They were superior to type 304L by a factor of 2.5. The weight loss for alloy 2541 was 50 mg/dm^2 after 949 hr of exposure to steam at 620°C (1150°F) and 69 atm and containing 20 ppm dissolved oxygen and low chloride (about 5 ppm). For comparison, Incoloy 800 showed 108 mg/dm^2 weight loss.

More recent results[15] of tests performed in superheated steam flowing at 20 ft/sec showed alloy 2541 to be four times as resistant as Incoloy 800 after almost 5000-hr exposure.

Four of a series of nickel-base alloys were found by Hanford[16] to be resistant to 650°C (1200°F) deoxygenated steam containing less than 50 ppb oxygen. Inconel 718, Incoloy 800, Inconel 600, and Hastelloy X-280 showed weight gains of less than 0.35 mg/cm^2 after 1680 hr in this steam circulating at 2 liters/hr.

OXIDATION BY GAS PHASES

The effects of contaminants in the coolant on materials for gas-cooled reactors are being studied at a number of sites. Hastelloy X and Haynes 25 have been found by Hanford[17] to carburize rapidly in 1120°C (2050°F) methane at 25 mm of pressure. For a 4000-min test, 88% of the attack occurred in the first 750 min. The Haynes 25 alloy was also exposed for 5000 min to 100 mm of oxygen with 28 mm of water vapor at 1120°C (2048°F) (Ref. 1). Upon cooling it showed rapid spalling of the oxide film starting at about 480°C (900°F).

In experiments at 815°C (1500°F), 921°C (1700°F), and 1030°C (1900°F) in helium containing water vapor (15 mm Hg), Hastelloy N was most resistant[16] at about 300 hr. A tight oxide film formed, and there was slight intergranular penetration at 1030°C.

Haynes 25 and Hastelloy X were found[18] to be resistant to 100 mm of nitrogen at 1200°C (2200°F).

An activation energy of 40 kcal/mole was obtained[19] for copper in a fluorine-plus-argon mixture at 550 to 700°C. Other metals are being investigated in this system.

In the Renfrew Laboratory of Babcock & Wilcox Limited,[20] seven heats of the 2.25 wt.% chromium–1 wt.% molybdenum alloy from different sources were compared for corrosion resistance in carbon dioxide with 5 vol.% carbon monoxide and 500 ppm water vapor at 550°C (1020°F). After almost 2800 hr of exposure, there was an 8-to-1 ratio between the least and the most resistant. Neither the chemical composition nor heat-treatment of the materials as supplied could account for the differences observed. (F. W. Fink)

Corrosion of Refractory Metals

Oxidation kinetics of tungsten and molybdenum at temperatures from over 1300°C to near the melting points and at oxygen pressures of 10^{-6} to 1 atm are described by Bartlett in a recent Air Force report.[21] Oxidation rates were determined by measuring the rates of surface recession in the metal rods. Arrhenius plots of recession rates are given in Figs. IV-1 and IV-2. Transport of oxygen through the boundary film of oxide vapors was found to limit the metal recession rates at the higher pressures. When tungsten was subjected to a hypersonic gas stream of 15,000 ft/sec (5 to

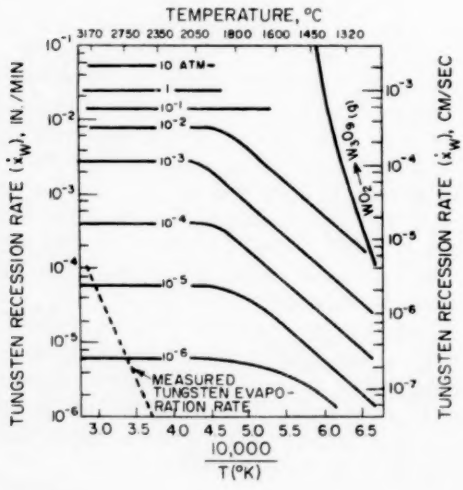

Fig. IV-1 Arrhenius plot of tungsten recession rate vs. reciprocal absolute temperature in oxygen.[21]

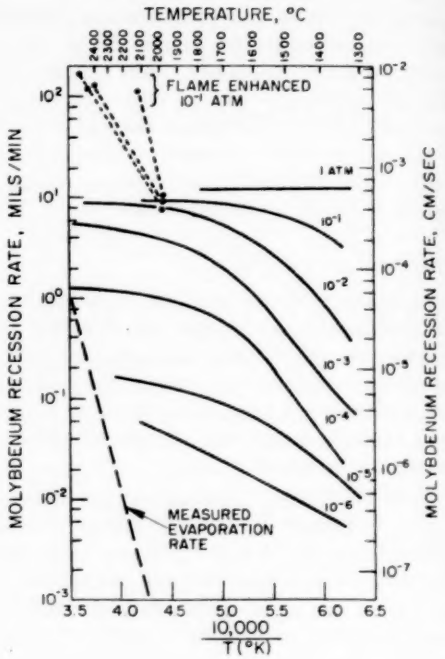

Fig. IV-2 Arrhenius plot of recession rates of molybdenum.[21]

20 vol.% oxygen mixtures in argon) at 2000°C, the recession rate could be increased five to six times that of the free-convection recession rates shown in Fig. IV-1 and would thus support the boundary-film concept. At the higher temperatures and pressures, molybdenum showed a large discontinuous increase in recession rate. This change in rate was accompanied by a sudden rise in temperature, and the sample was surrounded by a flame, indicating combustion in the gaseous phase rather than on the surface of the molybdenum rod. The author suggested that the highly exothermic reaction that accompanies the oxidation of MoO_2 to MoO_3 and the polymerization of MoO_3 might be the cause of this "flame-enhanced" oxidation phenomenon.

An investigation of the oxidation behavior of bulk silicides and silicide-coated molybdenum and tungsten in oxygen is described in an Air Force report[22] prepared by the Philco Corp. Figure IV-3 summarizes the oxidation behavior of the compounds $MoSi_2$ and Mo_5Si_3 as a function of temperature and pressure. In the "pest" temperature range (to ~550°C), a thick, non-

adherent oxide forms within a few hours, the oxide consisting of a mixture of MoO_2 and SiO_2. Above 1200°C and at high oxygen pressures, crystalline MoO_2 is not observed in the oxide scale. In this "passive" oxidation region (Fig. IV-3), there are negligible weight changes. Rapid weight loss occurs in the low-pressure, "active" oxidation region as the result of SiO vaporization. Between these two regions "active-passive" oxidation proceeds by an initial rapid weight loss followed by passive oxidation. This initial weight loss depletes the surface of silicon, which in turn reduces the silicon vapor pressure and permits the formation of protective SiO_2.

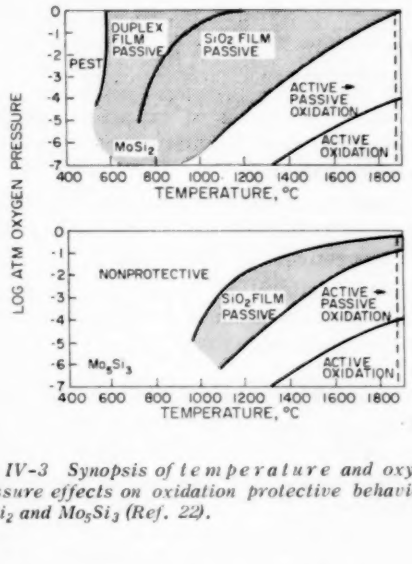

Fig. IV-3 Synopsis of temperature and oxygen-pressure effects on oxidation protective behavior of $MoSi_2$ and Mo_5Si_3 (Ref. 22).

Philco workers also measured the growth rates of Mo_5Si_3, Mo_3Si, and W_5Si_3 in this investigation. They were able to correlate the protective lives of the silicide coating on molybdenum with the rate of diffusion depletion of $MoSi_2$. Coating life was observed to decrease with increasing temperature, pass through a minimum, and then increase as the Mo_5Si_3 diffusion zone became passive.

Platinum and platinum-rhodium alloys were evaluated as oxidation-resistant claddings for niobium and molybdenum alloys by Metals & Controls, Inc.[23] The protective lives of 2-mil-thick claddings were found to be limited to only 5 to 15 hr at 2550°F because of interdiffusion between the cladding and refractory metal. Attempts to increase the diffusion stability of the composites by using intermediate diffusion barriers met with little success.

(J. J. English)

Corrosion by Liquid Metals

A static, isothermal capsule–corrosion study performed at Ames Laboratory[24] indicated degrees of corrosion attack ranging from limited to zero for the following combinations of materials:

1. Lead, tin, lead plus 2 wt.% uranium, or tin plus 1 wt.% uranium in tantalum at 1100°C and zinc in tantalum at 900°C.
2. Lead or lead plus 2 wt.% thorium in niobium at 900°C

Severe-attack combinations in the 800 to 1100°C range included:

1. Aluminum or aluminum plus 13 wt.% uranium in tantalum
2. Aluminum, zinc, or tin in niobium
3. Aluminum, lead, tin, or zinc in Inconel
4. The above liquid metals in yttrium

An investigation is in progress at Battelle Memorial Institute to find a heat-transfer fluid for use in approximately 1650°C irradiation capsules.[25] Requirements include fairly low vapor pressure and compatibility with the capsule components and clad irradiation specimens. Lithium is marginal on both counts. Several short-time isothermal tests with molybdenum containers have ruled out antimony and tin because of extensive molybdenum dissolution. Bismuth was somewhat better, but copper showed the most promise. Tests with about 1650°C molten copper contained in molybdenum or molybdenum–0.5 wt.% titanium–0.08 wt.% zirconium (TZM) revealed the following:

1. After 500 hr (isothermal), capsule-wall surface pits about 10 μ (0.4 mil) deep were found at grain boundaries.
2. When a tungsten–26 wt.% rhenium weld bead was placed in the capsule with the copper, the attack of the molybdenum grain boundaries adjacent to the bead was accelerated (pits were 70 μ deep in 70 hr).
3. When a 170°C temperature gradient was imposed on a molybdenum capsule containing a tungsten–26 wt.% rhenium weld bead in molten copper at a peak temperature of 1590°C, there

was undercutting of the capsule wall at the liquid-gas interface (200 μ in 225 hr) and heavy grain-boundary attack (200 μ deep) adjacent to the tungsten-rhenium bead.

4. With no tungsten-rhenium present, a TZM capsule showed no grain-boundary dissolution after 200 hr, but there was evidence that the copper was migrating all the way through the capsule wall along grain boundaries and evaporating from the outer surface.

Atomics International reports generally encouraging evidence of the behavior of cladding materials exposed to primary-system sodium during core II operation of the Sodium Graphite Reactor.[26] Zircaloy-2 cladding on the irradiation cans did not exhibit appreciable hydriding or oxidizing, nor did the stainless-steel fuel-element cladding exhibit serious carburization. Specific levels cited for the former are: hydrogen, 30 to 90 ppm compared with the as-received material level of 20 ppm (during core I operation hydrogen levels of 500 to 1000 ppm were observed); and oxygen, 730 to 1170 ppm compared with an original 1100 ppm. For the stainless steel the maximum carbon level observed was 0.24 wt.%, with 0.50 wt.% set as the acceptable operating limit.

AiResearch Manufacturing Company of Arizona operated a closed loop fabricated entirely of niobium–1 wt.% zirconium with potassium boiling at 1950°F and condensing at 1770°F (Ref. 27). A section contained orifices and molybdenum–0.5 wt.% titanium test samples. After 307 hr of operation, examinations revealed little, if any, erosion or corrosion damage to the test coupons and orifices as a result of the high-velocity flow of potassium vapor and/or liquid.

At Oak Ridge it was found[28] that pure niobium, tantalum, vanadium, titanium, and zirconium resist attack by lithium at temperatures of 800°C or higher. Small quantities of oxygen can destroy this immunity in either niobium or tantalum but do not seem to impair the resistance of the other three metals. Adding a small amount of zirconium to niobium renders the alloy resistant to lithium at 815°C if (1) the oxygen-to-zirconium atom ratio is less than 2:1 and (2) the alloy has been heat-treated for 2 hr at 1300°C (or for 1 hr at 1600°C or 5 hr at 1000°C) to stabilize the oxygen in the form of ZrO_2. Too high a heat-treating temperature (e.g., >1950°C) apparently redissolves the ZrO_2 and destroys the corrosion resistance to lithium. Additions of vanadium (up to 40 wt.%) to niobium do not have the same beneficial effect as zirconium in preventing attack by lithium.

Investigation of the corrosion behavior of niobium in 815°C potassium is also under way at Oak Ridge.[29] After a 500-hr test, a specimen containing an initial 2400 ppm oxygen in solid solution was recovered and the corrosion-product layers at the surface were closely examined. Next to the scale-potassium interface, a profusion of needlelike crystallites was found by electron microscopy. These crystallites were tentatively identified by electron diffraction as $KNbO_3$. The production of a stable niobate in the niobium-potassium system is cited as being significant and provides a hitherto missing link for the clarification of several prior Oak Ridge observations. The following are specifically mentioned:

1. Poor recoveries of oxygen by amalgamation and vacuum distillation of oxygen-doped potassium samples

2. Higher apparent solubilities of niobium in oxygen-contaminated potassium than predicted from theoretical considerations

3. Rapid migration of oxygen out of potassium-exposed niobium, in contradiction to available thermodynamic data

Potassium metallate formation, in this case K_2MoO_4, is also a key factor in a Battelle investigation of molybdenum-rich crystalline deposits that occur in potassium-containing molybdenum–0.5 wt.% titanium–0.05 wt.% zirconium (TZM) capsules tested in the 1500 to 2200°F range.[30] Most of the deposits are located near the liquid-vapor interface. Several parametric effects, including fluid temperature, temperature gradient through the liquid and vapor phases, and concentration of oxygen in the potassium, are being studied. Results to date indicate that the quantity of mass transfer is sensitive to fluid temperature, oxygen concentration, and partial pressure of noncondensable gas in the vapor zone (directly with the first two and inversely with the third). However, overall temperature gradient (to nearly 300°F) does not seem to be an important factor. In fact, the deposits were initially observed in potassium-containing hollow creep-test specimens operated without a purposely induced temperature gradient.

In the simplest terms the postulated mechanism involves the reaction

$$MoO_2 + MoO_3 + 4K \rightleftharpoons K_2MoO_4 + K_2O + Mo$$

The relatively high-vapor-pressure ingredients on the left-hand side exist in the vapor phase and, when the vapor is cooler than the liquid, as is normal in the refluxing capsule tests, the reaction proceeds toward the right. The molybdenum atoms formed diffuse to the wall and deposit. In the liquid bath the reaction tends to reverse and thus generates a cyclic process.

Attention is once again called to the series of High-Temperature Liquid-Metal Technology Reviews issued bimonthly by Brookhaven National Laboratory. These provide summaries of liquid-metals-corrosion investigations as well as investigations in the areas of heat-transfer, fluid flow, components design, analysis techniques, etc. They are available at $3.00 per copy from

Clearinghouse for Federal Scientific
and Technical Information
National Bureau of Standards
U. S. Department of Commerce
Springfield, Virginia 22151

(J. H. Stang)

Selected Mechanical Properties of Cladding and Structural Materials

Iron-Base Alloys

General Electric[15] is investigating the impact properties of a number of Fe-Cr-Al-Y alloys. Figure IV-4 shows the specimen used, and Fig. IV-5 shows the curves obtained to date. The 2541 alloy undergoes ductile-to-brittle transition at about 140°C, the 1541 alloy at about 170°C, and the 0561 alloy at about 200°C.

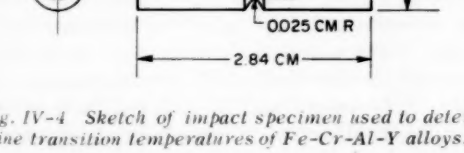

Fig. IV-4 Sketch of impact specimen used to determine transition temperatures of Fe-Cr-Al-Y alloys.[15]

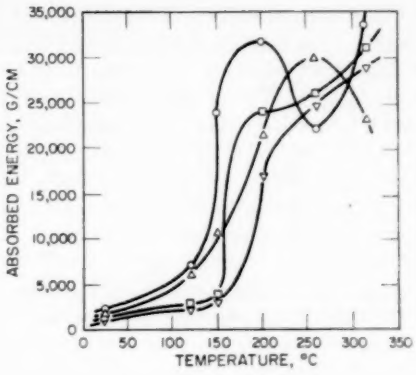

Fig. IV-5 Absorbed energy as a function of temperature for a series of Fe-Cr-Al-Y alloys tested in the annealed condition.[15] ○, 2541 (Fe–25 Cr–4 Al–1 Y, wt.%); △, 1541 (Fe–15 Cr–4 Al–1 Y); □, 1041 (Fe–10 Cr–4 Al–1 Y); ▽, 0561 (Fe–5 Cr–6 Al–1 Y). (The ductile-to-brittle transition temperature occurs at the midpoint between maximum and minimum energy.)

Refractory Metals

The stress-rupture and creep-test results[15] for the molybdenum–50 at.% rhenium alloy and a number of tungsten-rhenium-molybdenum alloys are given in Tables IV-1 and IV-2. Figure IV-6 shows stress-rupture curves for molybdenum, rhenium, and four refractory-metal alloys at 1600°C. The molybdenum–50 at.% rhenium alloy is considerably stronger than unalloyed molybdenum. Table IV-2 indicates that the tungsten–30 at.% rhenium alloy has twice the stress-rupture life of tungsten–25 at.% rhenium at 1600°C. This is attributed to the presence of a finely dispersed sigma phase at the 1600°C test temperature. At 2000°C the sigma phase is completely in solution, and the tungsten–25 at.% rhenium alloy shows a higher strength as expected because of its higher tungsten content.

The activation energy, the activation volume, and the frequency factor for the plastic deformation of niobium at low temperatures (below 20% of the absolute melting point) were derived from creep tests at Aerospace Corp.[31] The results support the theory that overcoming the Peierls-Nabarro stress is the rate-controlling factor during the plastic deformation of the

Table IV-1 STRESS-RUPTURE AND CREEP-TEST RESULTS[15] OF MOLYBDENUM–50 AT.% RHENIUM AT 1600°C IN HYDROGEN*

Stress kg/mm²	Elongation in 2.54-cm gauge length, %	Linear creep rate, min⁻¹		Time, hr				
		Total train load	2.54-cm gauge*	1% elongation†	3% elongation†	5% elongation†	10% elongation†	Rupture
1.41	56	3.1×10^{-5}	1.7×10^{-5}	4.5	24.0	44.0	93.1	232.6
1.76	47	5.8×10^{-5}	3.5×10^{-5}	4.7	14.1	22.8	40.9	66.7
2.11	56	1.2×10^{-4}						40.3
2.81	48	2.7×10^{-4}						9.2
3.37	98	5.8×10^{-4}						3.0
4.22	109	1.3×10^{-3}	6.7×10^{-4}	0.2	0.3	0.4	0.6	1.1

*Specimens were annealed for 2 hr at 1600°C in hydrogen prior to testing.
†Measurements obtained with twin cathetometer using a 2.54-cm gauge length.

Table IV-2 STRESS-RUPTURE TEST RESULTS[15] FOR TUNGSTEN-RHENIUM-MOLYBDENUM ALLOYS IN HYDROGEN

Sheet	Nominal composition, at.%			Test temp., °C	Stress, kg/mm²	Time to rupture, hr	Elongation in 2.54-cm gauge length, %	Linear creep rate, min⁻¹
	W	Re	Mo					
	75	25		1600	4.22	90.0		
362	70	30		1600	4.22	177.0	38	2.5×10^{-5}
	75	25		1600	3.37	190.0		
360	60	30	10	1600	3.37	124.0	46	4.2×10^{-5}
308	40	30	30	1600	3.37	17.1	24	1.4×10^{-4}
386	50	30	20	1650	3.37	13.7	15	1.2×10^{-4}
382	40	30	30	1650	3.37	7.8	19	2.4×10^{-4}
	75	25		2000	1.05	100.0		
362	70	30		2000	1.05	85.3	29	2.7×10^{-5}
308	40	30	30	2000	1.05	18.0		
308	40	30	30	2000	0.70	73.5	33	5.7×10^{-5}

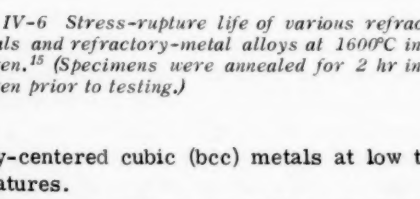

Fig. IV-6 Stress-rupture life of various refractory metals and refractory-metal alloys at 1600°C in hydrogen.[15] (Specimens were annealed for 2 hr in hydrogen prior to testing.)

body-centered cubic (bcc) metals at low temperatures.

The creep-rupture properties of electron-beam-melted niobium with additions of oxygen up to 0.35 wt.% were determined at 1038, 1260, and 1427°C at the Naval Research Laboratory.[32] Tests were conducted in vacuums of 1×10^{-5} torr or better. Rupture life was found to increase and the minimum creep rate to decrease with increasing oxygen content. There was no deleterious effect on ductility, even with high oxygen additions. The hardness increased as a function of cold work and oxygen content. Activation energies for high-temperature creep were determined which showed good agreement with the reported experimental activation energies for self-diffusion. At 1038°C, but not at 1260 or 1427°C, an anomalous behavior occurred, which was manifested by a rapid acceleration followed by a deceleration in the flow process. The irregularity, which is represented as a step in the creep curve, occurs only under certain combinations of temperature, stress, and oxygen content. It appears to be related to substructure formation and not to recrystallization or grain growth.

An investigation was carried out at ManLabs, Inc.,[33] to determine the nature of the tensile-ductility transition in recrystallized molybdenum strip of three interstitial contents. For a fine grain size, the tensile-ductility transition temperature (T_d) and the brittleness transition temperature (T_b) were found to be approximately the same; with increases in grain size, T_d is raised and T_b is lowered. A minimum in the fracture stress (σ_F) at T_d appears

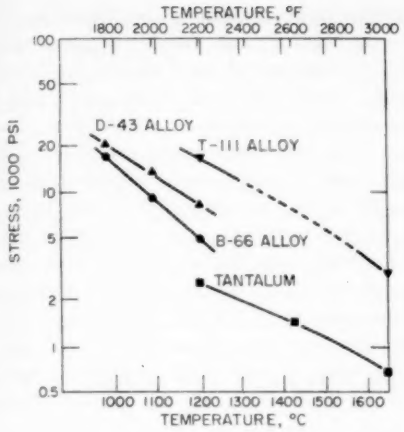

Fig. IV-7 Temperature dependence of stress to produce rupture in 1000 hr.[28]

to be associated with the temperature dependence of the "nicking" stress (σ_n). A 20% increase in σ_F was produced by prestraining above T_d. The mode of fracture initiation appears to be intergranular at T_d and below and cleavage above T_d. Crack initiation appears to be the controlling step in fracture for test temperatures above and below T_d. On the basis of a modification of the Cottrell relation for crack initiation, the increase in σ_F above T_d is associated with a decrease in both the flow locking parameter and the effective grain size.

The stress-rupture properties of tantalum, D-43, B-66, and T-111 are compared by investigators at Oak Ridge.[28] The T-111 alloy has superior stress-rupture properties, as is shown in Fig. IV-7. (J. A. De Mastry)

Metallurgical Aspects of Cladding Materials

Zirconium

Two relatively simple relaxation tests, uniaxial tensile and cantilever beam, have been developed by workers at Knolls[34] to provide a basis for judging the adequacy of annealing treatments in relieving stresses created in nuclear reactor components during fabrication. From these tests it is concluded that an annealing temperature of 1200°F for 3 hr will result in a reduction of residual stress to below 5000 psi for the following metals, listed in order of resistance to stress relaxation: hafnium, beta-quenched Zircaloy, Zircaloy weld metal, and alpha-annealed Zircaloy. It was desired to obtain the lowest values of time and temperature which would provide adequate relaxation but to avoid any deleterious metallurgical changes resulting from excessive time and temperature. Relaxation tests were performed in the range 932 to 1475°F for periods of less than 5 hr. Subsequently, nominal tensile properties were determined at 600°F.

Bassi and Camona[35] are using a new polishing and etching technique to determine metallographically the effects of annealing and high-temperature heat-treatments on Zircaloy-2. The effect of preferred orientation and stress on the directional precipitation of hydrides in Zircaloy-2 has been studied by workers at Oak Ridge.[36] Results to date indicate that preferred orientation has little, if any, influence on the orientation of hydride platelets in as-received sheet material, the hydride texture being similar to the orientation of slag inclusions in rolled steels. The observations also confirm a previous conclusion that hydrides precipitated under an elastic stress redistribute appreciably only when the stress axis is perpendicular to a high concentration of basal planes, and this redistribution increases as the stress increases.

An empirical method was developed[37] for determining the texture of polycrystalline Zircaloy-2 using Knoop microhardness data obtained from single crystals and from a specific pattern of hardness measurements on the unknown material. The microhardness measurements provide an approximation of the (0001) pole figure, and, with the use of a hardness contour map constructed from the single-crystal data, the hardness anisotropy of polycrystalline material can be determined.

The work by investigators at Knolls[38] on strengthening Zircaloy-4 by oxygen addition and/or beta heat-treatment has shown that strength increases can be obtained by both techniques. The addition of approximately 2800 ppm oxygen increases the longitudinal yield strength at 600°F about 40%; beta quenching plus a 932°F heat-treatment increases the longitudinal yield strength at 600°F about 100%. This work has also shown that other properties such as fatigue, weldability, and corrosion resistance are still acceptable and would not be

sacrificed for the increased strength. It has been shown that at least a 50% increase in yield strength at 600°F can be maintained in beta-quenched plus 932°F annealed Zircaloy-4 after subsequent heat-treatments of 2½ hr at 1300°F or 13½ hr at 1225°F, compared with alpha-worked and alpha-annealed Zircaloy-4. Beta holding time was observed to be relatively unimportant in producing a strength increase—the important factor being that all the piece attain the beta structure prior to quenching.

The effect of cooling rate and niobium content on the hardness of zirconium-niobium alloys was investigated[39] at Chalk River using a Jominy end-quench test. Specimens were subjected to cooling rates ranging from a water quench (1000°C/sec) to an air cool, and the niobium content ranged from 2.3 to 5.3 wt.%. The maximum as-quenched hardness of alloys containing more than 2.5 wt.% niobium was not produced by a water quench but by a cooling rate of 22°C/sec. After aging, the water-quenched material hardened appreciably to the highest value observed for the alloy, but the hardness of the material cooled at 22°C/sec changed very little. The maximum as-quenched hardness of alloys containing less than 2.5 wt.% niobium was produced by water quenching.

Group VIII Metals

The structure and properties of nickel-rich alloys of the nickel-cerium system have been investigated by the Russians[40] using microstructure analysis, hardness, and electrical-resistivity techniques. The alloys were cast, hot forged, annealed, and slow cooled. A cerium content of 0.05 wt.% is soluble in nickel and acts as a grain refiner. The solubility limit of cerium in nickel is 0.10 wt.% at room temperature and a maximum of 0.125 wt.% at 1200°C. Above the solubility limit the structure contains inclusions of Ni_5Ce. The addition of cerium to nickel in the solid-solution range increases the tensile strength of the alloy from 49.6 to 53.4 kg/mm².

The Japanese[41] have been investigating cobalt-tungsten alloys containing from 0 to 25 wt.% tungsten, especially their temper-hardening properties. Rods of the alloys were made by powder compaction, sintering, and hot swaging. Dilation behaviors through the alpha-to-beta and beta-to-alpha transformations and X-ray diffraction analyses of quenched or tempered specimens were examined in the alloys. The temper hardening and the time-temperature-transition diagram of the beta-to-alpha transformation were measured in detail for the cobalt–25 wt.% tungsten alloy. The crystal structure of this alloy quenched from 1100°C had the face-centered cubic lattice of the beta phase. When the quenched specimen was tempered at 600 to 675°C, the beta phase transformed slowly into the hexagonal close-packed lattice of the alpha phase, with an accompanying increase in hardness. The rate of the transformation was apparently controlled by diffusion. The maximum Vickers hardness number of 750 was attainable by optimum conditions of tempering.

Titanium

Russian investigators[42] have determined the modulus of elasticity and the shear modulus as a function of concentration in annealed (at 600°C) and quenched (from 900°C) ternary systems of titanium containing niobium and vanadium, niobium and molybdenum, vanadium and molybdenum, and the quaternary system containing the three alloying additions. The additions were made in equal amounts on a weight percent basis, and the alloys were prepared by melting under an argon atmosphere. Comparison of the results revealed that the elastic properties of the annealed specimens of the different alloys, plotted as a function of the concentration, exhibit identical behavior. This could be expected in view of the similarity of the behavior of titanium with the different alloying elements, indicated by the phase diagrams of the systems. The values of the elastic properties of alpha titanium are at least twice as great as those of the beta titanium; the alloying additions lowered these values in the case of the alpha phase but increased the values for the beta phase.

Refractory Metals

Deformation structures and glide dislocation configurations in zone-melted single crystals of molybdenum, deformed in tension at temperatures from 4.2 to 300°K, were examined by Lawley and Gaegher[43] using thin-film transmission electron microscopy. A majority of the crystals were oriented for single slip on the (0 1 1) [1 1 $\bar{1}$] system and were sliced and thinned parallel to the (0 1 1). At low temperatures

(≤200°K) the screw dislocations are straight and uniformly distributed on the slip plane. Glide configurations at 300°K are, in general, similar to those at the lower temperatures, except that the screw dislocations are wavy, the distribution is less uniform, and the number of secondary slip dislocations is lower. Dislocation tangling is restricted to the immediate vicinity of inclusions or grown-in dislocations. The observations are consistent with a picture of yielding in which the true elastic limit is largely independent of temperature and corresponds to the movement of edge segments. The large temperature dependence commonly associated with the macroscopic yield point is, in reality, a flow stress measured in a region of extremely high work hardening.

Cleavage surfaces produced in the brittle fracture of high-purity cast molybdenum have been shown by Limb[44] to vary greatly in appearance and in crystallographic relation. Some similarities with cleavage surfaces produced in high-purity cast chromium are notable. In addition, new types of characteristically marked cleavage surfaces have been identified, such as cleavage on (1 1 3) planes and on many planes of a ⟨1 1 3⟩ zone to give cylindrically shaped surfaces.

Twins in molybdenum-rhenium alloys containing 35 and 18 at.% rhenium, which were deformed at 20 and −195°C, were observed[45] by Ogawa and Maddin by means of transmission electron microscopy. A dislocation reaction between a slip dislocation and three twinning dislocations was often observed. Direct evidence of the operation of a pole mechanism for twinning was obtained. These observations suggest that the critical stage of twinning is the dissociation of slip dislocations in {1 1 2} planes into three twinning dislocations.

Researchers at General Electric[46] are investigating the tungsten-rhenium-molybdenum alloy system, with the primary objective of developing an alloy that will retain good ductility at room temperature after long exposure to hydrogen or argon at temperatures up to 2600°C. The tungsten−30 wt.% rhenium−30 wt.% molybdenum alloy has been developed, processed to sheet, and partially evaluated for service to 2600°C. The advantages of these alloys were identified as follows:

1. The molybdenum addition leads to a lower density than obtained in the tungsten−25 wt.% rhenium alloy (approximately 19% decrease).

2. The alloys are not embrittled by hydrogen at any temperature, a major advantage over tantalum alloys.

3. The alloy, as well as electron-beam welds of the alloy, appears to be resistant to embrittlement on prolonged heating (100 to 1000 hr) in hydrogen or argon in the 1200 to 2600°C temperature range.

4. Compacts of tungsten-rhenium-molybdenum can be successfully sintered at 2640°C, compared to the 3000°C temperature required for the tungsten−25 wt.% rhenium alloy. Other processing procedures employed for the latter alloy can be directly applicable to that of the molybdenum-containing alloys, which are more ductile and more fabricable.

5. The elevated-temperature strength approaches that of rhenium at 1600°C in the low stress range.

6. Measured melting point of the tungsten−30 wt.% rhenium−30 wt.% molybdenum alloy is above 2760°C.

The effects of grain size and impurity level on the tensile strength and ductility of powder-metallurgy tungsten has been investigated[47] at the Jet Propulsion Laboratory by comparing recrystallized coarse- and fine-grained undoped tungsten with recrystallized fine-grained doped tungsten. Tests were conducted in vacuum at a strain rate of 0.02/min from 2500 to 5000°F. Both fine-grained materials were about the same strength, and both were stronger than the coarse-grained material. Ductility for the doped (higher impurity level) fine-grained tungsten was lower than for the undoped fine-grained tungsten in which stress-induced grain growth occurred more readily. Stress-induced grain growth correlates in a general way with ductility, measured by either reduction in area or elongation. High and low values of stress-induced grain growth are associated with high and low values of ductility, respectively. In the intermediate-temperature region, between approximately 50 and 65% of the absolute melting point, where a ductility minimum occurs, grain-boundary sliding and its effects (i.e., void nucleation, growth, and intercrystalline fracture) appear to reduce ductility in both fine-grained materials.

The kinetics of yield-point return in commercially pure tungsten were determined by Baird and Hartley.[48] The activation energy for yield-point return is of the order of 96 kcal/

mole. The results demonstrate that the phenomena in impure tungsten can occur by a process other than interstitial pinning of free dislocations. The kinetics of the process and metallographic observations support the hypothesis that dislocations are immobilized by polygonization or removed by migration to large-angle grain boundaries.

Some answers to the question of the interaction between tungsten and niobium carbide have been provided by Vil'k et al.[49] who have studied the phase equilibrium between tungsten and the carbides of niobium, $NbC_{0.98}$ and $NbC_{0.85}$, in the temperature range of 2000 to 3000°C, using methods of metallographic and X-ray analysis and microhardness measurements. The investigated sections tungsten-$NbC_{0.98}$ (from 5 to 95 wt.% tungsten) and tungsten-$NbC_{0.85}$ (from 5 to 50 wt.% tungsten) are not pseudobinary and pass through the regions of two-phase equilibrium in the solid state alpha plus delta (solid solutions based on tungsten and W_2C), alpha plus gamma (solid solutions based on tungsten and NbC), alpha plus beta (solid solutions based on NbC and Nb_2C), and a region of three-phase equilibrium alpha plus delta plus gamma. The existence of ternary compounds of the tungsten-niobium-carbon system in the region of alloy compositions investigated was not detected, but a liquid phase exists at temperatures of a minimum of 2600°C. A binary eutectic alpha minus delta, a ternary eutectic alpha minus delta minus gamma, and a ternary peritectic alpha minus beta minus gamma exist in this region. The investigators present hypothetical isothermal sections of the concentration triangle tungsten-niobium-carbon for temperatures of 2000, 2600, 2700, and 3000°C and a polythermal vertical section of the tungsten-NbC system.

Deformation studies on niobium-vanadium alloys were made at Oak Ridge,[50] and results indicate good room-temperature ductility combined with exceptionally high hardness, work-hardening rates, and strength over the composition range from 20 to 70 wt.% vanadium. This behavior is due to the ability of the alloys to deform by twinning. The twinning transition temperature was found to increase with increasing vanadium content or annealing temperature and was a maximum at about 140°C in the 40 wt.% vanadium alloy. The addition of up to 0.7 wt.% oxygen lowered the twinning transition temperature in all alloys tested.

Hull, McIvor, and Owen have made studies[51] of the effects of grain size, temperature, and substructure on the change in dislocation density and distribution with plastic strain in tantalum and the relation of these changes to the change in flow stress with strain. In all specimens studied it was found that, as the deformation increased, the grain boundaries became thicker and more fuzzy because of dislocations either accumulating or initiating at the boundary. However, it is unlikely that these dislocations are formed by the blocking of a slip band because where this occurs the new dislocations are readily identified.

Available data concerning the effects of solutes on the strength and hardness of niobium, tantalum, tungsten, and molybdenum have been collected and reviewed by Siegle.[52] A correlation was found between the strengthening effects of substitutional solutes and group number in the periodic table, which suggests that the rate of strengthening of the above-mentioned refractory metals by substitutional solutes is related primarily to the increase in electron-to-atom ratio. Size effect played a secondary role in solid-solution strengthening. A feature of the alloying behavior of the refractory metals is the possibility of the interactions between interstitial and substitutional solutes, which are known, or presumed, to underlie several types of anomalies in the variation of strength and hardness with solute content.

The trends and status of the development of molybdenum, tungsten, tantalum, and niobium alloys for elevated-temperature applications were reviewed by Michael and Gentry[53] for the Agard Conference on Refractory Metals at Oslo-Blindern, Norway. The effects of alloying and metallurgical treatment on elevated-temperature strength are discussed in terms of available semiempirical concepts for strengthening. Other factors of importance which were considered in the discussion are low-temperature ductility, fabricability, and weldability.

The thermal expansion of tungsten, molybdenum, tantalum, and niobium up to 2000°C, and of zirconium up to 1450°C, has been determined by Amonenko, V'yugov, and Gumenyuk[54] using a vacuum resistance dilatometer. Graphs are given for the elongation and coefficients of linear expansion of the refractory metals as a function of temperature.

A bibliography[55] containing 916 references on the refractory metals tungsten, molybdenum,

tantalum, niobium, and rhenium and their alloys has been prepared, which covers U. S. and foreign journals and reports published from 1961 through 1963.

Miscellaneous

On the basis of data gathered by Ellis and Wilhelm[56] by means of X-ray diffraction, chemical analysis, and metallographic techniques, a constitution diagram is proposed for the niobium-tin binary system which is not in agreement with that of other investigators. The equilibrium solubility of niobium in liquid tin varies from 0.027 wt.% at 580°C to 0.198 wt.% at 1000°C. The equilibrium solubility of tin in niobium varies from approximately 2.5 wt.% at 550°C to about 3.0 wt.% at 1000°C. In addition to Nb_3Sn, two other intermetallic compounds, Nb_3Sn_2 and Nb_2Sn_3, were found in the alloys of the system. The compounds have body-centered and face-centered orthorhombic crystal structures, respectively. All compounds in the system decompose peritectically: Nb_3Sn at about 2130°C, Nb_3Sn_2 at about 915°C, and Nb_2Sn_3 at about 820°C. Lattice parameters of the compounds were determined and are presented.

A great deal of effort[57] has been concentrated on the phase equilibria, thermodynamic properties, alloy theory, and the plastic deformation behavior of rare-earth metals and alloys, including crystal-structure determinations of intermediate compounds of the rare earths. The effects of alloy additions of rare-earth metals on the mechanical and oxidation properties and crystal structure of zirconium have been investigated[58] at Rensselaer Polytechnic Institute.

Ukrainian investigators have reported[59] the results of their studies on the interaction between carbon and the transition metals of Groups IV, V, and VI of the periodic table in binary, ternary, and quaternary systems with respect to crystal structure and phase diagrams. (N. M. Griesenauer)

Diffusion Studies

An extensive investigation of self-diffusion in selected nickel-base solid solutions was made at Tohoku University in Sendai, Japan.[60] Self-diffusion coefficients of nickel and chromium in nickel-chromium alloys containing 0 to 30 at.% chromium were measured at 1040 to 1300°C, by means of lathe sectioning techniques, using polycrystalline specimens with a grain size of 1 to 4 mm. Also, self-diffusion coefficients of nickel and chromium in nickel-chromium alloys containing 0 to 100 at.% chromium and of nickel and tungsten in nickel-tungsten alloys containing 0 to 9 at.% tungsten were measured by the same method. In the nickel-chromium systems, studied in the temperature range of 1040 to 1300°C, chromium atoms diffused more rapidly than nickel atoms, and the ratio of the diffusion coefficient of chromium to that of nickel was about 1.6, independent of the chromium concentration over the whole temperature range. Diffusion rates of both elements decreased slightly with increasing chromium content. In the nickel-copper system, measurements were taken near the melting point of each alloy. Copper atoms appeared to diffuse more rapidly than nickel. The diffusion-coefficient ratios for copper/nickel ranged from 2.5 to 6 over the temperature range examined and increased with increasing copper content. In the nickel-tungsten system, the nickel atoms diffused more rapidly than tungsten, the ratio of diffusion coefficients for nickel/tungsten ranging between 3 and 4 over the temperature range of 1100 to 1400°C. Diffusion rates increased for both elements with increasing tungsten concentration. The results of these studies are given in Table IV-3 in the form of frequency factors and activation energies for Arrhenius type equations.

Reported in a French paper[61] is a study on the diffusion of plutonium in magnesium; used in the study were couples of a two-phase alloy of magnesium-plutonium precipitated against pure magnesium. Concentration was measured with an electron microprobe analyzer. The diffusion coefficients were calculated by the Matano method and ranged between 2×10^{-11} and 50×10^{-11} cm^2/sec for temperatures between 420 and 540°C, with concentrations of 1 at.% plutonium in magnesium.

The coefficients of self-diffusion of stabilized zirconium were derived from an analysis of experimental results as reported in a Russian journal.[62] For alpha-zirconium, $D = 1 \times 10^{-5} \exp(-40{,}000/RT)$ cm^2/sec, and for beta zirconium, $D = 2 \times 10^{-4} \exp(-40{,}000/RT)$ cm^2/sec. The author suggests that diffusion occurs by a cyclic mechanism that becomes complicated by

Table IV-3 ACTIVATION ENERGIES AND FREQUENCY FACTORS FOR SELF-DIFFUSION IN THE SYSTEMS[60] NICKEL-CHROMIUM, NICKEL-COPPER, AND NICKEL-TUNGSTEN

Diffusing element	At.% of second constituent	Frequency factor, cm^2/sec	Activation energy, kcal/mole
Ni	0 Cr	1.9	68.0
Ni	10.0 Cr	3.3	70.2
Ni	19.9 Cr	1.6	68.5
Ni	29.7 Cr	2.9	70.5
Cr	100 Ni	1.1	65.1
Cr	90 Ni	1.4	66.5
Cr	80.1 Ni	1.9	67.7
Cr	70.3 Ni	3.2	69.4
Ni	0 Cu	1.9	68.0
Ni	13.0 Cu	35	74.9
Ni	45.4 Cu	17	66.8
Ni	78.5 Cu	0.063	49.7
Ni	100.0 Cu	1.7	55.3
Cu	100 Ni	0.57	61.7
Cu	87 Ni	1.5	63.0
Cu	54.6 Ni	2.3	60.3
Cu	21.5 Ni	1.9	55.3
Cu	0 Ni	0.33	48.2
Ni	0 W	1.9	68.0
Ni	1.7 W	30	76.5
Ni	5.3 W	58	80.6
Ni	9.2 W	1.1	70.3
W	100 Ni	2.0	71.5
W	98.3 Ni	2.2	73.1
W	94.7 Ni	17	80.5
W	90.8	1.4	74.5

the existence of large numbers of defects in the unstabilized metal.

A paper was recently presented summarizing the extensive research that has been conducted at Oak Ridge[63] on diffusion in body-centered cubic metals. Included in the summary are results of investigations of diffusion in beta-zirconium, vanadium, niobium, and tantalum, some of which have been previously reviewed here. In the experimental work radioactive-tracer methods combined with mechanical sectioning techniques were used to determine activity profiles after the specimens had been subjected to isothermal diffusion anneals. One of the sectioning techniques included is the anodizing and stripping of the anodic film from the surface; this technique has permitted the removal of extremely thin sections, in some cases less than 100 A thick. Emphasized in the discussion in this paper is the marked curvature in Arrhenius type plots of the diffusion data over wide temperature ranges such as the data for diffusion of ^{95}Zr and ^{95}Nb in beta zirconium from 900 to 1800°C. The possibilities of the variation of the activation energy with temperature for a given diffusion process and of the variation in the mechanism in different temperature ranges are discussed in general terms. Also in the paper a previously reported "near-surface effect" for diffusion of ^{95}Nb in tantalum is clarified in terms of volume diffusion and diffusion enhancement within the specimens due to short-circuiting paths. The care required in interpreting low-temperature diffusion data because of the large structure-sensitive contributions to overall penetration plots is emphasized.

Radiation enhancement of diffusion can be the result of either the interstitials or vacancies that are produced in equal numbers during irradiation. It is of considerable interest in this regard to note analyses, also conducted at Oak Ridge,[37] of effects in a copper–15 at.% aluminum alloy on the basis of vacancy motion vs. interstitial motion. Analyses of the relative kinetics of different experimental runs and of interrupted irradiation runs indicate in both cases that the interstitial is the diffusion-enhancing, or active, defect.

(A. N. Ashurst and D. C. Carmichael)

Ceramic Technology

Oxygen pickup by powdered ZrO_2 has been shown by Smith[64] to be primarily a surface phenomenon. The proposed mechanism is that there is a primary adsorption of molecular oxygen and then a dissociation into an adsorbed monolayer of atomic oxygen. In studies covering the temperature range of 400 to 900°C and an oxygen pressure range of 10^{-5} to 760 mm Hg, the activation energy was found to be 35 kcal/mole for the adsorption of molecular oxygen and 58 kcal/mole for the adsorption of atomic oxygen. Only the molecular-oxygen adsorption was oxygen-pressure dependent. An atomic monolayer will adsorb irreversibly, but the adsorbed molecular oxygen can be reversibly adsorbed (35 kcal/mole) and desorbed (53 kcal/mole).

Determinations of electrical conductivity on monoclinic ZrO_2 show that this material is an amphoteric semiconductor at 1000°C, with the transition from n type to p type conductivity occurring at 10^{-16} atm of oxygen. Vest, Crawford, and Tripp[65] speculated that on the low-oxygen side of stoichiometry, assumed at an oxygen pressure of 10^{-16} atm, the conductivity

is attributable to ionized oxygen vacanices. On the high oxygen-partial-pressure side, there was a clear indication of conductivity attributed to completely ionized zirconium vacancies. In calcia-stabilized zirconia the conductivity behavior was so dominated by the calcium content as to make the determination on conductivity mechanisms difficult.

Unstabilized zirconia has been fabricated by hot pressing by Chaklader and Baker.[66] Optimum hot-pressing conditions are not yet established, but compressive strengths of 15,000 to 47,000 psi and densities of 90 to 95% of theoretical have been achieved.

The heats of formation of ZrC and HfC were determined by the Bureau of Mines[67] by using calorimetric measurements. Previous data are not known on HfC, and the data on ZrC vary with different investigators. The variations are attributed principally to uncertainties involved in correcting for impurities. The Bureau of Mines' data were determined on better materials than were available before, ZrC with 0.496 wt.% impurities and HfC with 0.137 wt.% impurities. The energies of combustion were measured by combustion calorimetry, and the heats of combustion and formation were derived. The results are the following:

For ZrC,

$$\Delta H_{298.15} \text{ (combustion)} = -308.60 \pm 0.55 \text{ kcal/mole}$$

$$\Delta H_{298.15} \text{ (formation)} = -47.0 \pm 0.6 \text{ kcal/mole}$$

and for HfC,

$$\Delta H_{298.15} \text{ (combustion)} = -306.08 \pm 0.20 \text{ kcal/mole}$$

$$\Delta H_{298.15} \text{ (formation)} = -52.3 \pm 0.4 \text{ kcal/mole}$$

When exposed to high rates of heat transfer, glasses and ceramics studied by Dugdale, McVickers, and Ford[68] crazed, flaked, weakened, and eroded, depending on the particular material and energy delivered. The exposure to pulsed-arc discharge heat sources that could deliver 17 and 30 joules/cm^2 to their surface caused glasses to flake off. The flakes appeared to be caused by tensile cracking on cooling after viscous flow during heating and not by cracking in compression. The behavior of electrical porcelains and alumina ceramics was more complex, showing cracking in compression and spalling during heating. The presence of a glassy phase tended to inhibit these effects. Deformation of alumina while hot involved twinning.

A refractory material of exceptional strength and thermal-shock resistance has been produced by pyrolytically codepositing ZrC and graphite[69] by Lepie. When codeposited with graphite, the carbide grains are kept very small, probably below 200 A. Flexural strengths ranged from 50,000 to 100,000 psi at room temperature and increased with temperature, at temperatures up to 2000°C. The very high-strength materials contained about 78 wt.% carbon. Pyrolytic ZrC in stoichiometric proportions has long, columnar grains. As greater amounts of excess carbon are deposited, the carbide grains become smaller and irregular. At high carbon contents, when the carbon becomes the continuous phase, the microstructure of the carbide and graphite composite resembles that of pyrolytic graphite.

Studies of yttria-bearing alumina metallized with tungsten (Ref. 70) indicate that the adherence is attributable primarily to the presence of an yttria-tungstate phase, $Y_2O_3 \cdot WO_3$. In the initial stages of the metallizing during firing in wet hydrogen, the tungsten oxidizes to WO_3 and some oxide remains at temperatures as high as 800°C. The WO_3 reacts with the Y_2O_3 at the grain boundaries of the alumina-yttria ceramic. As the firing temperature is raised, some of the $Y_2O_3 \cdot WO_3$ is reduced, and Y_2O_3 and some remaining $Y_2O_3 \cdot WO_3$ migrates into the tungsten. At the maturing temperature of 1700°C, the tungsten densifies and the tungsten-and-yttria mixture coalesces into a dense, hard structure. It is speculated that a similar adherence mechanism for tungsten metallizing of Al_2O_3 could be achieved with oxides other than Y_2O_3 which form tungstates. Examples are CaO, MgO, and Fe_2O_3.

For metallizing ceramics when it is desirable to avoid the high-temperature firing process usually required for maturing the metallized surface, a technique used at Sandia,[71] namely, deposition of metal with the aid of a gas discharge, may be suitable. In this technique the ceramic to be coated is made part of the cathode of a high-voltage d-c circuit, a gas discharge is established with an inert gas, and the metal to be deposited is evaporated into the positive glow region of the gas discharge. Prior to the evaporation step, the ceramic surface is cleaned by low-energy ion bombardment. The ionized metal atoms, during the metallizing stage, are accelerated across the electric field

and deposited on the ceramic. The energy is confined to the surface, giving high surface temperatures without the need to heat the bulk of the ceramic. Metallizing films of aluminum in combination with copper or gold have been deposited on ferroelectric ceramics, and films of titanium or chromium in combination with copper or gold have been used to metallize high-alumina ceramics. Joint strengths of 3000 to 8000 psi have been achieved. (D. J. Bowers)

Radiation Effects in Nonfuel Materials

Two excellent summaries have been published pertaining to the radiation-induced property changes in structural materials. One is a monograph by Trudeau[72] presented to show how neutron irradiation affects the toughness of ferritic steels and to point out the associated implications. The other is a summary of tabular data prepared by Bush,[73] including information on the effects of irradiation at elevated temperatures and the effects of postirradiation annealing.

Measurements were made by the Naval Research Laboratory[74] of Charpy V-notch transition temperatures of the modified type A-302B pressure-vessel steel used in construction of the pressure vessel for the Yankee Atomic Power Reactor and of a widely distributed and well-documented heat of A-302B steel after equal irradiations at about 282°C (540°F) to a maximum exposure of 9×10^{19} neutrons/cm^2. The difference in the effects on the two steels can be noted in Fig. IV-8. It appears that increase in transition temperature for the Yankee vessel is nearly 100°F greater than that for the reference steel. Postirradiation annealing at 400 and 455°C (750 and 850°F) resulted in significant recovery of initial properties.

Russian workers have demonstrated[75] that gamma irradiation of white iron at temperatures above the first-stage graphitizing temperature accelerates graphitization, providing the chromium content of the iron is low (<0.5 wt.%). This was found by comparing microstructures of control specimens annealed 12 hr at 800°C (1470°F) with those of specimens irradiated with 400 r/sec gammas from ^{60}Co sources for the same time at the same temperature. Gamma rays have the advantage over

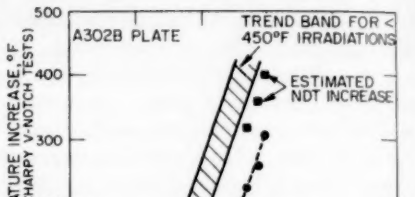

Fig. IV-8 Trend line for 540°F irradiations of A-302B steel, showing difference in neutron embrittlement between Yankee-vessel and reference steel.[74] ▲, ●, 6-in. reference steel; ■, 7⅞-in. Yankee-vessel steel.

neutrons or energetic beta particles for this application since they neither directly decompose the carbide phase nor induce radioactivity in the cast iron. Similar treatments at 700°C (1290°F) produced no visible changes in the white-iron structure, but X-ray analysis showed that the irradiation had caused pronounced internal changes in the cementite phase.

Researchers at Oak Ridge[37] have studied the effect of neutron irradiation at temperatures above and below one-half the absolute melting point on the tensile properties of type 304 stainless steel. The effect of the irradiation on the stress-strain behavior can be seen in Fig. IV-9. The curves indicate that irradiation at temperatures below 450°C, followed by tensile tests above 450°C, alters the deformation characteristic, whereas the same irradiation followed by tests at higher temperatures does not. In both cases the ductility is reduced, but, when the testing is done above 450°C, there is a greater reduction in ductility and the fracture is intergranular. The reduced ductility of specimens tested at the higher temperature, thought to result from thermal-neutron rather than fast-neutron effects, did not anneal out at temperatures as high as 1000°C. A study was made of the effects of various heat-treatments prior to irradiation on the postirradiation ductility. Results suggest that any heat-treatment that will improve the preirradiation ductility will also increase the postirradiation ductility of this alloy.

Workers at Vallecitos[3] studied the tensile and burst properties of Zircaloy-2 and Zircaloy-4 at room temperature and 345°C after exposures to 4×10^{20} and 1.6×10^{21} neutrons/cm^2. The ultimate strength showed an increase of about 25,000 psi at both temperatures after an exposure of 4.0×10^{20} neutrons/cm^2. The ductility as measured by total elongation was reduced considerably after 1.6×10^{21} neutrons/cm^2.

Koppenaal[76] determined the stress to produce a plastic strain of 2×10^{-6} in copper single crystals at 27 and −196°C (80 and −321°F) after exposures to approximately 10^{16} to 10^{20} neutrons/cm^2 at 60°C (140°F). At the higher temperature he found that the stresses were approximately 0.02 kg/mm^2 for annealed material, 0.3 kg/mm^2 for specimens irradiated to about 10^{16} neutrons/cm^2, and greater than 5.0 kg/mm^2 for specimens irradiated to about 10^{20} neutrons/cm^2. These results suggest that the stress is proportional to the cube root of the neutron dose.

Canadian workers[77] have studied the damage rate and recovery of the residual electrical resistivity in aluminum and gold after neutron irradiation at 1.74°K. The effects of impurities, quenched-in vacancies, and dislocations on the properties were studied. They found that the damage rate in aluminum was unchanged for impurity concentrations of less than 0.5 at.% and for quenched-in vacancy concentrations of less than 0.002 at.%. Dislocation concentrations of about 2×10^{10}/cm^2 in aluminum and about 1×10^{11}/cm^2 in gold were found to increase the damage rates by 35 and 50%, respectively. The results were interpreted in terms of channeling in aluminum and collision chains in gold.

Studies have been made by a Swedish investigator[78] to compare the energy release from irradiated molybdenum with that from cold-worked molybdenum. The samples compared were irradiated to 1×10^{17} fast neutrons/cm^2 at 35°C, and 40% cold worked in compression. The stored energy release, studied isothermally over the 75 to 186°C (170 to 370°F) temperature range, was about 20 times as much for the irradiated material (50 cal/mole) as for the cold-worked sample (2.6 cal/mole). The activation energy for the release process was greater by a factor of about 3 for the cold-worked material. (F. R. Shober)

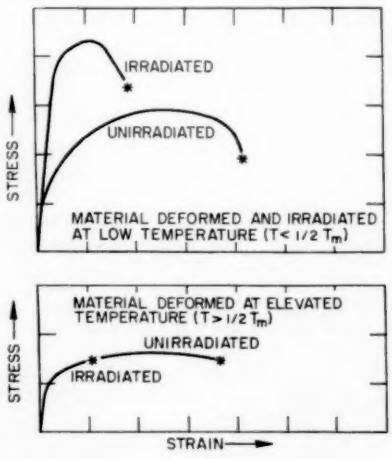

Fig. IV-9 Effect of irradiation on the stress-strain curve of stainless steel.[37]

References

1. Hanford Atomic Products Operation, Reactor and Fuels Laboratory Monthly Report, August 1964, USAEC Report HW-83820-A, Sept. 15, 1964. (Classified)
2. W. K. Winegardner, Fretting Corrosion in the Plutonium Recycle Test Reactor, USAEC Report HW-80021, Hanford Atomic Products Operation, March 1964.
3. General Electric Company, Atomic Power Equipment Department, Fuel Cycle Program. A Boiling Water Reactor Research and Development Program, Fifteenth Progress Report, January–June 1964, USAEC Report GEAP-4641, July 15, 1964.
4. I. H. Dyce, Corrosion of Zircaloy Fuel Cladding. The Influence of High Heat Fluxes, *Nucl. Eng.*, 9: 253-255 (July 1964).
5. C. Roy, Hydrogen Distribution in Oxidized Zirconium Alloys by Autoradiography, Canadian Report AECL-2085, September 1964.
6. D. L. Douglass, Corrosion Mechanism of Zirconium and Its Alloys, III, Solute Distribution Between Corrosion Films and Zirconium Alloy Substrates, USAEC Report GEAP-4521 (EURAEC-1181), General Electric Company, Vallecitos Atomic Laboratory, Apr. 1, 1964.
7. L. E. Link (Ed.), Reactor Technology, Selected Reviews—1964, USAEC Report TID-8540, Argonne National Laboratory, July 1964.
8. W. C. Rion, Jr. (Comp.), Stainless Steel Information Manual for the Savannah River Plant, Vol. I, Properties, USAEC Report DP-860 (Vol. 1), E. I. du Pont de Nemours & Co., Inc., July 1964.
9. E. L. Long, Jr., and C. Michelson, Some Observations of the Intergranular Corrosion of Irradi-

ated Type 304 Stainless Steel, USAEC Report ORNL-3684, Oak Ridge National Laboratory, November 1964.

10. Hanford Atomic Products Operation, Reactor and Fuels Laboratory Monthly Report, October 1964, USAEC Report HW-84474A, Nov. 16, 1964. (Classified)
11. Société d'Études de Recherches et d'Applications pour L'Industrie, Studies of Steel Corrosion in High-Temperature Water and Steam. Quarterly Report No. 8, April 1–June 30, 1964, USAEC-Euratom Report EURAEC-1122, July 29, 1964.
12. E. C. Potter and G. M. W. Mann, Oxidation of Mild Steel in High-Temperature Aqueous Systems, *First International Congress on Metallic Corrosion*, pp. 417-423, Butterworths & Co. (Publishers) Ltd., London, 1962.
13. Westinghouse Electric Corp., Atomic Power Division, Yankee Core Evaluation Program Quarterly Progress Report for the Period Ending September 30, 1964, USAEC Report WCAP-6064, October 1964.
14. W. L. R. Rice (Ed.), Nuclear Fuels and Materials Development, USAEC Report TID-11295(3rd ed.), July 1964.
15. General Electric Company, Advanced Technology Services, High Temperature Materials Program Progress Report No. 41, Part A, USAEC Report GEMP-41A, Nov. 30, 1964.
16. Hanford Atomic Products Operation, Metallurgy Research Operation, Quarterly Progress Report, April–June 1964, USAEC Report HW-82651, July 15, 1964.
17. F. W. Albaugh, Reactor and Fuels Laboratory Monthly Report, September 1964, USAEC Report HW-84291A, Hanford Atomic Products Operation, Oct. 15, 1964. (Classified)
18. Hanford Atomic Products Operation, Research and Development Programs Executed for Division of Reactor Development, Quarterly Progress Report, January–March 1964, USAEC Report HW-81984, September 1964.
19. General Electric Company, Advanced Technology Services, High Temperature Materials Program Progress Report No. 42, Part B, USAEC Report GEMP-42B, Dec. 18, 1964. (Classified)
20. S. N. Shah and J. A. Menzies, Oxidation of 2.25 Cr–1 Mo Steels from Different Sources in CO_2/5% CO/500 ppm H_2O at 550°C, Interim Report, British Report TRG-Report-757, March 1964.
21. R. W. Bartlett, Tungsten and Molybdenum Oxidation Kinetics at Extremely High Temperatures, Report ML-TDR-64-290, Philco Corporation, September 1964.
22. R. W. Bartlett and P. R. Gage, Investigation of Mechanisms for Oxidation Protection and Failure of Intermetallic Coatings for Refractory Metals, Report ASD-TDR-63-753 (Part II), Philco Corporation, July 1964.
23. J. J. Buchinski and E. H. Girard, Study of Ductile Coatings for the Oxidation Protection of Columbium and Molybdenum Alloys, Final Report on Bureau of Naval Weapons Contract NOw63-0706-C, Metals & Controls. Inc., October 1964.
24. R. J. Cash, R. M. Fisher, and M. R. Core, Compatibility Studies of Several Molten Uranium and Thorium Alloys in Niobium, Tantalum, and Yttrium, USAEC Report IS-888, Ames Laboratory, Iowa State University, February 1964.
25. W. Chubb and S. J. Paprocki, Development of Advanced High-Temperature Nuclear Materials During August Through October 1964, USAEC Report BMI-1702, Battelle Memorial Institute, Nov. 1, 1964. (Classified)
26. Atomics International, AEC Unclassified Programs, Quarterly Technical Progress Report, July–September 1964, USAEC Report NAA-SR-10501, Dec. 1, 1964.
27. E. A. Kovacevich and R. L. Salley, Mass Transfer Tests with Two-Phase Flow, Report APL-TDR-64-119, Garrett Corp., AiResearch Mfg. Division of Arizona, Nov. 20, 1964.
28. Oak Ridge National Laboratory, Metals and Ceramics Division Annual Progress Report for Period Ending June 30, 1964, USAEC Report ORNL-3670, October 1964.
29. Oak Ridge National Laboratory, Nov. 5, 1964. (Unpublished)
30. Quarterly Technical Progress Report for Period Ending December 31, 1964. SNAP 50/SPUR for Period Ending December 31, 1964, Report APS-5152-R1, Garrett Corp., AiResearch Mfg. Division of Arizona, Jan. 18, 1964.
31. G. A. Stone and H. Conrad, Creep of Niobium at Low Temperatures, Report ATN-64 (9236)-9, Aerospace Corp., Feb. 21, 1964.
32. J. Stoop and P. Shahinian, Effect of Oxygen on Creep-Rupture of Niobium, USAEC Report NRL-6095, Naval Research Laboratory, Mar. 18, 1964.
33. B. S. Lement and K. Kreder, The Tensile Ductility-Transition in Molybdenum, Report WADD-TR-61-181 (Pt. IV), ManLabs, Inc., July 1964.
34. P. T. Lovejoy and G. J. Moyar, Stress Relaxation Studies of Hafnium and Zircaloy-2 and -4, USAEC Report KAPL-M-6155, Knolls Atomic Power Laboratory, Apr. 24, 1964.
35. A. Bassi and G. Camona, Metallographic Observations on Annealing and High Temperature Processing of Zircaloy-2, *Energia Nucl. (Milan)*, 11: 370-378 (July 1964).
36. Oak Ridge National Laboratory, November 1964. (Unpublished)
37. Oak Ridge National Laboratory, September 1964. (Unpublished)
38. A. E. Bibb, A. P. Beard, and J. R. Fascia, Investigations on Strengthening of Zircaloy-4 by Heat Treatment and Addition of Oxygen, USAEC Report KAPL-3036, Knolls Atomic Power Laboratory, May 1964.
39. B. A. Cheadle, The Effect of Cooling Rate on the Hardness of Zirconium-Niobium Alloys, Canadian Report CRRM-1200, June 1964.
40. U. K. Duysemaliev, Solubility of Cerium in Nickel and Mechanical Properties of Nickel-Cerium Alloys, *Akad. Nauk Kaz. SSR, Tr. Inst. Met. i Obogashch.*, 10(3): 59-62 (1964).
41. T. Toda, On the Temper Hardening Properties of Cobalt-Tungsten Alloys, *Nippon Kinzoku Gakkaishi*, 28: 72-78 (1964).
42. S. G. Fedotov and O. K. Belousov, Elastic Properties of Multicomponent Titanium Alloys with Molybdenum, Vanadium, and Niobium, *Dokl. Akad. Nauk SSSR*, 155: 1387-1390 (Apr. 21, 1964).
43. A. Lawley and H. L. Gaigher, Deformation Struc-

tures in Zone-Melted Molybdenum, *Phil. Mag.*, Series 8, 10: 15-33 (July 1964).

44. H. R. Limb, Cleavage Fracture in Cast Molybdenum of High Purity, *J. Inst. Metals*, 92: 423-426 (August 1964).
45. K. Ogawa and R. Maddin, Transmission Electron-Microscopic Studies of Twinning in Molybdenum-Rhenium Alloys, *Acta Met.*, 12: 713-721 (June 1964).
46. General Electric Company, Advanced Technology Services, High-Temperature Materials Program Progress Report No. 39, Part A, USAEC Report GEMP-39A, Sept. 30, 1964.
47. J. L. Taylor, D. H. Boone, and O. W. Simmons, Effect of Grain Size and Impurities on Tensile Strength and Ductility of Tungsten from 2500 to 5000°F in Vacuum, USAEC Report JPL-TR-32-632, Jet Propulsion Laboratory, July 1, 1964.
48. W. R. Baird and C. S. Hartley, Kinetics of Yield-Point Return in Unalloyed Tungsten, *J. Inst. Metals*, 92: 181-182 (February 1964).
49. Yu. N. Vil'k, R. G. Avardbe, V. S. Neshpor, T. P. Ryzhkova, and Yu. A. Omelchenko, On the Question of the Interaction of Niobium Carbide and Tungsten, *Teplofiz. Vysokikh. Temp.*, 2: 274-279 (1964).
50. D. O. Hobson, Deformation Twinning in the Columbium-Vanadium Alloy System, USAEC Report ORNL-3678, Oak Ridge National Laboratory, September 1964.
51. D. Hull, I. D. McIvor, and W. S. Owen, The Variation of Flow Stress with Substructure in Tantalum, *The Reaction Between the Structure and Mechanical Properties of Metals, Vol. II*, pp. 595-612, Her Majesty's Stationery Office, London, 1963.
52. L. L. Siegle, Structural Considerations in Developing Refractory Metal Alloys, *The Science and Technology of Tungsten, Molybdenum, Tantalum, Niobium, and Their Alloys*, pp. 63-93, Pergamon Press, Inc., Oxford, 1964.
53. A. B. Michael and W. O. Gentry, The Trend and Status of Development of Refractory Metal Alloys, *The Science and Technology of Tungsten, Tantalum, Molybdenum, Niobium, and Their Alloys*, pp. 111-129, Pergamon Press, Inc., Oxford, 1964.
54. V. M. Amonenko, P. N. V'yugov, and V. S. Gumenyuk, Study of the Thermal Expansion of Tungsten, Molybdenum, Tantalum, Niobium, and Zirconium at High Temperatures, *Teplofiz. Vysokikh. Temp.*, 2: 29-31 (January–February 1964).
55. H. H. Hausner and H. C. Friedemann, *Bibliography on Refractory Metals and Alloys*, Metallwerk Plansee Aktiengesellschaft, 1964.
56. T. G. Ellis and H. A. Wilhelm, Phase Equilibria and Crystallography for the Niobium-Tin System, *J. Less-Common Metals*, 7: 67-83 (July 1964).
57. Ames Laboratory, Iowa State University, Annual Summary Research Report of Chemistry, Engineering, Metallurgy, Physics and Reactor Divisions, July 1, 1963–June 30, 1964, USAEC Report IS-900, September 1964.
58. W. R. Clough, Metallurgical Studies of Zirconium and Thorium and of the Alloying Behavior of Rare Earth–Transition Metal Systems, Annual Progress Report, August 1, 1963–July 31, 1964, USAEC Report TID-20862, Rensselaer Polytechnic Institute.
59. T. V. Fedorov and E. I. Gladyshevskii, Interaction Between Carbon and the Transition Metals of the Fourth, Fifth, and Sixth Groups of the Periodic Table, *High Temp.*, 1: 401-406 (November–December 1963); translated from *Teplofiz. Vysokikh. Temp.*, 1: 449-455 (November–December 1963).
60. K. Monma, H. Suto, and H. Oikawa, On the Relation Between High-Temperature Creep and Diffusion in Nickel Base Solid Solutions, *Nippon Kinzoku Gakkaishi*, 28: 188-192 (1964).
61. A. Van Craeynest and M. D. Calais, Plutonium-Magnesium Diffusion, *Mem. Sci. Rev. Met.*, 61: 459-465 (June 1964).
62. G. B. Fedorov, Some Features of the Strength and Diffusion Characteristics of Zirconium, *Issled. po Zharoprock. Splavam. Akad. Nauk SSSR, Inst. Met.*, 10: 46-52 (1963).
63. T. S. Lundy, J. I. Federer, R. E. Pawel, and F. R. Winslow, A Summary of ORNL Work on Diffusion in β-Zr, V, Nb, and Ta, USAEC Report ORNL-P-425 (CONF-711-1), Oak Ridge National Laboratory, 1964.
64. T. Smith, Zirconium Dioxide-Oxygen Reactions. I. Molecular Oxygen Adsorption with Electron Transfer, *J. Electrochem. Soc.*, 111: 1020-1027 (September 1964); II. Chemisorption of Atomic Oxygen, *ibid.*, pp. 1027-1031.
65. R. W. Vest, J. A. Crawford, and W. C. Tripp, The Electrical Behavior of Refractory Oxides: II, Report ARL-64-122, Systems Research Laboratories, Inc., August 1964.
66. A. C. D. Chaklader and V. T. Baker, Bulletin, American Ceramic Society, Vol. 44, March 1965.
67. A. D. Mah, Heats of Formation of Zirconium Carbide and Hafnium Carbide, Report BM-RI-6518, Bureau of Mines, Berkeley Thermodynamics Laboratory, April 1964.
68. R. A. Dugdale, R. C. McVickers, and S. D. Ford, The Behavior of Glasses and Ceramics at High Rates of Heat Transfer, *J. Nucl. Mater.*, 12: 1-15 (May-June 1964).
69. M. P. Lepie, The Properties of Pyrolytic ZrC, *Trans. Brit. Ceram. Soc.*, 63: 431-449 (August 1964).
70. R. E. Cowan, C. C. Herrick, and S. D. Stoddard, Mechanism of Adherence of Tungsten to Bodies Containing Yttria, USAEC Report LA-DC-6468 (CONF-716-3), Los Alamos Scientific Laboratory, 1964.
71. D. M. Mattox, Metallizing Ceramics Using a Gas Discharge, USAEC Report SC-R-64-1330 (CONF-716-2), Sandia Corp., September 1964.
72. L. P. Trudeau, Radiation Effects on Toughness of Ferritic Steels for Reactor Vessels, *Monograph Series on Metallurgical and Nuclear Technology*, 187 pp., 1964.
73. S. H. Bush, Selected Mechanical Properties of Irradiated Metals and Alloys, USAEC Report HW-81334 (Part 2), Hanford Atomic Products Operation, Oct. 1, 1964.
74. C. Z. Serpan, Jr., H. E. Watson, J. R. Hawthorne, and L. E. Steele, Yankee Reactor Pressure Vessel Surveillance Evaluation of Specimens Exposed During the Second Core, Report NRL-6179, Naval Research Laboratory, Sept. 18, 1964.

75. V. A. Shalashov, Influence of Gamma Irradiation on Intensification of Annealing of Malleable Cast Iron (in Russian), *Liteinoe Proizv.*, No. 12: 20-22 (December 1963). *Russ. Castings Prod. (English Transl.)*

76. T. J. Koppenaal, Microstrain Yield Stress in Neutron Irradiated Copper Single Crystals, *J. Appl. Phys.*, 35: 2750-2753 (September 1964).

77. M. L. Swanson and G. R. Piercy, Low Temperature Neutron Irradiation Damage in Aluminum and Gold, *Can. J. Phys.*, 42: 1605-1673 (August 1964).

78. H. U. Astroem, Isothermal Measurements on the Release of Stored Energy from Reactor Irradiated and Cold-Work Molybdenum, *Arkiv Fysik*, 26: 83-92 (1964).

Section V

Reactor Materials

Special Fabrication Techniques

Melting and Hot and Cold Working

A complete account[1] of the work of Reactive Metals, Inc., on the application of Dynapak forming to the production of uranium tubing is now available. Among the accomplishments of this study were the design and evaluation of extrusion tools and mandrel materials for use in Dynapak extrusion and the establishment of the feasibility of this method of fabrication for the production of uranium tubing. During the study a technique was developed and patented for the alpha extrusion and beta heat-treatment of uranium in a single operation. It is stated, however, that further work is required on this technique. It was also found that conventional hot-work tool steels are not suitable for Dynapak extrusion of uranium.

Union Carbide Nuclear Division workers have been engaged in the production of prototype parts for a large, bare, high-flux, all-metal reactor.[2] The most interesting aspect of their efforts has been the furnace modifications necessary to handle the 400-kg charges of the uranium–10 wt.% molybdenum that will be used in production of large rings. Since the uranium is to contain 20 at.% ^{235}U, water cannot be permitted to enter the furnace, and the 28-in.-diameter induction coil must be cooled by air or other suitable gases. Because of the mass and shape of the castings, heat losses from them must be controlled to minimize shrinkage at the top of the 30½-in.-diameter rings. Seven castings have been made using a normal uranium alloy. One of these has been evaluated. This evaluation revealed extensive coring in the casting and the need for some type of homogenization heat-treatment. Because of the low carbon requirement, it is planned to evaluate several washes to be used on the graphite crucibles and molds.

A collapsible mold has been designed to permit the casting of threaded hafnium carbide specimens by Bureau of Mines research personnel.[3] Fifteen castings containing 7.52 to 10.70 wt.% carbon have been radiographed and examined visually and by metallographic techniques. The sounder castings contained about 9 wt.% or more carbon. The sound castings were stress relieved by heating to 1900°C for 5 min and cooling in 15 min. Three stress-relieved specimens tested at temperatures near 2450°C exhibited strengths of 5840 to 6540 psi and fractured in a brittle manner. The higher strength was exhibited by the specimen containing the least amount of carbon.

Argonne National Laboratory reports[4] the successful extrusion of tungsten tubes from pressed and sintered sleeves, vapor-deposited tubes, and preextruded tubes. Oak Ridge National Laboratory[5] extruded two sintered tungsten billets to tube shells using as the lubricant the WO_3 that formed on the billet surfaces during transfer of the billets from the furnace to the press. One of the billets was extruded at 1870°C, and the other, at 1705°C. A reduction ratio of 5.8 to 1 was used for both billets. The breakthrough pressure was lower for the billet extruded at the lower temperature due to the high rate of evaporation of the WO_3 at the higher temperature.

General Electric Company[6] and Nuclear Metals Division of Textron, Inc.,[7,8] have continued their studies concerned with the preparation of tungsten and tungsten-rhenium alloys. At General Electric the following process procedures have been tentatively established for the tungsten–25 wt.% rhenium alloy.

1. Wet-blend the powders, compact, and sinter at 3000°C in hydrogen.

2. Heat the sintered compacts in hydrogen at 1400°C and hot-roll in air, reheating between passes. A cumulative reduction of 80% or more is preferred.

3. Heat to temperatures of 1400 to 3000°C in hydrogen to remove oxygen. Temperatures closer to 1400°C are preferred because a finer grain structure results, although oxygen removal is slower.

4. Cold-roll, with 1400°C intermediate stress relieving, to final size. A reduction of more than 65% is preferred.

Sintered compacts of the tungsten–30 wt.% rhenium–30 wt.% molybdenum alloy were clad in molybdenum and extruded at 1650°C. Fabrication of 0.038-cm-thick sheets of the alloy into tubes and containers is also reported. The melting characteristics for the alloys as determined by heating the materials for 2 hr in hydrogen at various temperatures are as follows:

1. Tungsten–25 wt.% rhenium melts above 3000°C; tungsten–30 wt.% rhenium shows incipient melting at 3000°C.

2. None of the alloys melted below 2760°C.

3. Tungsten–25 wt.% rhenium with up to 20 wt.% molybdenum melts above 2900°C, whereas the alloy containing 30 wt.% molybdenum shows incipient melting at this temperature.

4. Tungsten–30 wt.% rhenium alloys with up to 20 wt.% molybdenum melt above 2800°C; the alloy containing 30 wt.% molybdenum shows melting at this temperature.

The studies at Nuclear Metals have been concerned with the production of small-diameter tungsten and tungsten–25 wt.% rhenium tubing by extrusion, drawing, and sinking. Since it was believed that PbO might prove satisfactory as a lubricant during plug-drawing operations, this compound was evaluated rather fully and found unsatisfactory for this purpose. Other studies showed that cumulative reductions of 30 to 40% can be achieved at both 510 and 580°C by low reductions per pass, using plug drawing aided by sinking, and that reductions of 25:1 can be obtained in both alloys by extruding at 1200°C.

The Bureau of Mines[9] has developed a water-free expendable graphite mold that is useful for reactive-metal casting. The primary advantage in using this mold lies in its adaptability to standard foundry techniques and its low curing and firing temperatures. The mold blend consists of powdered graphite, cornstarch, dextrin, cereal binder, linseed oil, and Carbowax. Proper venting of the mold is essential to remove the gases evolved during pouring. It is stated that surface contamination due to carbon is greater than when machined graphite molds are employed; however, when titanium was cast, contamination did not penetrate more than 0.04 in. (N. E. Daniel)

Cladding

Pressure Bonding

The compaction of metal and ceramic powders by gas-pressure bonding has been described by Hodge.[10] Fine-grain structures can be achieved by gas-pressure bonding, and a wide variety of shapes can be fabricated directly. The consolidation of tungsten powders into forging billets and rocket nozzles has been accomplished at 2700 to 2900°F (1485 to 1565°C) at pressures of 10,000 to 20,000 psi. The compaction of tantalum, niobium, and rhenium was achieved at temperatures of 2600°F (1425°C), 2100°F (1150°C), and 2900°F (1565°C), respectively, at similar pressures. Beryllium powder compacts have been successfully fabricated at 10,000 psi and 1400 to 1600°F by using both spherical powders and −200-mesh commercial types. Ceramic powders, including Al_2O_3, MgO, BeO, and UO_2, were examined in detail, and the necessary bonding parameters were established for various types of powders. The application of powder consolidation to the production of metal-ceramic joints was also noted. Cursory studies on the compaction of tantalum carbide, tungsten carbide, and graphite materials were described. The carbides required parameters of 2900 to 3200°F (1595 to 1760°C) at pressures of 10,000 to 15,000 psi to achieve full densification. High-density graphites were produced at 3000 to 4200°F (1650 to 2315°C) and 10,000 to 30,000 psi. Cermet structures have been found ideal for gas-pressure bonding, with cermet loadings of 5 to 80 vol.% in matrices of stainless steel, chromium, and the refractory metals.

The consolidation of AGOT graphite powders by gas-pressure bonding has been examined at Battelle Memorial Institute.[11] Powders contained in tantalum jackets and subjected to temperatures up to 4000°F and pressures to 30,000 psi have yielded structures having 95% of the theoretical density. In all cases the

graphite powders were cold hydrostatically pressed prior to jacketing. Currently the packing behavior of binary, ternary, and quaternary mixtures of particle sizes for several graphites is being examined. Outgassing treatments of 4 hr at 400°F in air or ½ hr at 1500°F in vacuum have been found desirable prior to bonding. Preliminary bonding studies of these graphites have shown that increasing the pressure from 10,000 to 30,000 psi at 3000°F produces a marked increase in density. Densities of the various grades of material ranged from 83 to 92% of theoretical at the lower pressure and 93 to 99% of theoretical at the higher pressure.

Surface-preparation methods, as they affect the nature of bonds, are also being investigated. Techniques employed in this Battelle study[11] include heating in a high vacuum, cathodic etching, chemical modification, and mechanical cleaning. It has been noted that a zirconium hydride surface promotes continuously bonded structures after pressure bonding at 1500°F (815°C). A fine-grained bond area that is high in hardness is being examined further. An aluminum–lithium hydride surface produced porous interfaces in aluminum structures after bonding at 950°F (510°C). (S. W. Porembka)

Canning

Two filling methods are being evaluated at Argonne[12] to produce uncontaminated vibratorily compacted irradiation specimens consisting of a 36-mm column of fuel in a 61-cm-long by 6.53-mm-ID jacket. The first method utilizes a sealed tube holder that screws into the platen of a vibrator, with charging being accomplished through an O-ring-sealed fill tube. The second method replaces the O-ring seal with a metallic compression fitting on the open end of the fuel jacket, whereas the base of the jacket is screwed onto a stud mounted on the vibrator platen.

At Hanford Atomic Products Operation,[13] a ⅜-in.-OD 0.035-in.-wall stainless-steel tube, 18 in. long, was vibratorily compacted with UO_2 to 85% of theoretical density by using the following ternary mixture: −12 +14 mesh, 68 wt.%; −60 +80 mesh, 15 wt.%; −200 mesh, 17 wt.%. The measured density was very close to that predicted by the theoretical model for powder packing of this ternary mixture. The compact was formed with a 110-mil-diameter tungsten wire along the axis, so that a central void could be generated by resistance heating (presumably by melting of the adjacent UO_2).

Vibratory-compaction loading of fused UO_2 particles in a thin-walled Zircaloy-2-clad tube-in-tube fuel element at Hanford[13] resulted in greater than 86% of theoretical density in both the inner and outer tubes.

In a continuing study of vibratory compaction of thoria–urania powder mixtures at Oak Ridge,[14] five designs were evaluated for mounting and coupling a NAVCO BH 1⅝-in. pneumatic vibrator to a fuel tube. A method employing a floating anvil 8½ in. long yielded the highest bulk density for the lowest air pressure.

Vibratory compaction is being studied at Oak Ridge as a means of preparing high-density-oxide fuel rods.[15] A spring-loaded anvil with a spring constant of 2580 lb/in. was tried on a Branford vibrator and gave a marked improvement in the bulk density achieved. The vibration pulse generated in the anvil during impact indicated a peak acceleration of 10,000 g measured at a chamber pressure of 35 psig and a pulse composed of damped, complex sinusoidal waves having a duration of 6 msec.

A British patent[16] describes a method for fabricating a fuel body containing a fissionable fuel and a metal-hydride moderator. The method involves the forming of a solid body from a mixture of fuel (enriched uranium) and a hydride-forming metal (zirconium), enclosing the body within a stainless-steel sheath that is permeable to hydrogen at 700 to 900°C, and passing hydrogen through the sheath at this temperature to form a hydride. (V. D. Linse)

Electroplating

Electroforming has proved useful for shaping complex articles for nuclear energy applications. Improved capabilities based on research on aircraft and missile applications were reviewed in part at a recent American Society for Metals Conference.[17] This review pointed out that nickel could be electroformed with a tensile strength of 200,000 psi, which is expected to increase the usefulness of electroforming for a greater number of applications. A comprehensive state-of-the-art survey of electroforming was recently completed for Redstone Scientific Information Center.[18]

Niobium, titanium, and tantalum were codeposited with nickel by electrodeposition in

anhydrous solutions of nickel and niobium, titanium, or tantalum chlorides in acetyl, propyl, or butyl alcohol, according to a Russian report.[19] The alloys were deposited with a current density of 0.1 to 0.3 amp/cm^2. With an alcohol solution of hydrated zirconium oxychloride and anhydrous nickel chloride, no metal was electrodeposited. Unalloyed nickel could be deposited in anhydrous alcohol solutions of nickel chloride, but unalloyed niobium, titanium, or tantalum was not electrodeposited in anhydrous alcohol solutions of the metal chlorides.

A new procedure reported by Dow Chemical Co.[20] for cleaning copper–2 wt.% beryllium alloy ensured complete removal of oxides and other contaminants but avoided the uneven etching observed while employing prior-art methods. Dow's procedure included (1) ultrasonic degreasing in perchloroethylene, (2) immersion alkaline cleaning, (3) anodic treatment in sodium carbonate or immersion in nitric or nitric-sulfuric acid solution, and (4) immersion in sodium cyanide solution. Thereafter the copper-beryllium alloy was electroplated uniformly with a copper strike, a silver strike, and 1 mil of gold in an acid cyanide bath.

Oxides of thorium, uranium, plutonium, and other metals were precipitated by an electrolytic process developed in Russia.[21] Oxide coatings weighing 1 to 3 mg/cm^2 were precipitated in isobutyl alcohol, methyl ethyl ketone, or acetone solutions of the hydrated metal nitrate with a current density of 5 ma/cm^2 on aluminum and other metal substrates. The required potential for a 5- to 50-mm electrode spacing was in the range of 500 to 1000 volts. Thin films (100 to 150 μg/cm^2) were deposited in 10 to 15 min and heated to 500 or 600°C to drive off volatile compounds and were recoated several times to build up thicker deposits.

A method for plating Zircaloy with copper[22] included degreasing, activating by immersion for 1 min in a solution containing 29 g of potassium fluoride per liter and 50 g of 40% hydrofluoric acid per liter, depositing 5 μ of copper in an alkaline or acid solution, and heating at 700°C in an argon atmosphere. After the undiffused copper was removed by immersion in concentrated nitric acid, the thickness of the copper diffusion layer ranged from 5 to 15 μ.

(W. H. Safranek)

Nonelectrolytic Chemical Plating

The use of vapor-deposition processes to prepare high-purity metallic and nonmetallic materials in quantity and in useful shapes is reviewed. Additional applications include the deposition of protective metallic and nonmetallic overlay and diffusion coatings on various structural substrates.

A U. S. patent[23] describes a process for producing long whiskers of Group IB and Group VIII metals on copper substrates. Self-gettering and impurity transfer in the preparation of thorium by the carbide-iodide process[24] were discussed. Metal containing 1 ppm nitrogen and hydrogen, 9 to 13 ppm oxygen, and an estimated 3 to 6 wt.% carbon was prepared.

The formation of structural parts from pyrolytic tungsten, employing deposition from hydrogen-WF_6 atmospheres, is being widely investigated. Prestressed tungsten deposits,[25a] thermocouple wells, melting crucibles, spiral heaters, and thermionic-converter emitter shells,[26] and tubing $\frac{3}{4}$ to $\frac{1}{2}$ in. outside diameter and 14 in. long, formed on the inside of a tubular mandrel,[27] were described. Tungsten-rhenium alloys containing up to 35 wt.% rhenium are being codeposited.[27,28]

The deposition of boron in consolidated form[29] as well as in the form of continuous filaments ($\frac{1}{2}$-mil tungsten-wire substrate)[30] was described. In the latter case a superior reinforcing fiber is being sought. The mechanism involved in the deposition of carbon by low-temperature (500 to 1000°C) pyrolysis of acetylene[31] was investigated. The rate of consumption of C_2H_2 obeys a second-order kinetic law. Codeposition of boron-carbon "alloys" in the composition range 19 wt.% boron–81 wt.% carbon to 82 wt.% boron–18 wt.% carbon and of silicon-carbon from 69 wt.% silicon–31 wt.% carbon to 75 wt.% silicon–25 wt.% carbon was carried out.[27,28] A $\frac{1}{2}$-in.-OD by 0.030-in.-wall B_4C tube was fabricated.[28] Whiskers of Al_2O_3 and SiO_2 (Ref. 32*a*) and needle-shaped deposits of UO_2 (Ref. 33) were formed by using vapor-phase reactions. Crystals of Si_3N_4 also were prepared.[32a]

Overlay coatings, which have received much less attention than silicide type diffusion coatings, now are being actively investigated.

United States patents were issued covering a method of metallizing porous refractory substrates by low-temperature (120 to 260°C)

decomposition of volatile metal-bearing compounds[34] and coating heated substrates with chromium, molybdenum, vanadium, and tungsten by immersion in the respective liquid carbonyls.[35] Niobium–1 wt.% zirconium substrates were vapor plated with molybdenum coatings ($< 5 \times 10^{-5}$ in. thick) by hydrogen reduction of $MoCl_5$ as a means of reducing contamination by residual gases *in vacuo* of the order of 10^{-6} torr (Ref. 36). Pyrolytic-tungsten (PyW) overlay coatings are considered useful in many applications.[26] The influence of deposition parameters on the quality of PyW coatings on nickel-tube substrates is under investigation.[37] Silicon carbide coatings are used to protect tungsten against high-temperature oxidation.[25b,38] Graphite substrates are coated with thin films of ZrO_2–5 mole % Y_2O_3, TiC, and TiN (Ref. 32*b*). Alkoxide compound layers, deposited by physical vapor deposition (evaporation), are subsequently decomposed thermally to yield the desired coatings.

Interest still is high in modified silicide type diffusion coatings applied by pack-cementation, fluidized-bed, chemical vapor deposition, and slurry coating methods, which are competitive processes in aerospace application.[39] Current research programs and semicommercial processes involve pack-cementation and fluidized-bed coating of molybdenum alloys,[25c,40] niobium and niobium alloys,[25c,40–43] and tantalum alloys.[42,43] Progress is being made in securing increased stability and low-pressure-oxidation protective life of the coatings, but it is not rapid. A coating process yielding a 50% longer life than those currently obtained would be considered a breakthrough. (E. M. Sherwood)

Explosive Joining

In support of the U. S. Atomic Energy Commission–General Nuclear Engineering Corporation BONUS Reactor Program, Battelle conducted an experimental program[44] on the explosive welding of tubular sections of Zircaloy to Inconel 600. In the initial stages of the program, simple lap type interface designs (part *a* of Fig. V-1) were studied to provide preliminary data on the critical range of the various explosive-welding parameters. Subsequently development was shifted to a uniform-wall-thickness tapered-lap configuration (part *b* of Fig. V-1).

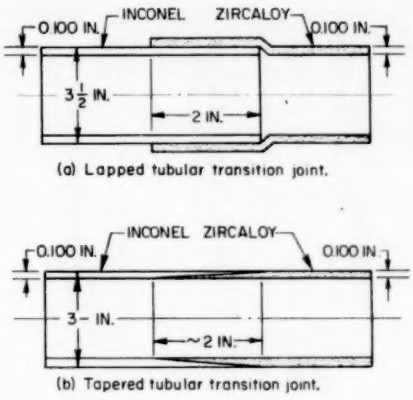

Fig. V-1 Sketches of the basic lap and tapered configurations for tubular transition joints.[44]

Lap-Joint Studies

The lap-joint interface specimens were prepared by machining to provide the desired initial interface clearance, degreasing in methyl ethyl ketone, and wire brushing the mating surfaces. The specimen components were then inserted into a mild-steel die, with a Parawax plug in the inside diameter of the specimen to act as the transfer medium. Next the assembly was sealed with Apiezon* putty and the joint interface evacuated. An explosive charge of the desired weight and configuration was then inserted into a hole in the center of the Parawax plug and the charge detonated.

A series of experiments utilizing the three lap-joint interface designs shown in Fig. V-2 led to the following observations:

1. No welding was achieved with a 40-g charge. With 50- and 60-g charge weights and a smooth joint interface (part *a* of Fig. V-2), partial welding was achieved.

2. Initial radial clearances of 50 to 80 mils resulted in sufficient closure velocity and suitable dynamic angle to effect welding. Clearances of 10 to 40 mils were inadequate.

3. Best welding was achieved at the base of grooves and threads with the interface designs shown in parts *b* and *c* of Fig. V-2. This was apparently due to the geometry being conducive to rupture of the surface-oxide films and to maintenance of the closure angle.

*A product of Apiezon Products Ltd. which is distributed by the Shell Oil Company.

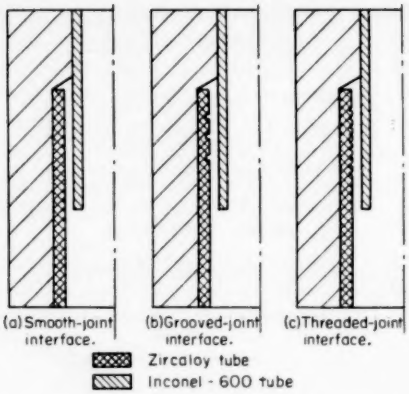

Fig. V-2 Sketches depicting various lap-joint interface designs.[44]

Tapered-Joint Studies

Explosive-joining tests were carried out with tapered-joint interface designs. The specimen preparation and testing procedures were the same as those used for the lap-joint studies except for the sealing of the interface prior to evacuation. The final method adopted was to machine O-ring grooves in the ends of the die and seal with aluminum disks. This permitted much better evacuation (to $<10\,\mu$) than was possible when Apiezon putty was used for sealing. Figure V-3 is a photograph of a completed explosively welded specimen.

The experiments led to the following observations:

1. Welding was relatively insensitive to taper angle or surface roughness; a taper of 2° and an interface surface roughness of 250 μin. rms were adopted.

2. The extent of welding increased with increasing charge density in the range 3 to 12 g/sq in., however, with the higher charge densities (7 to 12 g/sq in.), it was necessary to feather the charge to 4 g/sq in. near the base to prevent splitting of the Zircaloy in this area.

3. As with the lap-joint specimens, grooving the interface improved the weld continuity. Of the two designs shown in Fig. V-4, the scalloped-joint interface gave the most complete welds.

Physical Testing

Bend-test specimens were prepared by removing 0.250-in.-wide longitudinal sections

Fig. V-3 Tubular section of Zircaloy-2 and Inconel 600 explosively welded in a backup die.[44]

from explosively welded 5-in.-long transition joints. The welds achieved with grooved- and scalloped-joint specimens, when bent with the Inconel in tension and Zircaloy in compression, were capable of withstanding a minimum of a 2T radius bend without separation at the joint interface. Bending these specimens with the Zircaloy in tension and the Inconel in compression resulted in a rupturing of the Zircaloy

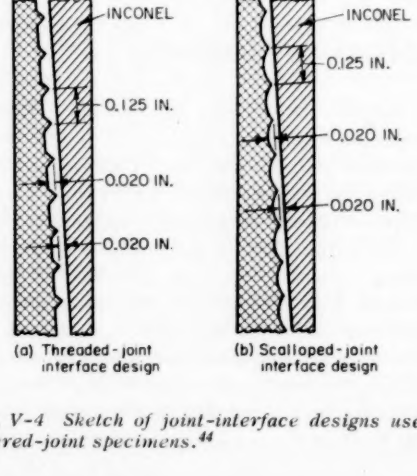

Fig. V-4 Sketch of joint-interface designs used for tapered-joint specimens.[44]

component when bent to a 3T radius. The smooth-joint interface, however, was found to rupture at the weld joint at a 5T radius bend. Cracking observed in the base materials in the scalloped-joint specimens after test was attributed to the greater shock hardening resulting from the higher charge density used to weld the scalloped-joint specimens. Table V-1 illustrates the substantial increase in hardness produced by explosive welding and verifies the fact that the specimen welded with a charge density of 12 g/sq in. was slightly harder than that welded with 10 g/sq in.

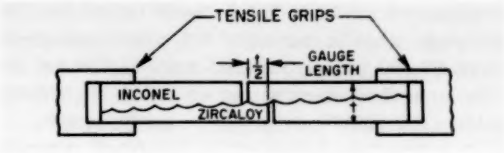

Fig. V-5 Tensile-shear test specimen for 5-in.-long transition joints.[44]

Table V-1 HARDNESS MEASUREMENTS* OF AS-RECEIVED AND EXPLOSIVELY WELDED SECTIONS[44]

Material	Condition	Hardness readings 1	2	3	4	Average hardness
Zircaloy	As received	197	223	298	206	206
Inconel	As received	151	150	151	149	150
Zircaloy	Explosively welded at 10 g/sq in.	229	240	247		235
Inconel	Explosively welded at 10 g/sq in.	325	344	309	315	324
Zircaloy	Explosively welded at 12 g/sq in.	258	262	265	258	261
Inconel	Explosively welded at 12 g/sq in.	334	341	330	328	348

*Knoop tester; diamond penetrator, 200-g load.

Several 1/4-in.-wide longitudinal sections were removed from 5-in.-long tubular transition joints possessing smooth- and scalloped-joint interface designs that had been explosively welded at 12 g/sq in. These specimens were each subjected to 1500 3-min thermal cycles between 150 and 750°F, after which they were removed and examined visually and metallographically. Prior to thermal cycling the smooth-joint specimens were found to be only partially welded at the upper end of the joint, whereas the scalloped-joint specimens were welded over the entire joint length. Following thermal cycling it was noted that in a few areas some slight separation at the weld joint had occurred with the smooth-joint interface specimens in the partially welded area. With the scalloped-joint interface, the weld joint remained unaffected except for some slight separation that occurred in an area in which intermetallic compound had formed during welding. It was concluded that thermal cycling would not be detrimental to contamination-free welds made with scalloped-joint interfaces.

The results of tensile-shear tests, conducted on specimens of the design shown in Fig. V-5, demonstrated that the strength of the welds is directly related to the degree of evacuation of the joint interface obtained prior to welding. Poor evacuation leads to the formation of brittle intermetallics, with consequent low tensile strength. In tests conducted with tensile specimens of the design shown in Fig. V-6, the specimen invariably failed in the Zircaloy

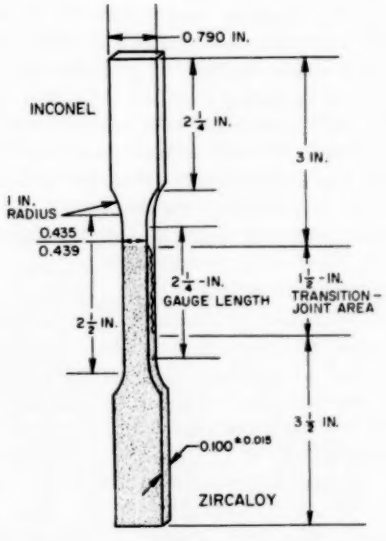

Fig. V-6 Tensile specimens prepared from 8-in.-long tubular transition joints.[44]

component and not in the weld interface. The average tensile strength for these specimens was 97,500 psi (compared with 65,000 psi for the annealed starting material) at an average elongation of 10% over a 2-in. gauge length.

(C. C. Simons)

Welding and Brazing

General Electric has completed studies[45] on the stability of welds in niobium alloys. Bend ductility of electron-beam and tungsten-arc–inert-gas (TIG) welds in D-43 and B-66 alloys served as the basis of the study. The relations between welding parameters, interdendritic spacing, and weld properties were evaluated, and these showed that, as the spacing increased (welding speed decreased), the normal niobium-base-alloy metallurgical reactions became sluggish. The ductile-brittle bend-transition temperature of as-welded specimens increased with decreased welding speed. Interstitial nitrogen also greatly increased the transition temperature and sluggishness of aging reactions. Oxygen did the same thing, but to a lesser degree. It was also shown that welds in these alloys can be overaged sufficiently to cause embrittlement at room temperature.

Recently reported results[27] of bend ductility of welds in niobium alloys by Oak Ridge verifies at least one of the above conclusions. Reducing the welding speed raises the ductile-brittle transition temperature of welds in D-43. The Oak Ridge studies are summarized in Fig. V-7. The superior ductility of electron-beam welds in all the alloys studied is evident. Also, welds in the C-129Y and T-111 alloys appear much more ductile than the rest. Studies still in progress to define better the curve between −73 and −200°C can furnish further

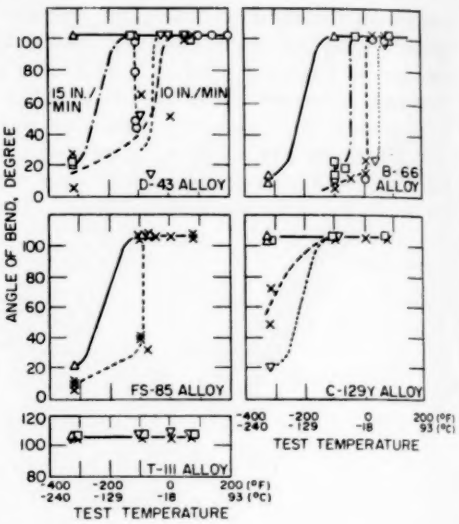

Fig. V-7 Bend-transition curves of welds in refractory-metal alloys D-43, B-66, FS-85, C-129Y, and T-111 (Ref. 27). Points plotted at 105° indicate completion of the test without failure (4T punch radius, 0.5 in./min deflection rate). ——△, unwelded. – – –×○, automatic tungsten arc. —·—□, electron beam. ----- ▽□, manual tungsten arc.

substantiation of the ductility of welds in C-129Y. The conditions used to make the welds covered by Fig. V-7 are given in Table V-2. The overaging of welds in niobium alloys is under further study at Oak Ridge.

At the Norair Division of Northrop Corp., a novel method for making a brazing alloy useful on niobium alloys has been developed.[46] Chromium was vacuum deposited on 0.0015-in.-thick pure titanium foil and then given a diffusion treatment as part of the brazing cycle. The result is titanium–33 wt.% chromium brazing filler metal that can be handled in foil form. The reliability of the titanium–33

Table V-2 WELDING CONDITIONS FOR REFRACTORY-ALLOY SHEET SPECIMENS[27]

Alloy	Sheet thickness, in.	Automatic gas tungsten arc (argon gas, 9-volt arc)		Electron beam, 30 in./min		Manual gas tungsten arc (argon gas)	
		Welding speed, in./min	Welding current, amp	Welding current, ma	Voltage, kv	Welding speed, in./min	Welding current, amp
D-43	0.060	15	210 to 240				
	0.060	10	200 to 240	6.5	130	~3	140 to 150
B-66	0.060	10	190 to 240	4.5	130	~3	140 to 150
FS-85	0.050	10	165 to 175			~4	155 to 180
C-129Y	0.030	10	70 to 100	3.5	130	~6	~80
T-111	0.060	10	245 to 260	6.8	120	~3	190 to 220

wt.% chromium alloy for structural honeycomb panels useful to 1370°C was demonstrated with the D-36 niobium alloy. Heat shield panels brazed with titanium–13 wt.% vanadium–11 wt.% chromium–3 wt.% aluminum (B120VCA) commercial alloys were serviceable at 1480°C.

The Oak Ridge studies[27] to develop alloys for brazing of niobium alloys have emphasized the niobium-vanadium-tantalum and titanium-vanadium-tantalum systems. This work has been reviewed previously. Ternary diagrams for the two systems are now available. The shear strength of joints made with these alloys and tested at 1090 and 1200°C are given in Table V-3. Tantalum T joints made with the same alloys have been aged for 500 hr at 1370°C in vacuum. Loss of titanium from the high-titanium alloys and loss of ductility of some of the higher vanadium alloys were observed as a result of aging.

Table V-3 ELEVATED-TEMPERATURE SHEAR STRENGTH OF BRAZED JOINTS[27]

Composition, wt.%	Brazing temp., °C	Test temp., °C	Shear strength, psi	No. of specimens tested
		Niobium-Vanadium-Titanium		
65 V–30 Ta–5 Nb	1870	1090	23,400	2
65 V–5 Ta–30 Nb	1820	1090	22,900	2
80 V–10 Ta–10 Nb	1870	1200	13,800	4
30 V–30 Ta–40 Nb	2010	1200	13,400	4
40 V–30 Ta–30 Nb	1930	1200	15,600	4
50 V–25 Ta–25 Nb	1870	1200	16,800	4
90 V–5 Ta–5 Nb	1870	1200	13,900	4
60 V–20 Ta–20 Nb	1870	1200	12,400	4
		Titanium-Vanadium-Tantalum		
40 V–10 Ta–50 Ti	1730	1200	12,600	4
25 V–15 Ta–60 Ti	1650	1200	7,800	4
20 V–5 Ta–75 Ti	1650	1200	7,100	4
20 V–10 Ta–70 Ti	1650	1200	7,600	4
35 V–35 Ti–30 Ta	1700	1200	10,000	4
50 V–20 Ta–30 Ti	1760	1200	13,100	4
65 V–30 Ta–5 Ti	1840	1200	13,500	4
55 V–25 Ta–20 Ti	1840	1200	13,800	4

René 62 is a new high-strength superalloy similar to the well-known René 41 but having properties that minimize strain-age cracking during postwelding heat-treatments. The results of a short study of the brazing of this new alloy are given in Table V-4. The data indicate that the precautions necessary to the successful brazing of most titanium and/or aluminum-bearing superalloys must also be used for René 62.

General Electric has completed the initial phases of a program designed to develop techniques for producing jet-engine and aerospace parts from TD nickel.[47] The joining methods under study, all of which minimize agglomeration or loss of dispersed thoria, are resistance welding, flash welding, brazing, diffusion bonding by resistance heating, and diffusion bonding by hot pressing. The initial evaluation of all these methods indicates that normal parameters can be varied sufficiently to produce high-quality joints in TD nickel.

Union Carbide investigators have made a comparison of the electron-beam and TIG welding processes for joining uranium.[2] Butt joints in vacuum-annealed uranium sheet were very porous when electron-beam welded on a Hamilton–Zeiss 3-kw machine. This was not true when TIG welding was used. The electron-beam welding parameters are shown in Table V-5. The work is continuing in an effort to produce porosity-free welds.

Studies of the welding of iron-chromium-aluminum-yttrium alloys at General Electric[6] have indicated that a problem exists with the formation of a film of intergranular iron-Y_9. This compound causes cracking with minor cold reductions, and annealing at 1000°C does not improve the results. It was learned that the iron-Y_9 is spheroidized when the alloy is held for 500 hr at 1100°C. Thus the possibility of imparting ductility exists through the use of long-time heat-treatments.

Many recent studies have been concerned with the joining of aluminum alloys in many different forms and to other metals. Lockheed

Table V-4 RESULTS OF BRAZING STUDIES ON RENÉ 62 T JOINTS[27]

Brazing alloy	Composition, wt.%	Specimen pretreatment	Brazing temp., °C	Atmosphere	Remarks
Coast Metals 52	4 Si–3 B–93 Ni	0.002-in. nickel plate	1060	Hydrogen	Good wetting and flow
Copper		0.002-in. nickel plate	1100	Hydrogen	Fair wetting and flow
Gold-nickel	82 Au–18 Ni	0.002-in. nickel plate	1010	Hydrogen	Good wetting and flow
Nicrobraz 50	10 P–12 Cr–78 Ni	0.002-in. nickel plate	1000	Hydrogen	Fair wetting and flow
Coast Metals 52	4 Si–3 B–93 Ni	Bare specimen	1060	Helium	Fair wetting, no flow
GE-8600	4 Si–32 Cr–24 Pd–40 Ni	Bare specimen	1170	Helium	Fair wetting, no flow
Gold-nickel	82 Au–18 Ni	Bare specimen	1010	Helium	Fair wetting, no flow
GE-8102	15 Cr–8 Si–77 Ni		1170	Vacuum	Fair wetting and flow
GE-8400	18 Cr–16 Ni–8 Si–4 W–1 B–53 Co		1170	Vacuum	Poor wetting and flow
GE-8600	4 Si–32 Cr–24 Pd–40 Ni		1170	Vacuum	Good wetting and flow
Gold-nickel	82 Au–18 Ni		1010	Vacuum	Very good wetting and flow
Nicrobraz 50	10 P–12 Cr–78 Ni		1010	Vacuum	Fair wetting, no flow
Coast Metals 52	4 Si–3 B–93 Ni		1060	Vacuum	Excellent wetting and flow
Coast Metals 62	16 Ni–16 Co–1 B–67 Mn		1100	Vacuum	Poor wetting and flow; skulling
GE-8202	2 Cr–2.5 Si–1.5 B–94 Ni		1100	Vacuum	Good wetting and flow

Table V-5 ELECTRON-BEAM WELD STUDIES[2]
(Flat Plate or Square Butt Joints)

Material	Dimensions, in.	Welding parameters					Remarks
		kv	ma	Travel speed, in./min	Distance from heat shield, in.	Other	
Tungsten	1 by 3 by 0.060	110 to 150	10 to 17.5	10 to 96	1½ to 5	Deflection and circle	Preliminary studies
Tungsten	2 by 6 by 0.060	140	10	20	2½	0.025-in.-diameter circle	Final conditions for foil penetration with no undercut
Uranium	2 by 6 by 0.010	120	1.0	30	3		Full penetration
Uranium	2 by 6 by 0.006	100	0.5	30	3¾		Full penetration
Uranium	2 by 8 by 0.250	150	10	15½	2¾		90% penetration
Uranium	2 by 8 by 0.375	150	15	20	2½		90% penetration; focus at ½T
Uranium	2 by 8 by 0.500	150	17.5	13	2¾		90% penetration; focus at ½T
Uranium	2 by 8 by 0.625	150	20	5	2⅛		Two passes, one from each side; focus at ½T
Type 1100 aluminum	1 by 2 by 0.005	120	1.0	20	2¼	0.010-in. transverse deflection; pulse width, 4; pulse frequency, 7	Blind T-weld with three-leg sections 0.005 in. thick

investigators have reported on the fracture toughness of welds in 0.5-in. X7039-T6 aluminum alloy.[48] The "precracked Charpy impact" technique was used. Flat-welded test panels, from which the impact specimens were taken, were made with the base-metal grains so oriented as to simulate circumferential and longitudinal welds in cylindrical pressure vessels. Notches were carefully located to show the properties of the heat-affected zone, weld metal, fusion line, etc.

Transverse specimens with the notch passing through the thickness of the base-metal plate had the lowest resistance to crack propagation. Conditions of plane stress fracture were encountered with all notch orientations and loca-

tions in the fusion zone and the heat-affected zone. The fracture toughness of double-pass and single-pass welds was equal, and the weld and heat-affected-zone values were greater than those of the base metal. Using Irwin's equation for "through thickness" based on plane stress conditions gave the room-temperature critical crack size of 9.7 in.; at −305°F, the critical size was 5.25 in. The average critical size for the base metal was about 1.0 in.

The feasibility of repairing foundry defects in A-356 aluminum-alloy castings was demonstrated by work at Douglas.[49] If welding procedures are used which maintain the magnesium content and produce sound welds, minimum strength requirements are met. A major criterion is that repairs be made only in areas that can be properly inspected for soundness.

Because it is often desirable to weld wrought aluminum to cast aluminum, Frankford Arsenal studied the properties of several such combinations.[50] Cast alloys 214, 356-T6, and Almag 35 plates 0.375 in. thick were welded to wrought 5456 alloy using double-V joints and two passes on each side. Several different filler metals were used with standard gas–tungsten-arc welding procedures. The resulting welds were defect free except for minor tungsten inclusions. The results are shown in Table V-6.

Table V-6 PROPERTIES OF CAST ALUMINUM-TO-WROUGHT ALUMINUM WELDMENTS[50]

Weld combination, cast-filler-wrought	Approximate strength, 1000 psi		Approximate joint efficiency,* %
	Yield	Tensile	
Almag 35/5183/5456 Almag 35/5556/5456	19.6	37.0	95
214/5183/5456 214/5556/5456	14.2	22.0	99
356-T6/5556/5456 356-T6/4043/5456	14.2	21.0	53

*Based on tensile strength.

The joining of aluminum to steel and other metals is an old problem. No really new method has been developed. Boeing Co. was able to join 6061 aluminum-alloy tubing to AISI type 304L stainless-steel tubing by precoating the steel with a zinc electroplate, followed by a hot dip in 1100 aluminum, and then brazing.[51] The joint gap found best was 0.002 to 0.006 in.; thus control of the hot-dip coating thickness was important. They also were able to make these tubing joints by oxyhydrogen and TIG welding. In this case the zinc plate was replaced with a copper plate. Tensile properties of both types of joints were good, but the "welded" joints had poor fatigue properties.

At Frankford Arsenal the interest was in joining steel and other wear-resistant metals to aluminum.[52] Arc welding and diffusion bonding were studied. The steel members used had a coating of either silver brazing alloy, zinc, or aluminum. It was found that 2024 aluminum alloy can be welded to steel that has been coated with zinc, aluminum, or a silver alloy, provided the welding arc is directed toward the aluminum member of the joint. The diffusion-bonding process can be used to join 2024 aluminum alloy to silver-alloy-coated steel.

(R. M. Evans)

Nondestructive Testing

Ultrasonic Techniques

Ultrasonic transducers for nondestructive testing of similar design and manufacture may differ considerably in their operating characteristics. These differences affect interpretation of test results. Immersion type transducers may be evaluated by a practical method used at Hanford,[53,54] in which a transducer under test is immersed in a water bath containing a small reflector. The transducer is translated and pulsed simultaneously, and the amplitude of the echo signal from the reflector is displayed on the vertical axis of an oscilloscope. The location of the vertical display (echo-pulse amplitude) on the horizontal axis of the oscilloscope corresponds to the position of the transducer on either the x or the y scan. Patterns of an x scan and of a y scan and an echo with the reflector located on the axis of the transducer are photographed with a Polaroid camera and mounted on a sheet containing all information concerning the test. The data sheet provides a valuable permanent record of the characteristics of each transducer.

Among the characteristics of ultrasonic-wave propagation which an inspector should understand in order to use ultrasonic methods to greatest advantage are those of diffraction and attenuation. Although attenuation increases with frequency, the inverse is true with diffraction. The two phenomena are in competition with each other. Most ultrasonic tests use pulses of a range of frequencies, which makes an under-

standing of the diffraction process essential to proper interpretation of test results. According to Fitch of Hanford,[53] diffraction effects are subdued within three times the near-field distance of large transducers. Studies at Hanford show that:

1. At the center of the beam the amplitude of the approximate center frequency, f_c, is about five times greater than the amplitude of $2f_c$.
2. At the edge of the beam the amplitude of f_c is approximately equal to that of $2f_c$.
3. The center of the beam contains a higher percentage of low frequencies than does the edge of the beam.

In a study[55] for the Allison Division of General Motors Corp., Automation Industries, Inc., determined that ultrasonic measurements of the depth of weld penetration in tube-to-header joints in heat-exchanger manifolds are accurate to within 0.010 in. of penetration depth as measured destructively. (D. Ensminger)

NDT Methods Other Than Ultrasonic

A report issued by the Division of Reactor Development, AEC,[56] summarizes developments in nondestructive testing (NDT) during 1963 at Argonne, Hanford, and Oak Ridge. The information presented on neutron radiography studies at Argonne deals with intensities and resolutions that have been obtained with collimated and uncollimated beams by several techniques. Other application requirements of interest to the prospective user are included. The state of development and accomplishments with infrared heat-transfer and imaging studies at Argonne are also summarized. Accomplishments at Hanford and Oak Ridge were summarized previously in this Review. Hanford achievements in NDT from 1952 to 1964 are summarized in a more recent report.[54] A comprehensive reference listing of more detailed reports is included. Activities in NDT at Oak Ridge for the period ending June 30, 1964, are presented in the annual report of the Metals and Ceramics Division.[27]

Television X-ray imaging techniques have received continuing attention at Oak Ridge.[28] A beryllium-window vidicon provided increased sensitivity, particularly to low-voltage X rays, over earlier glass-window vidicons. Good X-ray images of masking tape and graphite have been obtained at 12 kvp by the closed-circuit-television system. The observation is aided considerably when the specimen being examined is moved. Speeds comparable to those required for examination of a radiograph are realized, and magnifications of 10 to 30× are in use. A 0.0005-in. tungsten wire was plainly visible, as was a 200-mesh screen. Defects in aluminum plug welds were discernible in specimen sizes up to ½ in. in diameter. With materials of higher atomic number, techniques for masking and orienting must be developed for maximum resolution. The technique is being developed for measurement of a specimen motion as it is subjected to rapid temperature excursions while enclosed in other apparatus.

An investigation[33] of the phase-sensitive eddy-current instrument developed at Oak Ridge has been conducted. Specimens consisted of cores of 1100 aluminum, 0.065 and 0.052 in. in diameter, that were clad on either side with shims of copper. With a 200-mil-diameter coil and an operating frequency of 10 kc, it is reported that the copper cladding thickness was measured to within 1 mil of the true 10- to 19-mil value with no visible influence as a function of varying core thickness or variation in cladding on the opposite surface. The conductivity ratio between the cladding and core in this case was less than the 2:1 value that had been considered minimum for accurate cladding-thickness measurements. As reported in the literature,[57] the device offers advantages in reduced sensitivity to lift-off, linearity for "through-transmission" operation, and in examination of thicker sections. The application of the instrument is being extended by use of additional operating frequencies, up to 2 Mc, and selective time differentiating circuits. Scanning at a constant speed with the new circuits provides an apparent increase of 10 or more times in sensitivity to defects.

The use of laser interferometry techniques for length measurement is under study at Oak Ridge.[2] An electronic counter counts the interference fringes at a translation speed of 4 in./min with the use of a Moore carriage. Parallelism of optical components and vibration of lead-screw drive motors have been the principal sources of early problems. Integral fringe counts have permitted the length of a 4-in. gauge block to be measured to six significant figures, with a seventh figure obtainable by averaging several measurement runs. Interpolation counting will be used to improve the measurements. It is expected that continued improvement of

the system will be realized with the use of newer lasers and hydraulic drive to reduce the sensitivity of the measurements to adverse environmental conditions. (A. F. Leatherman)

References

1. Q. C. Carloni and L. Robins, Summary of the Dynapak Extrusion of Uranium Tubes, USAEC Report BRB-83, Reactive Metals, Inc., Sept. 11, 1964.
2. Union Carbide Corporation, Nuclear Division, Y-12 Plant, Y-12 Development Activities Progress Report, August–October 1963, USAEC Report Y-1472, Oct. 30, 1964. (Classified)
3. Bureau of Mines, Albany Metallurgy Research Center, Quarterly Metallurgical Progress Report No. 24, July 1–September 30, 1964, USAEC Report USBM-RC-1135.
4. W. R. Burt, Jr., H. C. Katiyar, and R. M. Mayfield, Development of Techniques for Fabrication of Small-Diameter Thin-Wall Tungsten Tubing, Interim Progress Report, July 1–December 31, 1963, USAEC Report ANL-6806, Argonne National Laboratory.
5. Oak Ridge National Laboratory, Space Power Program Semiannual Progress Report for Period Ending June 30, 1964, USAEC Report ORNL-3683, October 1964. (Classified)
6. General Electric Company, Advanced Technology Services, High-Temperature Materials Program Progress Report No. 41, Part A, USAEC Report GEMP-41A, Nov. 30, 1964.
7. Nuclear Metals Division of Textron Inc., Fundamental and Applied Research and Development in Metallurgy, USAEC Report NMI-2130, Sept. 25, 1964.
8. Nuclear Metals Division of Textron Inc., Fundamental and Applied Research and Development in Metallurgy, USAEC Report NMI-2131, Oct. 8, 1964.
9. S. L. Ausmus and R. A. Beall, Expendable Casting Molds for Reactive Metals, Report BM-RI-6509, Bureau of Mines, Albany Metallurgy Research Center, November 1963.
10. E. S. Hodge, Elevated Temperature Compaction of Metals and Ceramics by Gas Pressures, *Powder Met.*, 7(14): 168-201 (Autumn 1964).
11. R. W. Dayton and R. F. Dickerson, Progress Relating to Civilian Applications During October 1964, USAEC Report BMI-1697, Battelle Memorial Institute, Nov. 1, 1964. (Classified)
12. Argonne National Laboratory, Reactor Development Program Progress Report, July 1964, USAEC Report ANL-6923, Aug. 20, 1964.
13. Hanford Atomic Products Operation, Reactor and Fuels Laboratory Monthly Report, August 1964, USAEC Report HW-83820A, Sept. 15, 1964. (Classified)
14. Oak Ridge National Laboratory, Aug. 6, 1964. (Unpublished)
15. Oak Ridge National Laboratory, Nov. 5, 1964. (Unpublished)
16. Improvements in/or Relating to the Fabrication of Fuel Elements and Elements so Produced, British Patent 960,352 (to General Dynamics Corp.), June 10, 1964.
17. P. C. Silverstone, Electroforming, Its Use in the Aircraft and Missile Industry, American Society for Metals Technical Report No. W4-43, Electroforms, Inc., March 16–20, 1964.
18. W. H. Safranek, A Survey of Electroforming for Fabricating Structures, Report to Redstone Scientific Information Center on Contract DA-01-021-AMC-203(Z), Battelle Memorial Institute, July 15, 1964.
19. M. M. Godneva, Electrolytic Deposition of Nickel with Niobium, Tantalum, Titanium, and Zirconium from Anhydrous Solutions, *Zh. Neorgan. Khim.*, 9: 996-1001 (April 1964).
20. W. H. Roberts, Plating Beryllium–Copper Alloy with a Copper–Silver-Gold Laminate, USAEC Report RFP-366, Dow Chemical Co., Jan. 11, 1964.
21. B. A. Gvozdev and Yu. T. Chuburkov, Preparation of Th, U, and Pu Oxide and Rare Earth Coatings by Electrolytic Precipitation from Organic Solutions, Report KFK-tr-157 [translated from *Radiokhimiya*, 5(6): 712-715 (1963)].
22. E. Caretta, R. Di Pietro, and R. Sesini, Electroplating on Zircaloy-2 With Copper, *Energia Nucl. (Milan)*, 11(9): 505-508 (1964).
23. W. J. Allan and W. W. Webb, Process for Production of Long Metallic Whiskers Using a Polycrystalline Copper Substrate, U. S. Patent 3,144,358 (to Union Carbide Corp.), Aug. 11, 1964.
24. A. F. Reid, Self-Gettering and Impurity Transfer in the Vapor Deposition of Thorium by the Carbide-Iodide Process, *J. Electrochem. Soc.*, 111(12): 1400-1403 (December 1964).
25. Papers presented at Eighth Meeting, Refractory Composites Working Group, Fort Worth, Texas, January 14–16, 1964.
    a. H. Leggett, Selected Activities of the Douglas Aircraft Company in the Development of Refractory Composites.
    b. G. Wakefield, Overlay Concept Applied to Protective Coatings.
    c. B. S. Payne, Research in Protective Coatings for Refractory Metals.
26. M. Basche, Pyrolytic Tungsten Parts and Coatings Resist Heat, *Mater. Design Eng.*, 60(2): 82-85 (August 1964).
27. Oak Ridge National Laboratory, Metals and Ceramics Division Annual Progress Report for Period Ending June 30, 1964, USAEC Report ORNL-3670, October 1964.
28. Oak Ridge National Laboratory, September 1964. (Unpublished)
29. E. Sirtl, Process of Producing Compact Boron, Particularly in Monocrystalline Form, U. S. Patent 3,160,476 (to Siemens and Halske AG), Dec. 8, 1964.
30. R. M. Witucki, Boron Filaments, Astro Research Corp., 1964.
31. C. F. Cullis and N. H. Franklin, The Pyrolysis of Acetylene at Temperatures from 500 to 1000°C, *Proc. Roy. Soc. (London)*, 280A: 139-152 (July 7, 1964).
32. Papers presented at Joint Meeting, Basic Science Division, American Ceramic Society, Western Clay Products Association, San Francisco, California, October 28–30, 1964.
    a. W. B. Campbell, Vapor Phase Crystal Growth of Oxides.

b. K. S. Mazdeyasni, C. T. Lynch, and J. S. Smith, Alkoxide Pyrolysis to Oxide Films and Powders.

33. Oak Ridge National Laboratory, November 1964. (Unpublished)
34. W. C. Jenkin, Method of Depositing Metals and Metallic Compounds Throughout the Pores of a Porous Body, U. S. Patent 3,160,517 (to Union Carbide Corp.), Dec. 8, 1964.
35. J. M. Basile, Metal Plating Process, U. S. Patent 3,155,532 (to Union Carbide Corp.), Nov. 3, 1964.
36. H. Inouye, Contamination of Refractory Metals by Residual Gases in Vacuums Below 10^{-6} Torr, USAEC Report ORNL-3674, Oak Ridge National Laboratory, September 1964.
37. J. H. Connor and A. Brenner, Deposition of Tungsten by Reduction of the Hexafluoride with Hydrogen in the Vapor Phase, Quarterly Report for the Period May 1 to August 1, 1964, National Bureau of Standards, Aug. 14, 1964.
38. R. Moreton, The Protection of Tungsten from Oxidation at High Temperatures with Silicon Carbide Coatings, British Report RAE-CPM-67, March 1964.
39. B. S. Payne, Cementation Coatings for Refractory Metals, *Am. Ceram. Soc. Bull.*, 43(8): 567-571 (August 1964).
40. W. L. Aves, G. Bourland, and G. M. Ecord, Investigation and Development of Techniques To Extend the Utility of Pack Processes and Compositions for Coating Molybdenum and Columbium Alloys, First Quarterly Progress Report, June 1–September 1, 1964, Ling-Temco-Vought, Inc.
41. Pratt & Whitney Aircraft Division, United Aircraft Corp., Advanced Materials Program for July and August 1964, USAEC Report PWAC-1016, Nov. 11, 1964. (Classified)
42. Lockheed Missiles and Space Company, Investigation of Modified Silicide Coatings for Refractory Metal Alloys With Improved Low-Pressure Oxidation Behavior, First Progress Report, June 1–Aug. 31, 1964.
43. Thompson Ramo Wooldridge Inc., Advancement of Protective Coating Systems for Columbium and Tantalum Alloys, Second Quarterly Technical Progress Report, July 1–October 1, 1964.
44. R. J. Carlson and C. C. Simons, Joining of Zircaloy and Inconel 600 Tubes by Explosive Welding, USAEC Report BMI-1715, Battelle Memorial Institute, Feb. 19, 1964.
45. R. E. Yount and D. L. Keller, The Structural Stability of Welds in Columbium Alloys, Report ML-TDR-64-210, General Electric Company, June 1964.
46. A. H. Freedman and E. B. Mikus, Brazing of Columbium D-36 Honeycomb Structures, *Welding J. (N. Y.)*, 43(9): 385s-392s (September 1964).
47. T. K. Redden, R. E. Kutchera, and R. G. Carlson, Development of Joining Techniques for TD Nickel, Interim Progress Report No. 1-8-211, May 1–July 31, 1964, General Electric Company, Advanced Engine Technology Department, August 1964.
48. A. T. D'Annessa, Fracture Toughness of X7039-T6 Aluminum Alloy Plate Weldments, Technical Report 6-62-64-6, Lockheed Aircraft Corp., April 1964.
49. E. N. Bossing, Mechanical Properties Tests of Welded A-356-T6 Aluminum Alloy, Report SM-45949, Douglas Aircraft Co., Inc., Apr. 20, 1964.
50. M. S. Orysh and I. G. Betz, Welding 214, 356, and Almag 35 Cast Aluminum Alloy, Report R-1726, Frankford Arsenal Laboratories, July 1964.
51. C. H. Crane, Steel to Aluminum Brazing, Report No. D2-81106, Boeing Co., Jan. 23, 1964.
52. M. S. Orysh, L. G. Betz, and F. W. Hussey, Joining of Steel and Other Wear-Resistant Metals to Aluminum Alloys, Technical Memorandum M64-8-1, Frankford Arsenal Laboratories, August 1963.
53. Hanford Atomic Products Operation, Research and Development Programs Executed for the Division of Reactor Development, Quarterly Progress Report, January–March, 1964, USAEC Report HW-81984, September 1964.
54. D. C. Worlton, Progress in Nondestructive Testing. A Summary of Hanford Achievements in These Programs Under General Electric 1952–1964, USAEC Report HW-83608, Hanford Atomic Products Operation, August 1964.
55. General Motors Corp., Allison Division, MCR Quarterly Technical Progress Report for Period July 1–September 30, 1964, USAEC Report GMAD-3078-13 (EDR-4016), Oct. 30, 1964. (Classified)
56. W. L. R. Rice (Ed.), Nuclear Fuels and Materials Development, USAEC Report TID-11295 (3rd Ed.), July 1964.
57. C. V. Dodd, Applications of a Phase-Sensitive Eddy Current Instrument, *Materials Evaluation*, 22(6): 260-264 (June 1964).

LEGAL NOTICE

This journal was prepared under the sponsorship of the U. S. Atomic Energy Commission. Neither the United States, nor the Commission, nor any person acting on behalf of the Commission:

A. Makes any warranty or representation, expressed or implied, with respect to the accuracy, completeness, or usefulness of the information contained in this journal, or that the use of any information, apparatus, method, or process disclosed in this journal may not infringe privately owned rights; or

B. Assumes any liabilities with respect to the use of, or for damages resulting from the use of any information, apparatus, method, or process disclosed in this journal.

As used in the above, "person acting on behalf of the Commission" includes any employee or contractor of the Commission, or employee of such contractor, to the extent that such employee or contractor of the Commission, or employee of such contractor prepares, disseminates, or provides access to, any information pursuant to his employment or contract with the Commission, or his employment with such contractor.

NUCLEAR SCIENCE ABSTRACTS

The U. S. Atomic Energy Commission, Division of Technical Information, publishes *Nuclear Science Abstracts (NSA)*, a semimonthly journal containing abstracts of the literature of nuclear science and engineering.

NSA covers (1) research reports of the U. S. Atomic Energy Commission and its contractors; (2) research reports of government agencies, universities, and industrial research organizations on a world-wide basis; and (3) translations, patents, books, and articles appearing in technical and scientific journals.

Complete indexes covering subject, author, source, and report number are included in each issue. These are cumulated quarterly, semiannually, and annually providing a detailed and convenient key to the literature.

Availability of *NSA*

SALE *NSA* is available on subscription from the Superintendent of Documents, U. S. Government Printing Office, Washington, D. C., 20402, at $30.00 per year for the semimonthly abstract issues and $22.00 per year for the four cumulated-index issues. Subscriptions are postpaid within the United States, Canada, Mexico, and all Central and South American countries, except Argentina, Brazil, British and French Guiana, Surinam, and British Honduras. Subscribers in these Central and South American countries, and in all other countries throughout the world, should remit $37.00 per year for subscriptions to semimonthly abstract issues and $25.00 per year for the four cumulated-index issues.

EXCHANGE *NSA* is also available on an exchange basis to universities, research institutions, industrial firms, and publishers of scientific information. Inquiries should be directed to the Division of Technical Information Extension, U. S. Atomic Energy Commission, P. O. Box 62, Oak Ridge, Tennessee, 37831.

TECHNICAL PROGRESS REVIEWS may be purchased from Superintendent of Documents, U. S. Government Printing Office, Washington, D. C., 20402. *Isotopes and Radiation Technology* at $2.00 per year for each subscription or $0.55 per issue; the other four journals at $2.50 per year and $0.70 per issue. The use of the coupon below will facilitate the handling of your order.

POSTAGE AND REMITTANCE: Postpaid within the United States, Canada, Mexico, and all Central and South American countries except as hereinafter noted. Add $0.50 per year, or $0.15 per single issue for the *Isotopes and Radiation Technology* journal and $0.75 per year or $0.20 per single issue for the other four journals for postage to all other countries, including Argentina, Brazil, British and French Guiana, Surinam, and British Honduras. Payment should be by check, money order, or document coupons, and MUST accompany order. Remittances from foreign countries should be made by international money order, or draft on an American bank, payable to the Superintendent of Documents, or by UNESCO book coupons.

order form

SUPERINTENDENT OF DOCUMENTS
U. S. GOVERNMENT PRINTING OFFICE
WASHINGTON , D. C., 20402

Enclosed:
document coupons ☐ check ☐ money order ☐

Charge to Superintendent of Documents No. _____

Please send a one-year subscription to

☐ NUCLEAR SAFETY

☐ POWER REACTOR TECHNOLOGY

☐ REACTOR FUEL PROCESSING

☐ REACTOR MATERIALS

(Each subscription $2.50 per year; $0.70 per issue.)

☐ ISOTOPES AND RADIATION TECHNOLOGY

(Each subscription $2.00 a year; $0.55 per issue.)

SUPERINTENDENT OF DOCUMENTS
U. S. GOVERNMENT PRINTING OFFICE
WASHINGTON, D. C., 20402

(Print clearly)

Name _____

Street _____

City _____ Zone ____ State _____